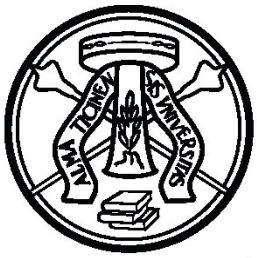

UNIVERSITÀ
DI PAVIA

PhD IN BIOMEDICAL SCIENCES
DEPARTMENT OF BRAIN AND BEHAVIORAL SCIENCES
UNIT OF NEUROPHYSIOLOGY
Coordinator: Prof. Antonio Pisani

HERG Channel Agonists:

A Novel, Substrate-Based Therapeutic Approach for

Long QT Syndrome

Scientific Supervisor:
Eminent Professor Silvia G. Priori

PhD Candidate:
Dr. Deni Kukavica

Academic Year 2021/2022

S ljubavlju, mami i tati

ABSTRACT

Long QT Syndrome (LQTS) is a potentially fatal genetic arrhythmia syndrome, characterized by prolongation of ventricular repolarization, which predisposes young and otherwise healthy individuals to sudden cardiac death.

Despite quantum leaps in our understanding of LQTS, the mainstay of treatment remains the use of beta-adrenergic blockers, which are aimed at control of the arrhythmic trigger, and which do not modify the QT interval duration. Since the duration of the QT interval is a potent predictor of outcomes, our group championed a substrate-based approach aimed at shortening the duration of the QT interval using mexiletine, a class I antiarrhythmic for treatment of Long QT Syndrome type 3 (LQT3). Currently, mexiletine is indicated as a standard-of-care for all patients with LQT3, suggesting that in principle shortening the QTc interval may be an effective strategy to treat *all forms* of LQTS.

We tested the efficacy and safety of 3-nitro-N-(4-phenoxyphenyl) benzamide (ICA-105574), the most potent HERG1 channel agonist, in different models of LQTS. In Phase One, we successfully developed drug-induced models of type 2, type 3, and type 8 LQTS and used them to investigate the ability of ICA-105574 to safely abbreviate the QT interval in different forms of LQTS. Following the successful preliminary demonstration of efficacy and safety, we exploited the opportunity to study *in vivo* the effects and safety of ICA-105574 using the first successful knock-in large mammal model of a cardiac channelopathy. Using state-of-the art, clinical grade, ultra-high density mapping of ventricular repolarization, we showed that ICA-105574 significantly reduces the arrhythmogenic gradients of ventricular repolarization identified in our knock-in model of LQTS.

These results offer evidence to support the view that development of HERG1 channel agonists, as a novel class of antiarrhythmics, could have clinical application.

PHASE ONE:
Drug-Induced Models

PHASE TWO:
Knock-In Model of LQT8

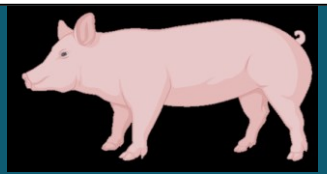

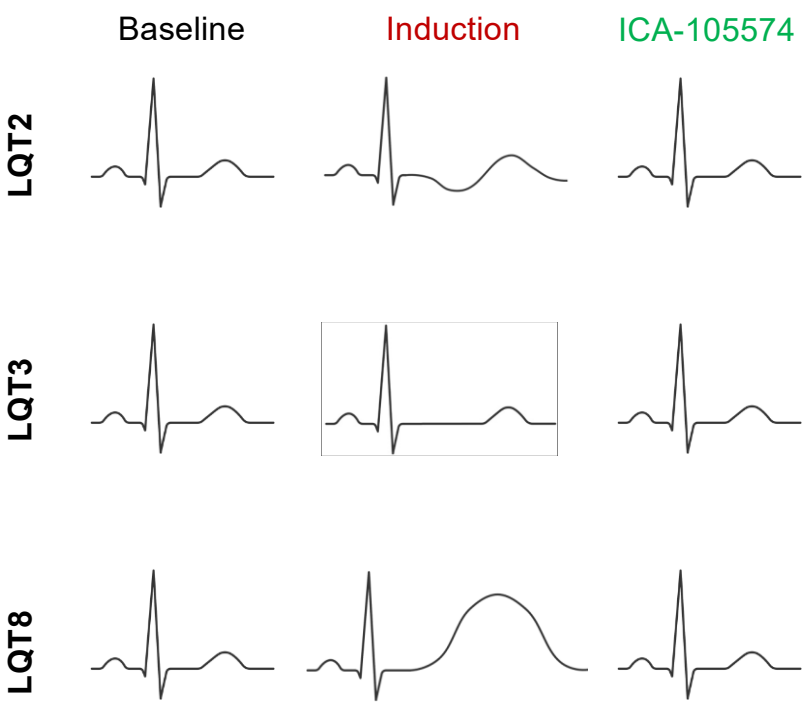

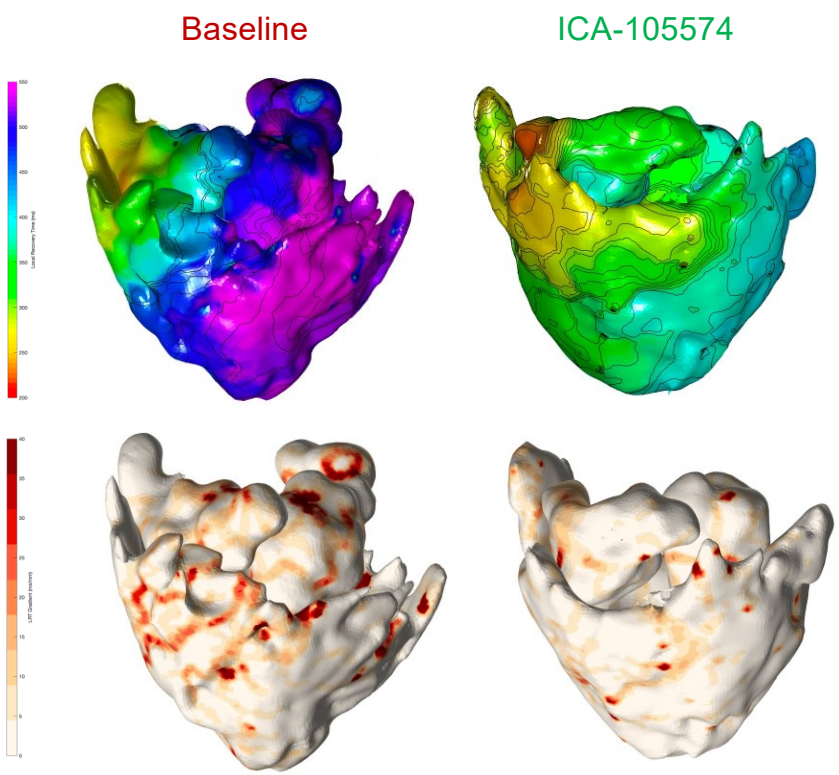

TABLE OF CONTENTS

TABLES

FIGURES

1 LONG QT SYNDROME: AN INTRODUCTION

1.1 Definition and Epidemiology

Long QT Syndrome (LQTS) is a collective term for a group of cardiac electrical disorders characterized by prolonged ventricular repolarization, represented by the QT interval on surface electrocardiogram (ECG), and by the predisposition to develop polymorphic ventricular tachycardia and ventricular fibrillation leading to syncope or sudden cardiac death (SCD)[1].

Congenital LQTS is mainly related to mutations in genes encoding for cardiac ion channels. Patients with congenital LQTS have been described in all ethnic groups. The prevalence of the autosomal dominant (AD) LQTS in Caucasians is estimated at 1:2000[2], whereas the autosomal recessive (AR) form is less frequent (1 in 200,000)[3].

Acquired LQTS is usually secondary to drug adverse effects or electrolyte disturbance. Its precise incidence in the general population is difficult to estimate, but a recent study on in-patients revealed a prevalence QT interval prolongation of 28%[4].

The focus of this dissertation will be exclusively congenital, genetically-mediated forms of LQTS.

1.2 Genetic Bases

In the context of genetic cardiac diseases, LQTS constitutes the archetype of monogenic diseases. Classical linkage-analysis studies conducted in the 1990's permitted to identify the three canonical LQTS-genes[5–7] that alone are responsible for about 75% of all LQTS patients[8]. This high yield of genetic analysis has also made it possible to assemble genetically homogeneous cohorts of patients, laying the foundations for a genotype-specific approach in the clinical management of patients with LQTS[2] and other inherited arrhythmogenic conditions. More in detail, 70% of LQTS is secondary to loss-of-function mutations affecting either the Kv7.1 potassium channel (LQT1, gene *KCNQ1*[5]) or the Kv11.1 potassium channel (LQT2, gene *KCNH2*[6]), while about 5-10% is secondary to gain-of-function mutations in the Nav1.5 sodium channel (LQT3, gene *SCN5A*[7]).

In addition to the three abovementioned canonical genes, which account for the majority of cases of congenital LQTS, a plethora of other genes have been associated to LQTS (Table 1.1).

Table 1.1. Genetic Bases of Congenital LQTS.

Gene	LQTS Type	Frequency (%)	Locus	Protein	Functional Effect	Evidence for LQTS causation
KCNQ1	LQT1	40-55	11p15.5-p15.4	Potassium channel, voltage-gated, KQT-like subfamily, member 1	Loss-of-function; reduction of IKs current	Definitive
KCNH2	LQT2	30-45	7q36.1	Potassium channel, voltage-gated, subfamily H, member 2	Loss-of-function; reduction of IKr current	Definitive
SCN5A	LQT3	5-10	3p22.2	Sodium channel, voltage-gated, type V, alpha subunit	Gain-of-function; increase of sodium current	Definitive
CALM1	LQT14	<1	14q32.11	Calmodulin 1	Loss-of-function, reduction in calcium-binding affinity	Definitive
CALM2	LQT15	<1	2p21	Calmodulin 2	Loss-of-function, reduction in calcium-binding affinity	Definitive
CALM3	LQT16	<1	19q13.2-q13.3	Calmodulin 3	Loss-of-function, reduction in calcium-binding affinity	Definitive
TRDN (Homozygous	-	<1	6q22.31	Triadin	Loss-of-function, loss of cardiac Ca2+ release units, impaired	Strong/moderate

mutations)					excitation-contraction coupling	
CACNA1C	LQT8 (TS)	<1	12p13.33	Calcium channel, voltage-dependen, L-type, alpha-1C subunit	Gain-of-function; increase of calcium current	Strong/moderate
KCNJ2	LQT7 (ATS)	<1	17q24.3	Potassium channel, inwardly rectifying, subfamily J, member 2	Loss-of-function; reduction of IK1 current	Definitive for ATS Limited for LQTS
KCNE1	LQT5	<1	21q22.11-q22.12	Potassium channel, voltage-gated, ISK-related subfamily, member1	Loss-of-function; reduction of IKs current	Limited *
CAV3	LQT9	<1	3p25.3	Caveolin 3	Secondary gain of function of sodium channel	Limited
ANK2	LQT4	<1	4q25-q26	Ankyrin 2	Loss-of-function (several target proteins)	Disputed
KCNE2	LQT6	<1	21q22.11	Potassium channel, voltage-gated, ISK-related subfamily, member 2	Loss-of-function; reduction of IKr current	Disputed *
SCN4B	LQT10	<1	11q23.3	Sodium channel, voltage-gated, type IV, beta subunit	Secondary gain of function of sodium channel	Disputed

AKAP9	LQT11	<1	7q21.2	A-kinase anchor protein 9	Loss-of-function; reduction of IKs current	Disputed
SNTA1	LQT12	<1	20q11.21	Syntrophin, alpha-1	Secondary gain of function of sodium channel	Disputed
KCNJ5	LQT13	<1	11q24.3	Potassium channel, inwardly rectifying, subfamily J, member 5	Loss-of-function; reduction of IK-Ach current	Disputed
Autosomal Recessive LQTS with congenital deafness (Jervell and Lange-Nielsen Syndrome)						
KCNQ1	JLN1	<1	11p15.5-p15.4	Potassium channel, voltage-gated, KQT-like subfamily, member 1	Loss-of-function; reduction of IKs current	Definitive
KCNE1	JLN2	<1	21q22.11	Potassium channel, voltage-gated, ISK-related subfamily, member1	Loss-of-function; reduction of IKs current	Definitive

** Despite limited/disputed evidence classifications for congenital LQTS, KCNE1 and KCNE2 are both considered to be strong-evidence genes for acquired LQTS.*

Adapted from Adler et al.[9]

1.3 Pathogenesis

From a pathophysiological standpoint, QT interval prolongation derives from an increased duration of the action potential of the cardiomyocyte (Figure 1.1).

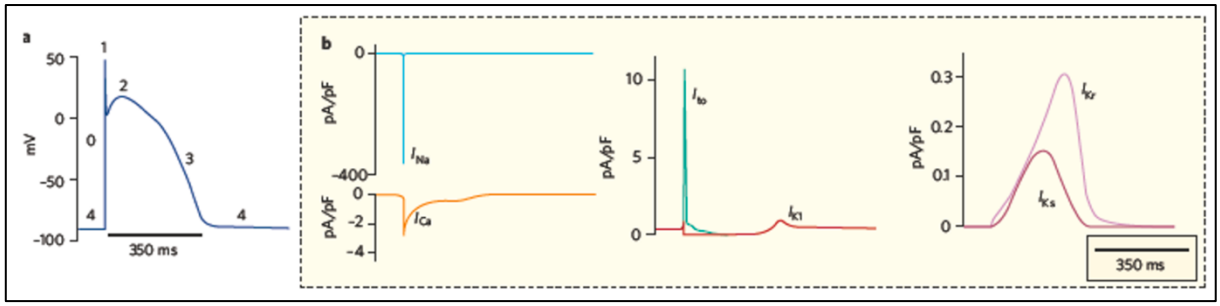

Figure 1.1. Ion channels shaping the ventricular action potential.

Ventricular action potential consists of four phases (Panel A). Phase 0 begins with the inward sodium current (I_{Na}; Panel B, blue line) triggering a rapid membrane depolarization. After the membrane depolarization, rapid and partial repolarization (Phase 1) occurs, dependent on the short-lasting effect of the transient outward potassium current (I_{To1}; Panel B, green line). In the plateau phase or phase 2, the interplay between L-type Ca^{2+} channels conducting inward I_{Ca} current (Panel B, orange line) and the slow counterbalancing outward potassium currents I_{Ks}, I_{k1}, I_{Kr} (Panel B; purple, red and pink lines, respectively) prolongs the duration of the repolarization. During the phase 3, repolarization is mediated by outward potassium currents, which bring the cell to its resting potential (Phase 4)
Adapted from Sangiunetti M and Tristani-Firouzi M[10].

The latter can result from both a reduction in repolarizing outward currents (e.g., IKs and IKr; LQT1 and LQT2, respectively[5,6]) or from an increase in depolarizing inward currents (e.g,. INa; LQT3[7]). In the latter case, while the peak sodium current is usually unaltered, the inactivation of the channel is disrupted, causing longer channel openings and an augmentation of the slowly inactivating Na current, called "late Na current" (INaL)[7].

Independently of the molecular substrate, the resulting abnormal prolongation of action potential can predispose to the development of early afterdepolarizations (EADs) secondary to reactivation of L-type Ca^{2+} channels or Na^{+}/Ca^{2+} exchanger[11–15]. EADs, in turn, can trigger premature ventricular beats that may initiate polymorphic reentrant ventricular tachycardia (VT) when infringing on a substrate of heterogeneous repolarization[12].

1.3.1 Long QT Syndrome, type 2

Long QT Syndrome type 2 (LQT2) is the second most common type of congenital LQTS. According to the most recent data, it is thought that LQT2 accounts for 35-40% of all cases of LQTS[16].

In 1995, laboratory of Prof. Keating identified that mutations in *KCNH2* gene, located on chromosome 7, are the molecular mechanism underlying the LQT2, and by doing so proved the genetic basis of the disease. *KCNH2* codes for the alpha subunit of the potassium channel (HERG1 channel) responsible for conducting the delayed rectifier IKr current, which activates during repolarization and rapidly inactivates at the end of it[17,18]. The ensuing current is a relatively small potassium repolarizing outward current at the end of phase 3 of the action potential (Figure 1.2).

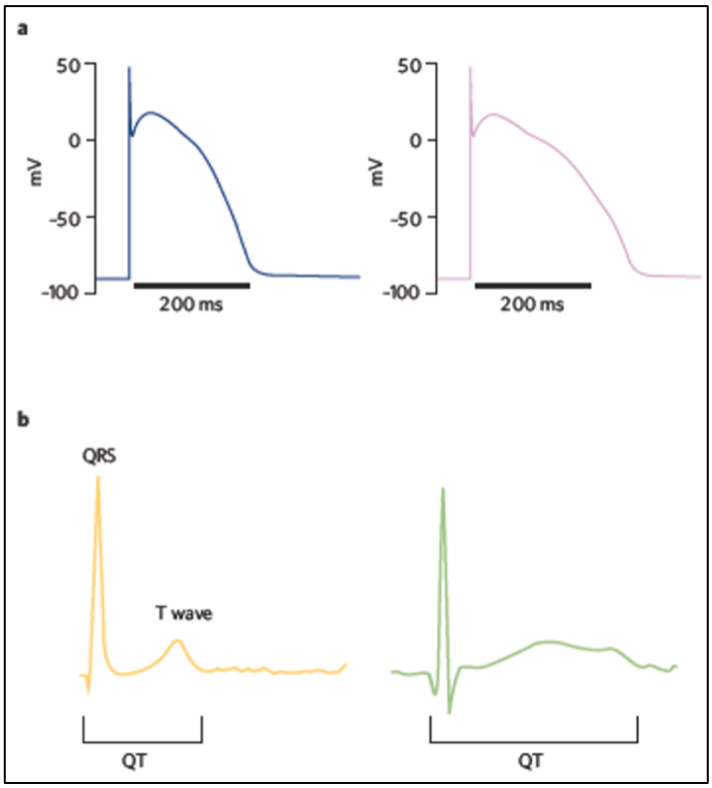

Figure 1.2. Effects of Reduction of HERG1 Current.

Reduction of the HERG1-mediated IKr results in the lengthening of the ventricular action potential (Panel A; the blue line represents the normal action potential, and the pink line represents the prolonged action potential). Adapted from Sangiunetti M and Tristani-Firouzi M[10].

The clinical phenotype is usually caused loss-of-function mutations: either missense mutations, or nonsense or frameshift mutations.

A single missense mutation which leads to a loss-of-function effect does so by causing either a defect in exposition of the mutated protein on the cytoplasmic membrane or in an translation of immature protein leading to a defective IKr current[18–22]. This is typically the result of trafficking defects[23] with dominant negative loss-of-function due to heteromerization of the mutant protein with the wild type protein, rendering also the healthy subunits hypofunctional or nonfunctional[24].

On the other hand nonsense and frameshift variants, do not lead to dominant negative loss of function but to a "simple" haploinsufficiency, by preventing transcription of the mutant protein from the affected allele[18]. Although they also cause a reduction in IKr current, their effect is less conspicuous than in mutations showing dominant negative loss effect, leading paradoxically to a milder phenotype[25].

1.3.2 Long QT Syndrome, type 3

In tandem with the discovery of *KCNH2* mutations as the cause of LQT2, the laboratory of Prof. Keating published the finding that mutations on *SCN5A*, located on chromosome 3, are responsible for Long QT Syndrome type 3 (LQT3)[7].
SCN5A gene encodes for the alpha subunit of the cardiac isoform of protein $Na_V1.5$, a voltage-dependent sodium channel (Figure 1.3)[18,26].

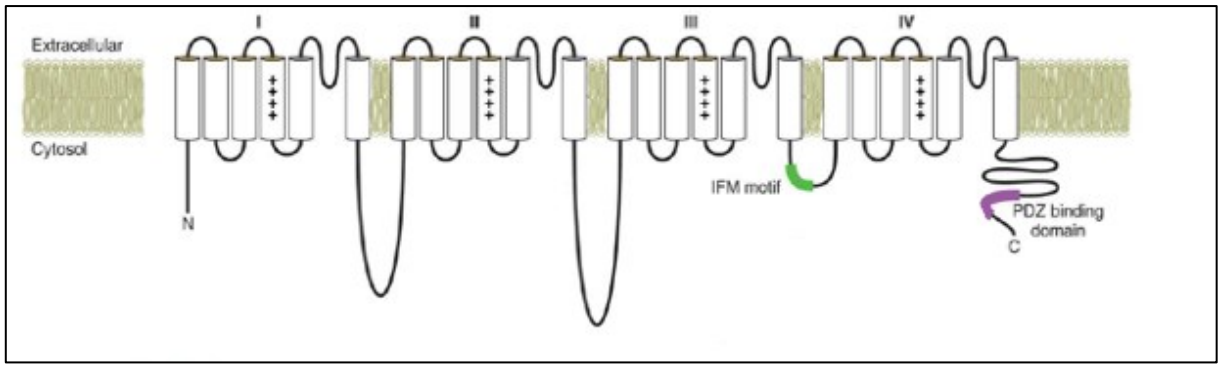

Figure 1.3. Schematic Structure of $Na_V1.5$.

Unlike most types of LQTS, LQT3 is caused by mutations inducing a gain-of-function effect. Specifically, LQT3-causing mutations affect the inactivation of the channel, causing longer channel openings and augment the slowly inactivating Na current, called "late Na current" (INaL)[7].

1.3.3 Long QT Syndrome, type 8

Long QT type 8, known also as Timothy syndrome type 1 (TS1), is a rare multisystemic inherited arrhythmogenic disorder, characterized by a complex set of cardiac manifestations, both (1) electrical disturbances such as QT interval prolongation, second degree atrio-ventricular blocks, ventricular arrhythmias and (2) structural anomalies, such as interatrial and interventricular defects, patent ductus arteriosus, cardiac hypertrophy.

Seminal work by Splawski and colleagues permitted to identify *CACNA1C* as the causative gene, with all 13 patients for whom DNA samples were available carrying a single, *de novo*, missense mutation in the exon 8A (c.1216G>A, p.G406R)[27]. *CACNA1C* encodes for the voltage-dependent cardiac L-type calcium channel (LTCC), which conducts the inward depolarizing I_{Ca} current, which is largely responsible for the phase 2 of cardiac action potential. LTCC is activated by membrane depolarization, links membrane depolarization to myocardial contraction, and is inactivated in a voltage-dependent manner (VDI)[28] and calcium-dependent (CDI)[29].

Patch clamp studies have shown that in the presence of TS-causing p.G406R mutation, VDI component of the LTCC's inactivation is nearly completely lost, leading to the prolongation of phase 2 (17% longer)[27] and consequently cardiac action potential[27].

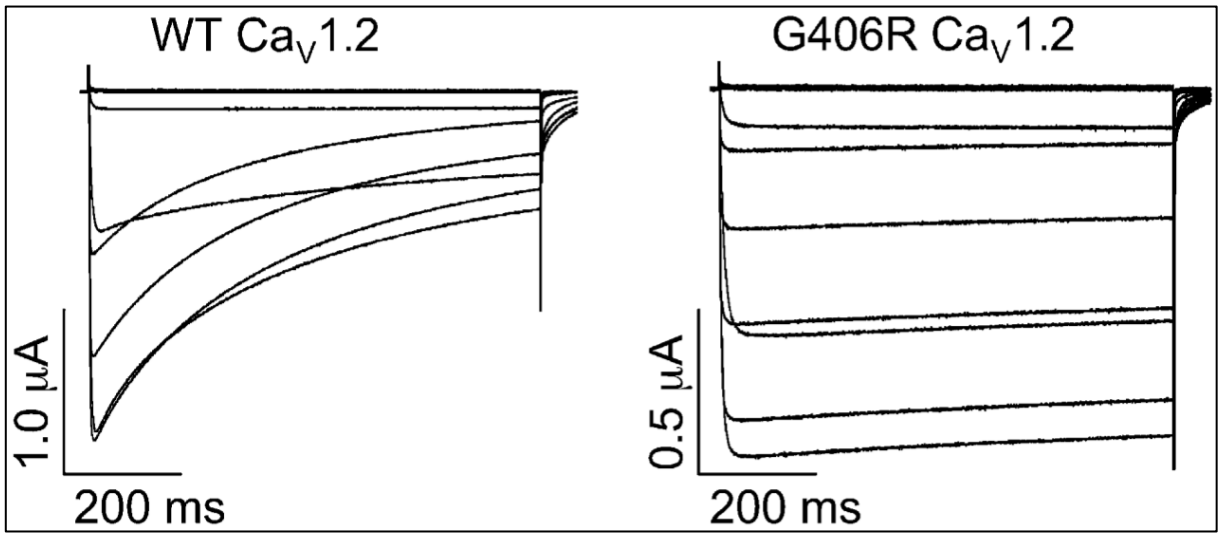

Figure 1.4. Patch Clamp Studies Showing Near-Complete Loss of Voltage-Dependent Inactivation in TS1.

Adapted from Splawski et al[27].

1.4 Clinical Manifestations and Diagnosis

The diagnosis of LQTS relies primarily on the corrected measurement of the QT interval for heart rate (QTc) using Bazett's formula[30]. Importantly, secondary causes of QT prolongation (drugs or electrolyte imbalance) need to be excluded when assessing the ECG of a patient with suspected LQTS[1].

According to the most recent guidelines of the European Society of Cardiology[1], LQTS is diagnosed with either:

- QTc ≥480 ms in repeated 12-lead electrocardiograms with or without symptoms (Figure 1.5)
- LQTS diagnostic score >3

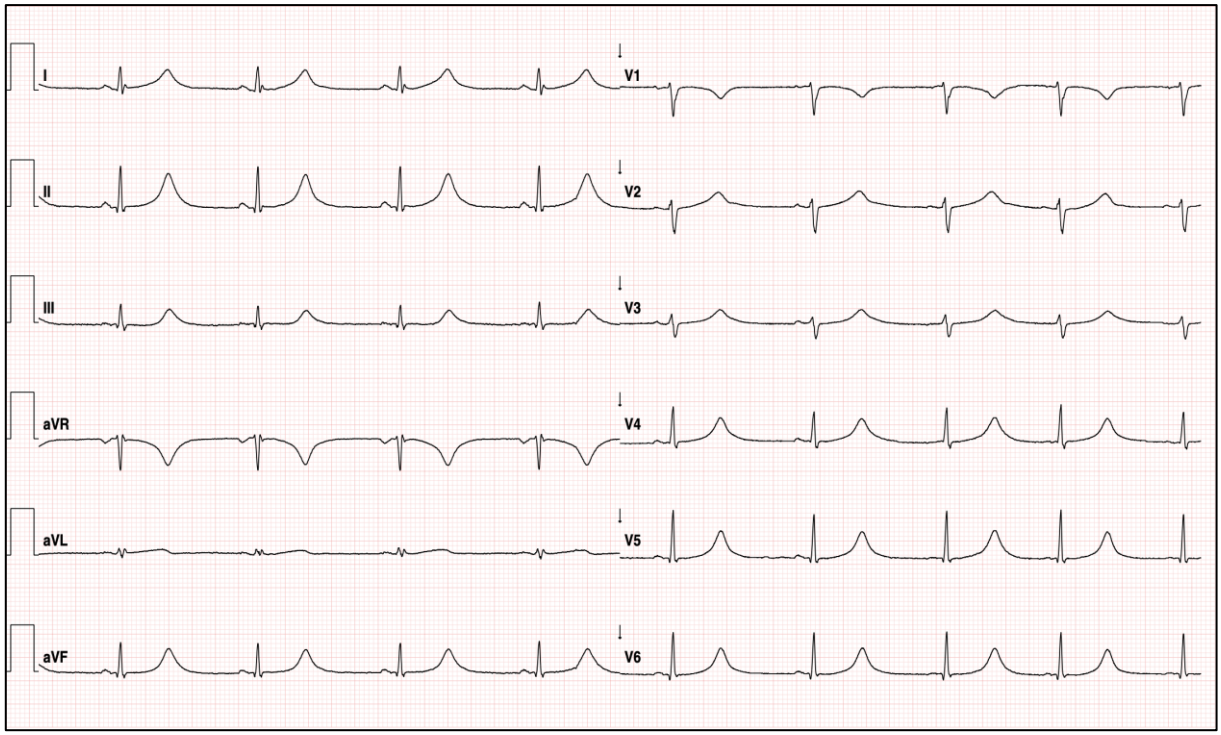

Figure 1.5. Example of an Electrocardiogram of a Patient with Long QT Syndrome.

Moreover, the diagnosis may be considered in patients with QTc interval ≥460 ms, but < 480 ms, in repeated 12-lead electrocardiograms in patients with an arrhythmic syncope in the absence of secondary causes for QT prolongation[1].

Although prolonged ventricular repolarization is the hallmark of LQTS, 10 to 36% of carriers of a pathogenic mutation exhibit normal QTc values[2]. These "silent carriers" are also

considered affected according to the current guidelines; they have a higher risk of syncope or CA than the general population (approximately 10% from birth to 40 years[2]) and consequently ought to be treated[1].

Aside from the prolonged ventricular repolarization, patients with LQTS present with peculiar ECG alterations. These alterations tend to be gene-specific and may help in identifying the syndrome: notches on the T-wave, for instance, are typical for LQT2 and indicate a higher risk for arrhythmic events, while sinus pauses are common among LQT3 patients[31–33] (Figure 1.6).

Figure 1.6. Representative ECG Traces of Three Main Forms of LQTS.

Figure from the 2022 ESC Guidelines for the management of patients with ventricular arrhythmias and the prevention of sudden cardiac death[1].

1.5 Risk Stratification

Clinical, demographic, electrocardiographic and genetic parameters should be integrated in the risk stratification of patients with Long QT Syndrome.

Patients with a history of cardiac arrest or arrhythmic syncope present a higher risk of SCD as compared to asymptomatic ones, especially if arrhythmias occur during the first year of life. Survivors of a CA have a high risk of recurrences and should receive an ICD[1]. Similarly, the occurrence of syncope during therapy with adequate dosage of beta-blockers calls for a more aggressive treatment[1].

Regardless of the clinical presentation, two factors have been consistently associated with clear prognostic implications: 1) the duration of the QTc interval, and 2) the genotype[2,16,34]. In fact, QT interval duration >500 ms traditionally identifies patients at higher arrhythmic risk[2], and our group demonstrated that every 10 ms increment of QT interval translates into a 15% increase of arrhythmic risk[34].

Genetic background is another independent modulator of risk: patients with LQT2 and LQT3 are respectively 2 and 4 times more at risk of SCD than patients with LQT1[34]. Combining these two risk factors, our group has recently developed[34] and validated[16] a risk calculator that allows a granular estimate of 5-year risk of potentially fatal arrhythmias based on the duration of the QTc interval and the genotype (LQT1, LQT2 or LQT3) of an individual patient (http://molecularmedicine.unipv.it/reseach-groups/cardiology/priori/1-2-3-lqts-risk-calculator-an-independently-validated-risk-calculator-for-patients-with-long-qt-syndrome/; Figure 1.7).

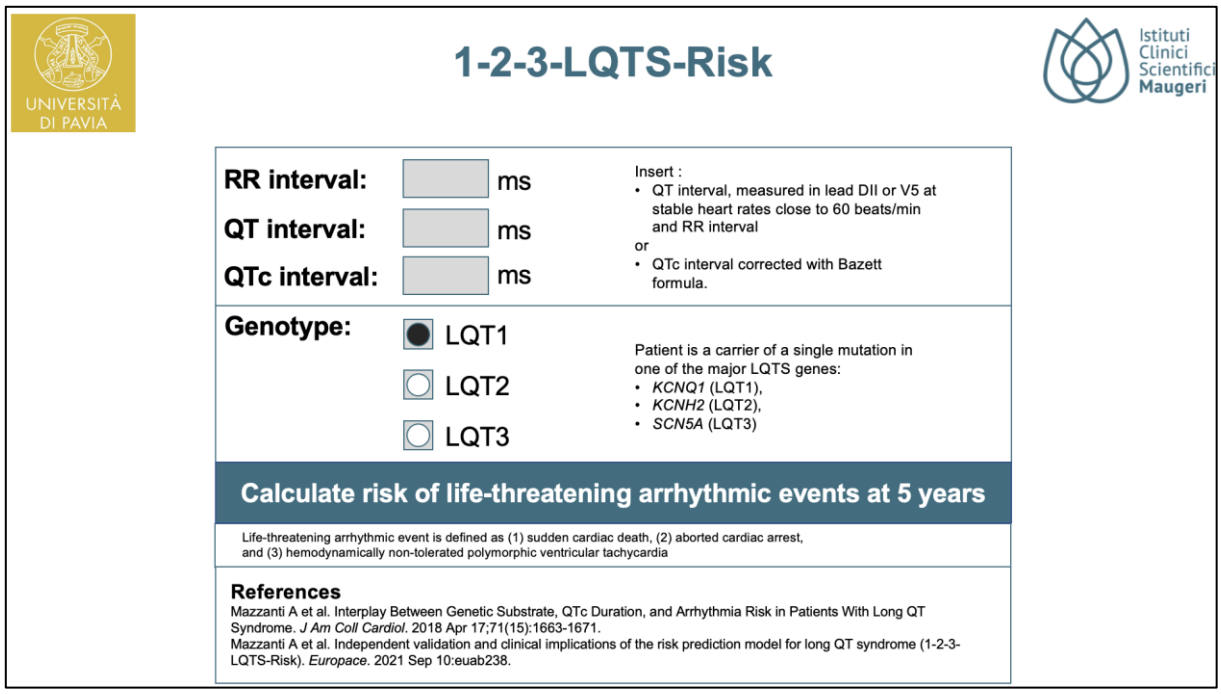

Figure 1.7. 1-2-3-LQTS Risk Calculator.

Regarding demographic factors, the interplay between age and sex is complex. Male gender is associated with a 3-fold increase in the risk of life-threatening cardiac events during childhood, especially in LQT1[5,35]. On the contrary, an opposite trend has been observed post-puberty and females maintain a higher risk than males during adulthood, especially in LQT2, with a peak of arrhythmic risk in the postpartum period[35].

Additionally, it is recognized that patients with calmodulinopathies[36], Jervell Lange-Nielsen syndrome[37], Timothy syndrome[27], Triadin knock-out syndrome[38], or compound heterozygosity represent high-risk categories. Furthermore, even within the same genotype it is possible to identify single genetic variants or portions of the gene that are associated with a particularly malignant phenotype, such as the A341V mutation of *KCNQ1*[39] or mutations in the pore region of HERG[25].

1.6 Current Therapeutic Approaches

The postulates of current therapeutic approaches as suggested by the 2022 European Society of Cardiology (ESC) Guidelines for the management of patients with ventricular arrhythmias and the prevention of sudden cardiac death[1] are summarized in Figure 1.8 and are discussed in relative subsections.

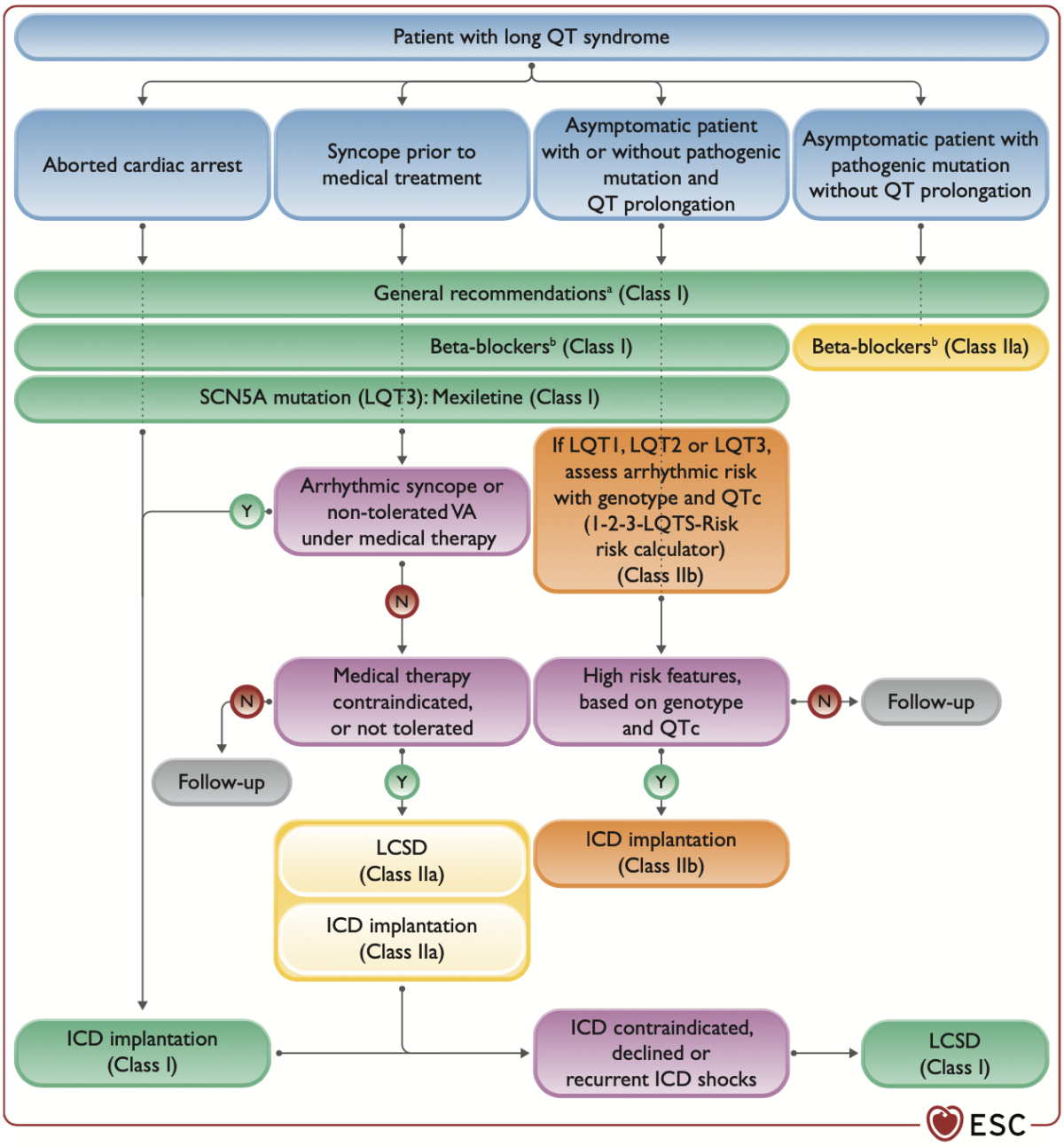

Figure 1.8. Algorithm for Management of Patients with Long QT Syndrome.

Figure from the 2022 ESC Guidelines for the management of patients with ventricular arrhythmias and the prevention of sudden cardiac death[1].

1.6.1 Lifestyle Changes

Lifestyle modifications to limit the exposure to arrhythmic triggers should be applied to all LQTS patients[1]. These include avoidance of drugs prolonging QT interval (for a comprehensive list: www.crediblemeds.org), abstention from strenuous exercise (especially swimming) in LQT1 patients, and reduction of exposure to abrupt loud noises in LQT2 patients[1]. Additionally, all patients should avoid and correct electrolyte abnormalities[1], such as hypokalemia.

1.6.2 Beta-Adrenergic Antagonists Therapy

β-blocker therapy (βB) is the mainstay pharmacological therapy for LQTS[1,40,41]. They are indicated in all LQTS patients, including those with a genetic diagnosis and normal QTc[1]. Nadolol (1-2 mg/kg per day), a potent long-acting non-selective beta-blocker, is the (βB)of choice, as it is the only molecule demonstrated to reduce arrhythmic risk in all genotypes[34].

1.6.3 Genotype-Specific Therapy

As will be discussed later, our group pioneered a genotype-specific therapy for LQTS. First, in 1996, our group showed that the use of the antiarrhythmic drug mexiletine, a sodium channel blocker, can counteract the gain-of-function mutations in the *SCN5A* gene which cause LQT3[42], and then more recently in showed that mexiletine not only shortens and often normalizes the QTc interval, but also provides a clinically relevant reduction of the number of patients with arrhythmic events, the number of events per patient, and the annual event rate at follow-up[43].

In the most recent 2022 ESC Guidelines, this approach has been fully endorsed and today, the use of mexiletine in patients with LQT3 is a class I indication[1].

1.6.4 Device Therapy

As mentioned earlier, the use of an implantable cardioverter defibrillator (ICD) is clearly indicated in all patients survivors of a cardiac arrest and patients who continue experiencing arrhythmic symptoms (i.e., arrhythmic syncope or hemodynamically non-tolerated ventricular arrhythmias) while receiving adequate medical therapy[1].

In a novel recommendation, 2022 ESC Guidelines suggest that either ICD or left cardiac sympathetic denervation (LCSD) should be considered in patients in patients who are

symptomatic (i.e., arrhythmic syncope or hemodynamically non-tolerated ventricular arrhythmias) when medical therapy is contraindicated or not tolerated[1].

Lastly, in an endorsement of the risk stratification scheme pioneered by our group, 2022 ESC Guidelines suggest that an ICD may be considered in patients deemed to be at high risk according to the 1-2-3-LQTS Risk calculator[16].

1.6.5 Left Cardiac Sympathetic Denervation

Left cardiac sympathetic denervation (LCSD) is currently indicated[1] in patients with symptomatic LQTS (i.e., arrhythmic syncope or hemodynamically non-tolerated ventricular arrhythmias) when:

- ICD therapy is contraindicated or declined;
- patient is on beta-blockers and genotype-specific drugs with an ICD and experiences multiple shocks or syncope due to VA .

As mentioned above, either ICD or left cardiac sympathetic denervation (LCSD) should be considered in patients in patients who are symptomatic (i.e., arrhythmic syncope or hemodynamically non-tolerated ventricular arrhythmias) when medical therapy is contraindicated or not tolerated[1].

1.7 Unmet Therapeutic Needs

Despite the success of βB and mexiletine in reducing the rates of arrhythmic events, it well known that event rates are genotype dependent.

The pioneering works led by Prof. Moss demonstrated, using a matched period analysis in 869 patients with LQTS, that the use of βB significantly reduced the event rate in patients with LQTS (Figure 1.9), providing the evidence-based rationale for the use of βB[40].

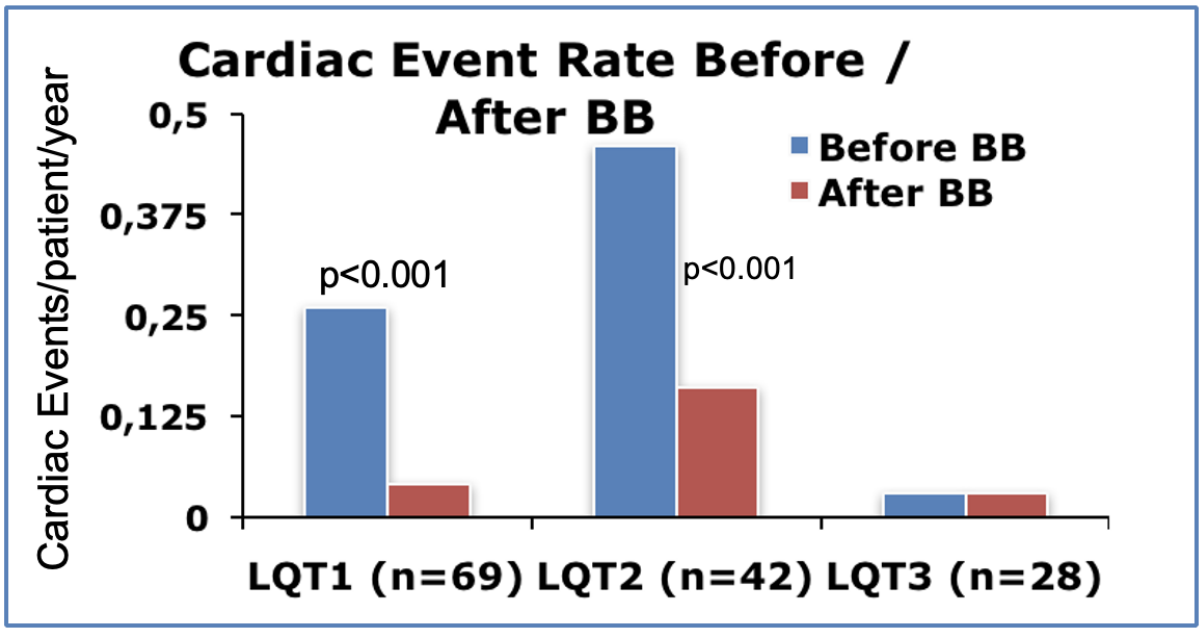

Figure 1.9. Beta-Blockers in LQTS: Matched Period Analysis

Adapted from Moss et al[40].

Shortly after, our group demonstrated that genetic background of patients with LQTS plays a fundamental role in response to βB therapy. Relevantly, the risk of cardiac events in patients with LQT2 (adjusted relative risk [ARR]: 2.81; 95% confidence interval [CI], 1.50-5.27; p=0.001) and LQT3 (ARR: 4.00; 95% CI, 2.45-8.03; p<0.001) was significantly higher than among LQT1 patients (Figure 1.10), suggesting inadequate protection from βB therapy[41].

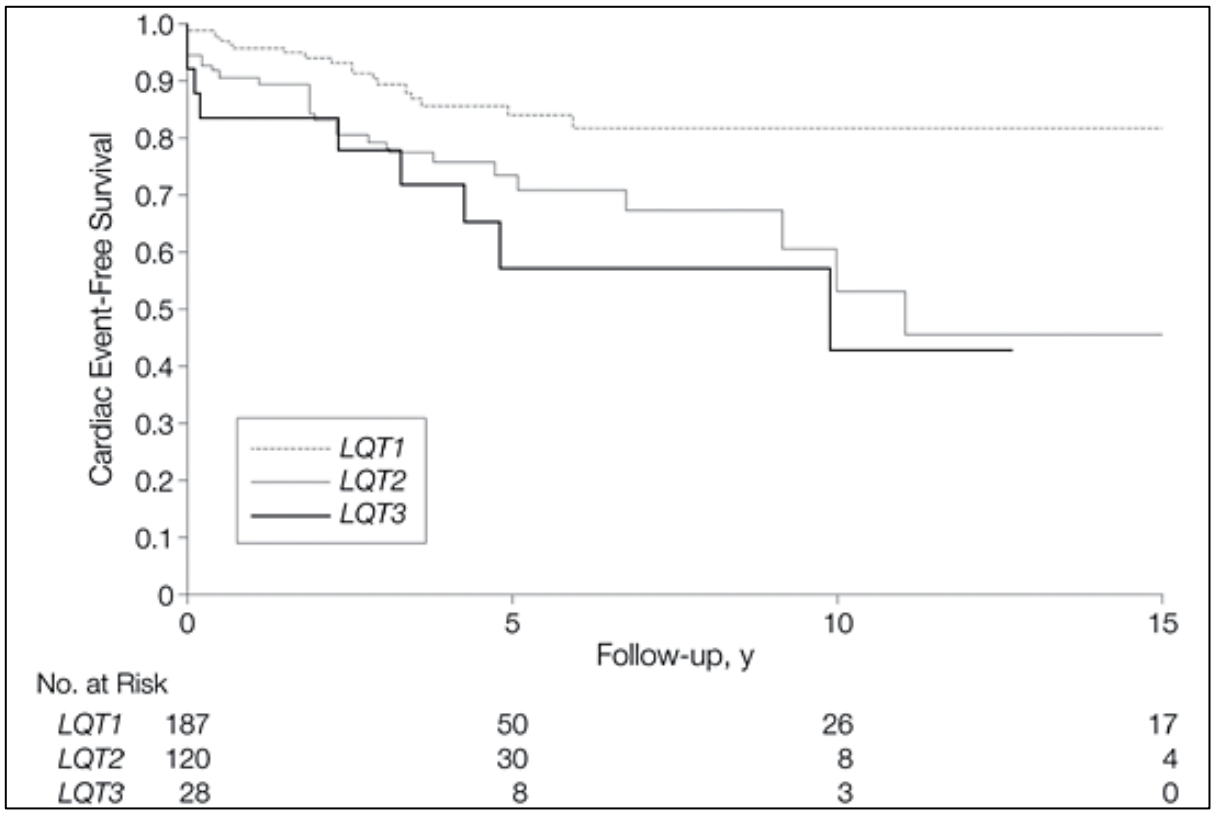

Figure 1.10. Kaplan-Meier analysis of cumulative cardiac event-free survival in LQTS Patients treated with βB.

Figure reproduced from Priori et al[41].

This finding was confirmed in our later study, conducted on 1710 patients, demonstrating in a multivariable analysis that in addition to gender, symptoms, the duration of QTc interval, and the type of βB, genotype was an independent predictor of outcomes of patients with LQTS treated with βB[34]. As shown in Figure 1.11, the cumulative probability of experiencing a first life-threatening arrhythmic event on βB therapy in patients with LQT2 was 4.9% (95% CI: 1.5%-8.1%) and in patients with LQT3 was 5.8% (95% CI: 1.4%-10.0%) at 5 years follow-up (unpublished data from Prof. Priori's laboratory).

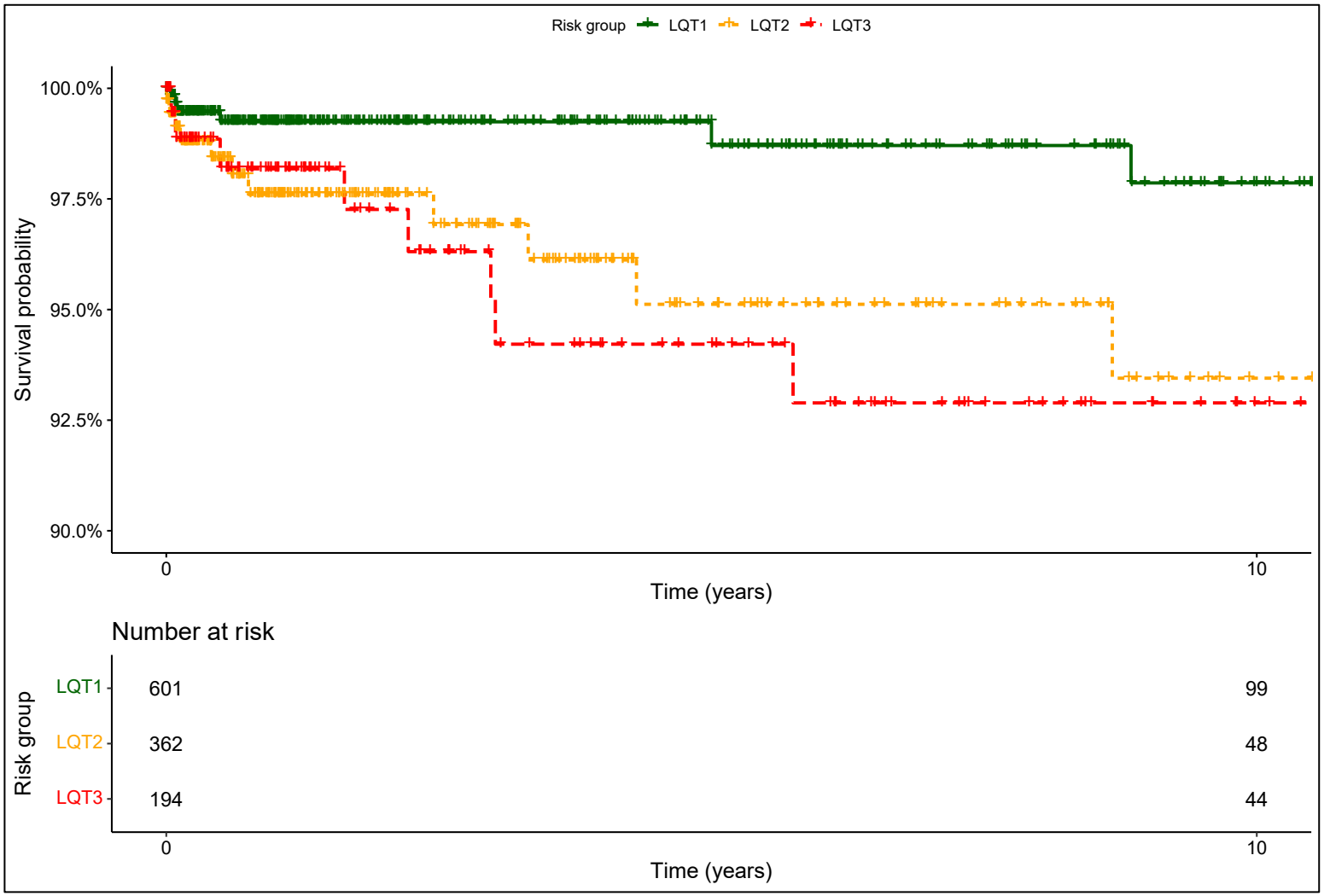

Figure 1.11. Kaplan-Meyer estimate of cumulative survival free from the first LAE in βB therapy in LQTS

Unpublished figure based the data published in Mazzanti et al[34].

On the other hand, LQT8 is considered the most lethal form of LQTS. In the original description of the disease back in 2004, Splawski and colleagues reported a mortality rate of 59%, with an average age of 2.5 years at the time of death[27].

These findings were later corroborated by the work of Dufendach and colleagues, who assessed the survival of the largest cohort of patients (N=17) over a median follow-up of 5 years. The authors report cardiac arrest rates of 65% (11/17 patients) and mortality rate of 24% (4/17 patients)[44].

Considering the aforementioned, it is evident that patients with LQT2, LQT3 and LQT8 are incompletely protected by βB, the gold standard of therapy for patients with LQTS[1].

1.8 Novel Therapeutic Approaches

Considering the incomplete arrhythmic protection conferred by βB therapy in patients with LQT2, LQT3 and LQT8, different novel therapeutic approaches have been investigated. Here, I will offer a brief overview of the therapies at the most advanced stage, starting from the use of mexiletine, which is currently considered the clinical gold standard from patients with LQT3, to other novel, experimental therapies, which are currently not approved for human use.

1.8.1 From Trigger-Based to Substrate-Based Therapy

The first substrate-specific therapeutic approach was envisioned by our group for genotype-specific treatment of LQT3. In 1996, our group demonstrated that the use of the antiarrhythmic drug mexiletine, a sodium channel blocker, can counteract the gain-of-function mutations in the *SCN5A* gene which cause LQT3[42]. More recently, we showed that mexiletine not only shortens and often normalizes the QTc interval, but also provides a clinically relevant reduction of the number of patients with arrhythmic events, the number of events per patient, and the annual event rate at follow-up[43] (Figure 1.12).

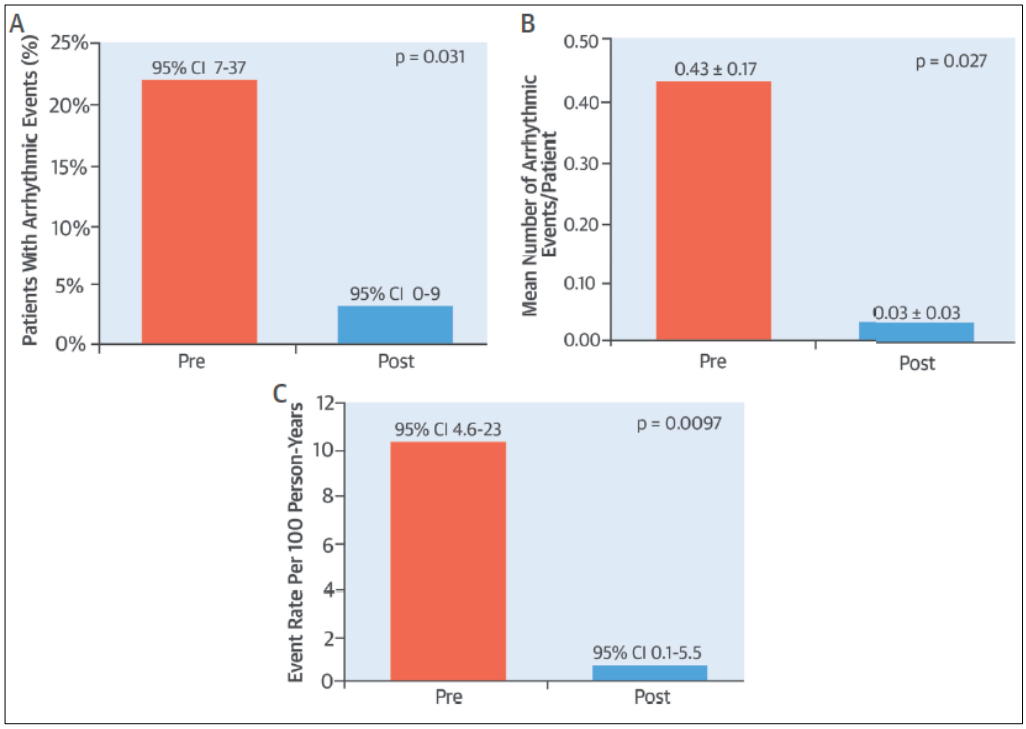

Figure 1.12. Effect of Mexiletine in Patients with LQT3.

Figure from Mazzanti et al[43].

Other sodium channel blockers, such as flecainide and ranolazine, have been shown to be effective in LQT3[45–48]. Nevertheless, it should be remembered that overlapping forms between LQT3 and BrS exist, and that administration of flecainide can unmask ST elevation in some patients with LQT3[49].

In the most recent 2022 ESC Guidelines, this approach has been fully endorsed and today, the use of mexiletine is indicated in all patients with LQT3 (class I indication)[1].

Following the promising results obtained in LQT3, mexiletine has been proposed also for the treatment of LQT2 and it has been shown to be partially effective in shortening the QTc interval duration in two-thirds of a small subset of patients (n=12) with LQT2[50].

Our unpublished data from 20 patients with LQT2 (55% males, age 23±15 years) who received an oral loading dose of mexiletine at a mean dosage of 9±2 mg/kg/day, show that in some patients clinically relevant responses are observed, but in others the drug fails to shorten QT interval (Figure 1.13). Before mexiletine, the mean QTc interval was 527±53 ms (range 462 ms to 650 ms) and 10/20 (50%) patients had high-risk QTc values (i.e., QTc >500 ms). After mexiletine, 18/20 (90%) patients showed a mean shortening of the QTc interval by 42±28 ms, with a high-interindividual variability (range of shortening from 86 ms to 8 ms), while 2/20 (10%) patients did not show any reduction of the QTc after receiving mexiletine. Overall, the effect of mexiletine in LQT2 patients was inferior to the one observed in a previously reported cohort of 34 patients with LQT3, who had equal baseline QTc values and received a similar dosage of mexiletine but showed a significantly higher reduction of the average QTc interval (63±37 ms in LQT3 vs. 42±28 ms in LQT2, p=0.02).

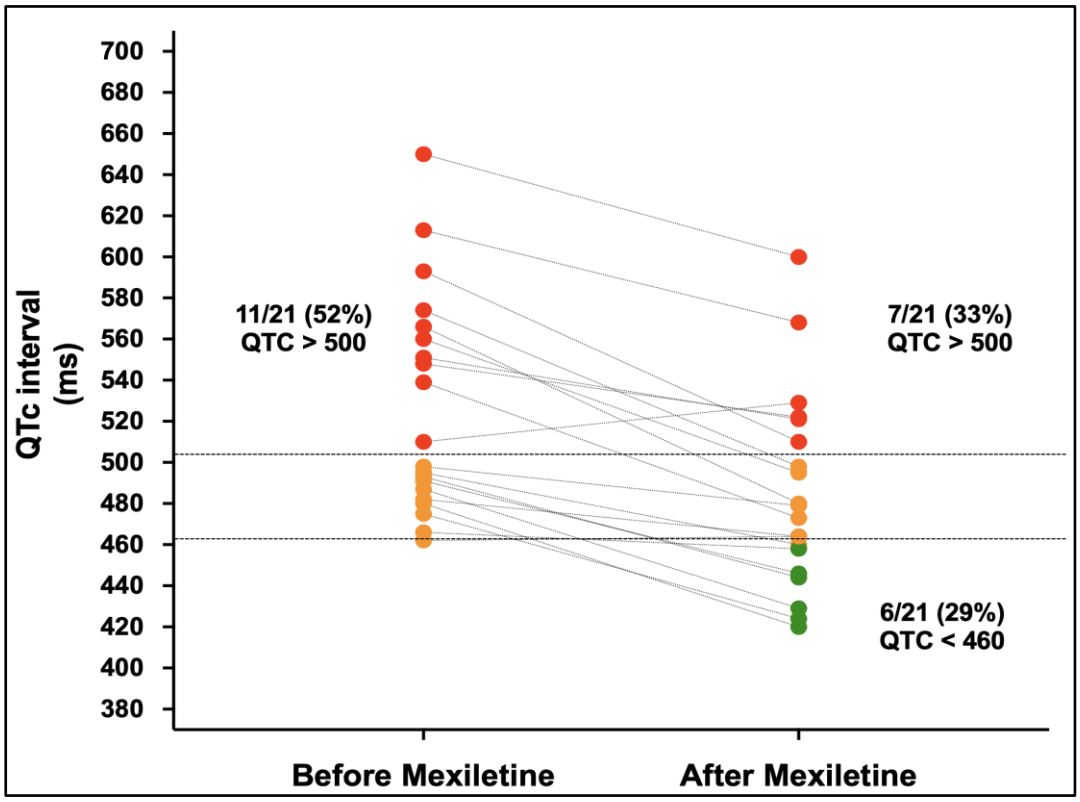

Figure 1.13. Comparison of QTc interval values in LQT2 patients before and after mexiletine loading dose.

Unpublished data from Prof. Priori's laboratory.

Considering the lethality of LQT8 and the insufficient antiarrhythmic protection conferred by βB, substrate-specific approach was also tested in LQT8. Specifically, this approach was clinically tested using mexiletine[51], ranolazine (selective late INa inhibitor)[52] and verapamil[53] (class IV antiarrhythmic), but only a modest QTc shortening was reported and no conclusions could be drawn about their antiarrhythmic efficacy.

1.8.2 Novel Pharmacological Agents for Shortening of Ventricular Repolarization

In addition to the mexiletine, other pharmacological and biological substrate-specific therapeutic approaches for LQTS have been proposed.

A novel substrate-specific therapeutic approach for LQT2 stems from the notion that over 50% of causative variants of LQT2 cause a trafficking defect. A therapeutic strategy based on the use of ***lumacaftor***, a chaperone during protein folding which has been shown to increase the number of CFTR protein trafficked to the cell surface in cystic fibrosis, has been proposed[54,55].

In vitro studies in human induced pluripotent stem cell-derived cardiomyocytes (iPSC-CMs) from patients carrying mutations inducing trafficking defects (IVS9-28A/G, p. R366X, p.S428X, p.A561V) showed that lumacaftor, a drug approved for treatment of cystic fibrosis, increased channel trafficking[54]. Subsequently, *in vivo* studies in patients carrying two of the aforementioned mutations demonstrated QT interval shortening[55]. However, a recent work observed a paradoxical effect of action potential elongation upon lumacaftor administration in one trafficking-defective mutation (p.G604S), underlining how, without completely comprehending the functionality of the mutant channel to be rescued, this therapy could be harmful[56].

Other *in vitro* studies have demonstrated that ***roscovitine***, a small molecule that inhibits cyclin-dependent kinases, is able to augment the voltage-dependent inactivation of $Ca_v1.2$ and restores the electrical and Ca^{2+} signaling properties of cardiomyocytes from patients with LQT8[57].

Most recently, Yazawa laboratory showed that a Food and Drug Administration (FDA)-approved cough suppressant ***dextromethorphan***, an agonist of sigma non-opioid intracellular receptor 1, can shorten the prolonged action potential in cardiomyocytes from patients with LQT8 and human cellular models of LQTS1 and LQTS2[58]. Following this proof-of-concept, dextromethorphan has also been successfully tested in a murine model of LQT8, confirming its ability to normalize the QT interval[58].

However, neither of these compounds have been tested in large animal models nor in humans.

Following the discovery of autoantibodies targeting the *KCNQ1* channel which have been shown to reduce the QT interval, biological therapy for LQT2 has been proposed.
Recent work by Maguy and colleagues demonstrated that ***KCNQ1 antibodies***, acting as IKs agonists, were able to restore alterations in cardiac repolarization and to suppress arrhythmias in iPSC-CMs from LQT2 patients[59], but *in vivo* results are lacking.

1.8.3 HERG1 Channel Agonists

Following the proof of concept that acting on a repolarizing current represents a viable therapeutic strategy to abbreviate repolarization (i.e., mexiletine in LQT3, and to a lesser degree in LQT2), we hypothesize that human ether-à-go-go" (HERG1) channel, a potassium-selective channel conducting the rapid component of the delayed rectifier potassium current (I_{kr}), which plays a fundamental role in the ventricular repolarization[6], may be a promising pharmacological target to further test this concept.

1.8.3.1 Physiology of HERG1 Potassium Channel

HERG1 channel (Figure 1.14) is a potassium-selective channel, expressed in different tissues, including neural, smooth muscle, tumor cells and myocardium[10].

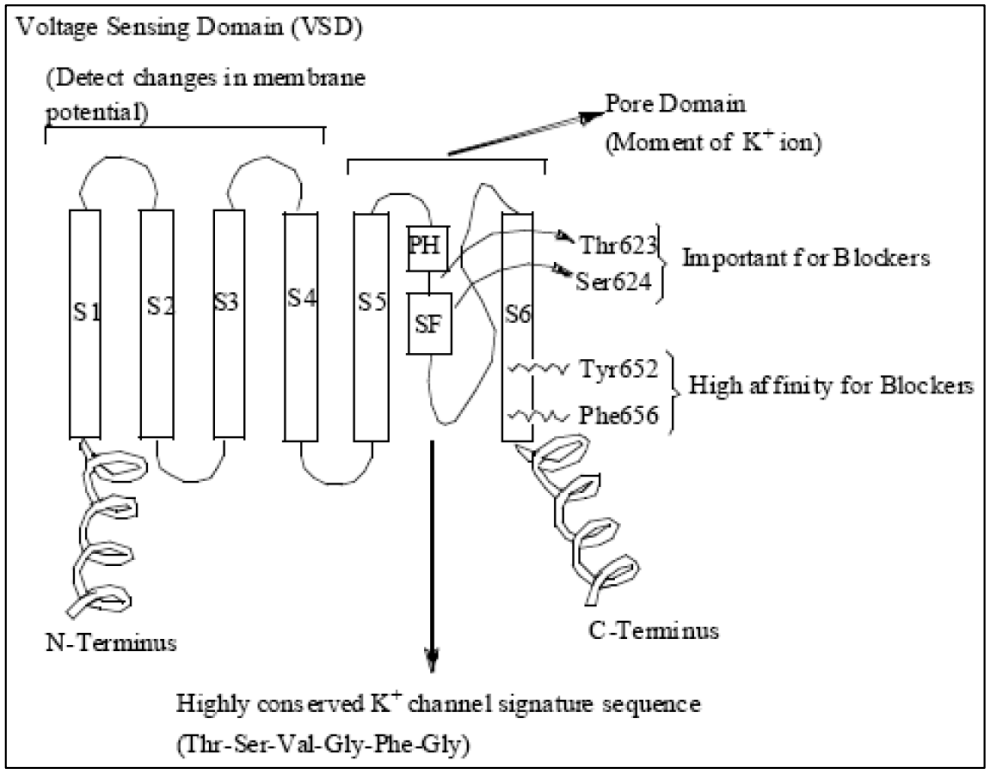

Figure 1.14. Structure of HERG1 channel.

HERG1 channel is a transmembrane protein (like other Kv channels) made of four α-subunits, each one consisting of six transmembrane spanning -helical segments (S1–S6). The S1-S4 helices form a voltage sensor domain (VSD). The S5 helix, together with the pore helix (PH) and selectivity filter (SF) to which it is linked, and the S6 helix form the pore domain.

Adapted from Moorthy et al[60].

In cardiomyocytes, it conducts the rapid component of the delayed rectifier potassium current (I_{Kr}) and plays a fundamental role in the ventricular repolarization. The most important contributor to the Phase 3 of the ventricular action potential (i.e., slow repolarization phase) is in fact I_{Kr} conducted by HERG1 channels.

Seminal work by Wang and MacKinnon permitted to resolve the cryo-EM structure of HERG1 in 2017[61] and by doing so resolved a long-standing mystery: why a large number of chemically unrelated drugs inhibit HERG1. Although mutagenesis studies had already identified the amino acids that form the high-affinity drug-binding site[62,63], the cryo-EM structure offers an explanation for their importance (Figure 1.15).

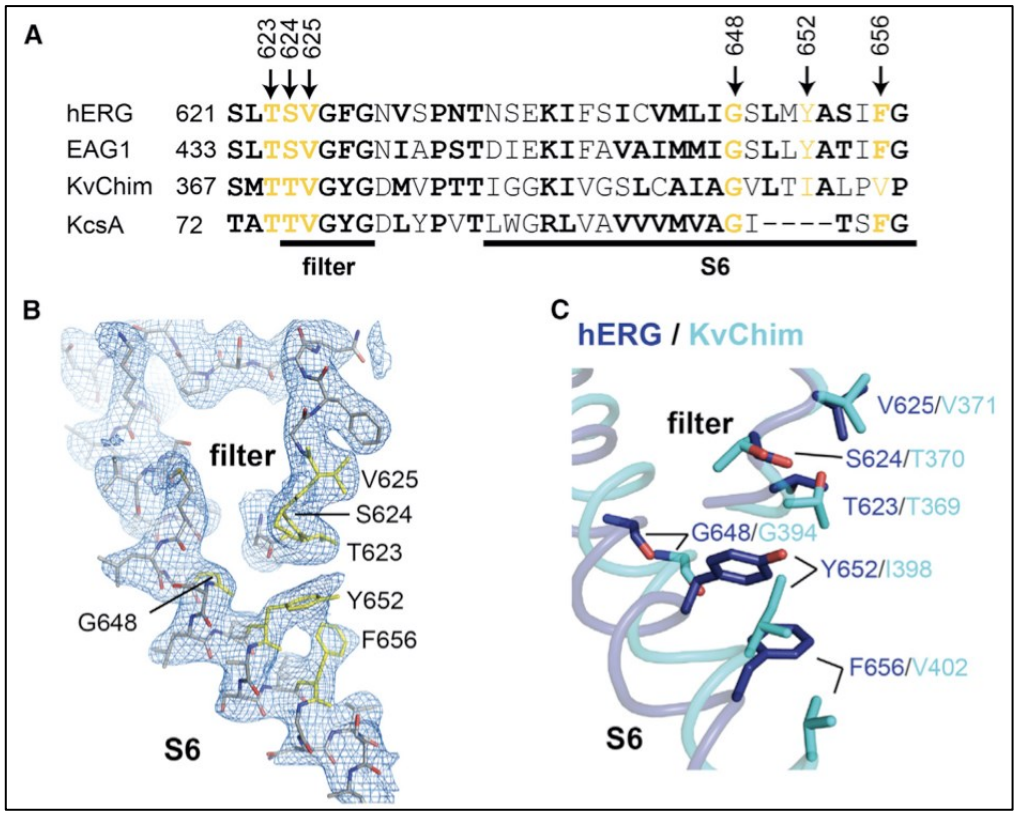

Figure 1.15. Putative Drug-Binding Site on a cryo-EM Model of hERG.

Panel A: Sequence of selected potassium channels, with conserved residues in bold. In yellow, residues related to drug binding; arrows indicate the amino acid residue number in HERG1.

Panel B: EM density map of the putative drug-binding site, shown as a blue mesh and molecular model shown as stick. In yellow, residues related to drug binding.

Panel C: Overlay of HERG1 and Kv1.2-2.1 paddle chimera (KvChim) near the central cavity, with drug-binding residues shown as sticks.

Modified from Wang and MacKinnon[61].

Specifically, it is now known that the amino acids involved span from Tyr-652 to Phe-656[62], and are located in a hydrophobic pocket in the pore [61]. It is thought that the small dimensions of the central cavity (cylindrically shaped, 8Å in diameter and 11Å in length) contributes to HERG1's unique susceptibility to a wide range of drugs. This can be explained by the fact that a smaller volume of high dielectric medium (e.g. water) surrounded by a relatively lower dielectric medium (e.g. protein) will exhibit a more negative electrostatic potential[61]. Specifically, the calculated potential at the center of the larger cavity of KvChim is approximately -125 mV, while in HERG1 is is -625 mV. As many HERG1-blocking drugs are positively charged, the drug affinity for the drug-binding site is increased.

1.8.3.2 Pharmacology of HERG1 Channel Agonists

In 2005, a compound known as RPR260243 was discovered to act as an HERG1 channel agonist[64]. Following this seminal discovery, a number of other HERG1 channel agonists have been discovered, all of which shorten the ventricular action potential and the QTc interval[65].

HERG1 channel agonists are a heterogenous group of compounds which augment the HERG1-conducted I_{Kr} current via four different mechanisms[65]:

1. slowed rate of channel deactivation,
2. attenuation of C-type inactivation,
3. shift of channel opening to more negative potentials,
4. increase in channel open probability.

Interestingly, most compounds of HERG1 channel agonist class exert their effect through multiple mechanisms[65], as shown in Figure 1.16.

Compound	Effect on hERG1 channel				EC_{50} (cell type)
	Slows rate of deactivation	Positive shift in V-dependence of inactivation	Negative shift in V-dependence of activation	Increases open probability (P_o)	
RPR260243	+++	+			n.d. (~3 μM) (CHO) [4]
Ginsenoside Rg3	+++		+		0.4 μM (X. o.) [17]
ICA-105574	+	+++	+		0.5 μM (HEK) [47]
Mallotoxin	+		++	+	0.4 μM (CHO) [22]
KB130015	+		++		12 μM (HEK) [23]
PD-118057		+		++	n.d. (~10 μM) (HEK) [24]
PD-307243		+		+	n.d. (~2 μM) (CHO) [27]
NS1643		+/−	++		10.4 μM (X. o.) [30]
NS3623		+		+	79 μM (X. o.) [48]
A-935142	+	+	+		n.d. (>20 μM) (HEK) [26]

n.d., not determined; CHO, Chinese hamster ovary cells; X. o., *Xenopus* oocytes; HEK, HEK293 cells.

Figure 1.16. Mechanisms of Action of HERG1 Channel Agonists.

Figure from Sanguinetti M, 2014[65].

1.8.3.3 ICA-105574

3-nitro-N-(4-phenoxyphenyl) benzamide (ICA-105574) is a novel[66] and most potent HERG1 channel agonist[65]. It has a complex pharmacology, but currently it is thought that most of its effect on increasing the I_{Kr} current (Figure 1.17) derives from important positive shift in voltage-dependent of the C-type inactivation (estimated to be +182 mV at 2 μM)[65].

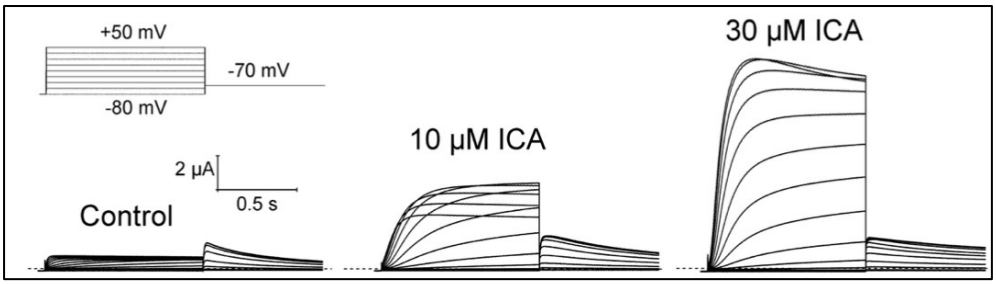

Figure 1.17. Voltage-dependent Activation of I_{Kr} current by ICA-105574.

Figure from Garg et al[67].

This concept is corroborated by elegant experiments demonstrating lesser effect of ICA-105574 on mutant channels, known to present impaired inactivation[67] (Figure 1.18). Additionally, it is believed that ICA-105574 slows the rate of deactivation and causes a negative shift in voltage-dependent of activation[65].

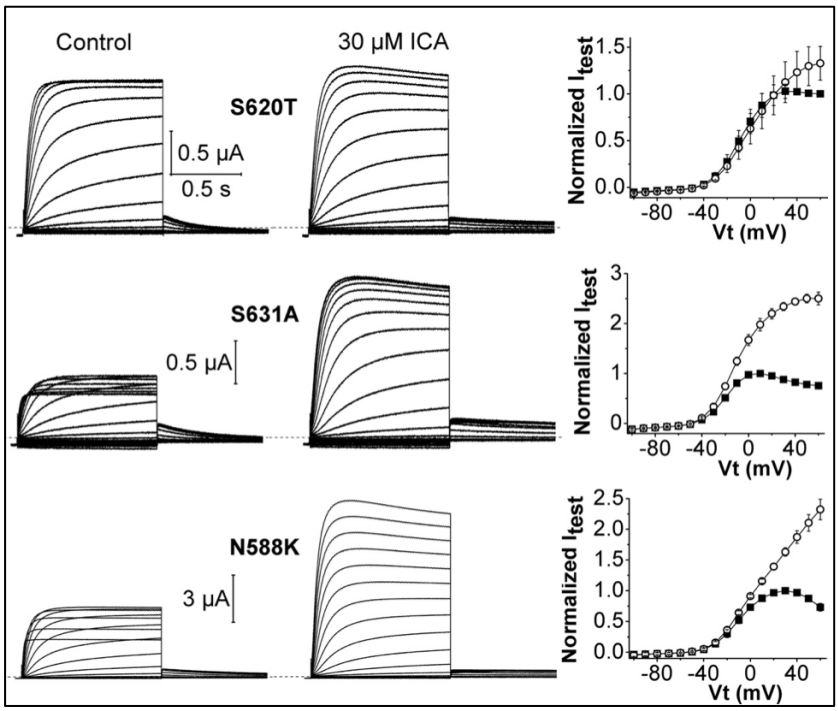

Figure 1.18. Effect of ICA-105574 on Mutant Channels with Known Defect of Inactivation.

Figure from Garg et al[67].

Currently, it is thought that ICA-105574 exerts its effect by docking into the HERG1 channel and binding to the residue F557[67]. More recent works from the authors who demonstrated ICA-105574's binding site show that this binding increases the stability of the ion selectivity filter, which results in the attenuation of the voltage-dependent C-type inactivation[68].

Importantly for the purposes of this study, in addition to the carefully studied mechanism of action and known binding site, ICA-105574 has already been tested in different models of LQTS.

First, ICA-105574 had been tested in a guinea pig model in 2013. In this work the Authors demonstrated that ICA-105574 shortened significantly the action potential duration (APD) in ventricular cardiomyocytes in a concentration-dependent manner[69] (Figure 1.19).

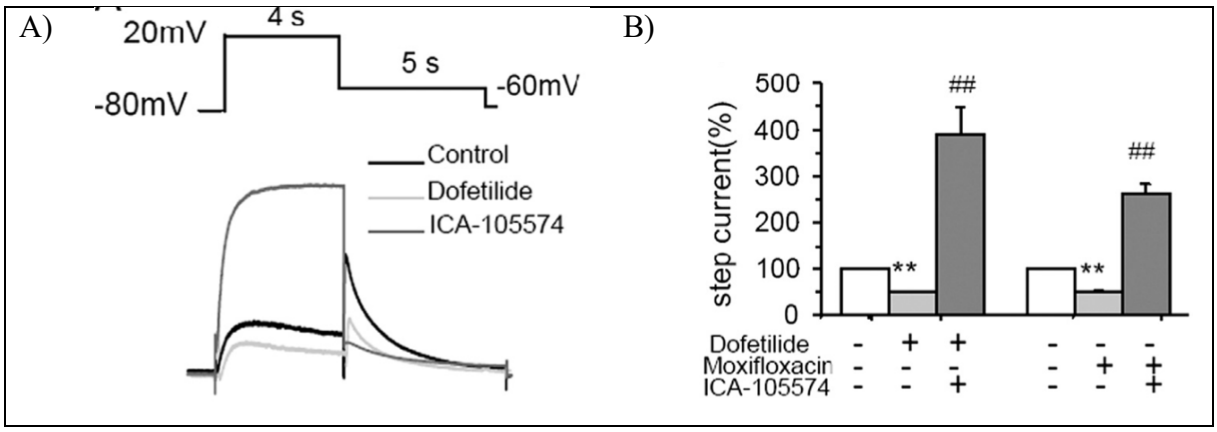

Figure 1.19. Effects of ICA-105574 on Guinea Pig Cardiomyocyte Action Potential Duration. Figure adapted from Meng et al[69].

Following the demonstration of ICA-105574's ability to shorten the APD, effects of the drug were assessed in Langendorff-perfused guinea-pig hearts. As shown in Figure 1.20, ICA-105574 shortened the QTc interval significantly[69].

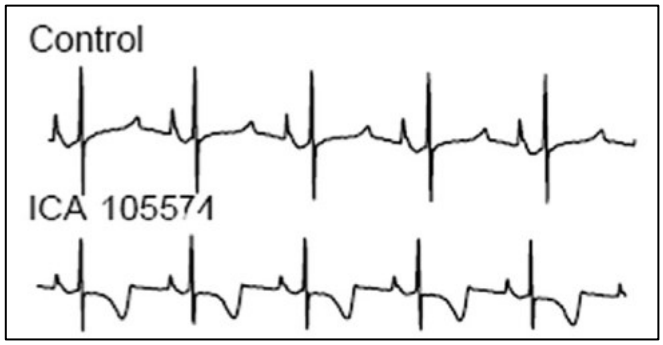

Figure 1.20. Effect of ICA-105574 on QTc in Langendorff-perfused Guinea Pig Hearts

Figure adapted from Meng et al[69].

Relevantly, the authors showed that excessive shortening of QT interval may be obtained with extremely high doses of ICA-105574 (i.e., 10 μM) and that this leads to spontaneous occurrence of ventricular fibrillation in 33% of cases (2/6 hearts; Figure 1.21).

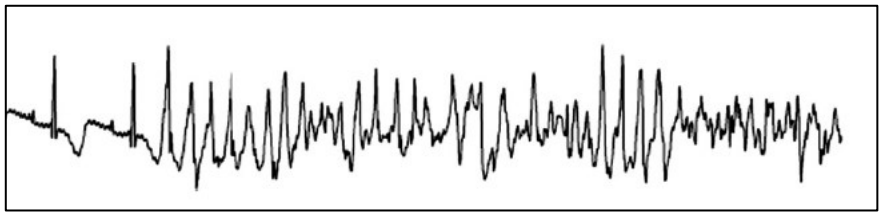

Figure 1.21. Representative Trace of Ventricular Fibrillation Occurring After Treatment with 10 μM ICA-105574

Figure adapted from Meng et al[69].

In the same year, Asayama and colleagues published a study investigating the effects of ICA-105574 on electrophysiological properties of canine hearts. Prolonged ECG recording in anesthetized dogs showed that intravenous administration ICA-105574 at a dose of 10 mg/kg significantly shortened the QTc interval[70] (Figure 1.22). Relevantly, the Authors demonstrated that the maximal drug effect corresponded to a free plasma concentration of 1.7 μM, significantly less than the 10 μM, which has been shown to be arrhythmogenic by Meng and colleagues[69].

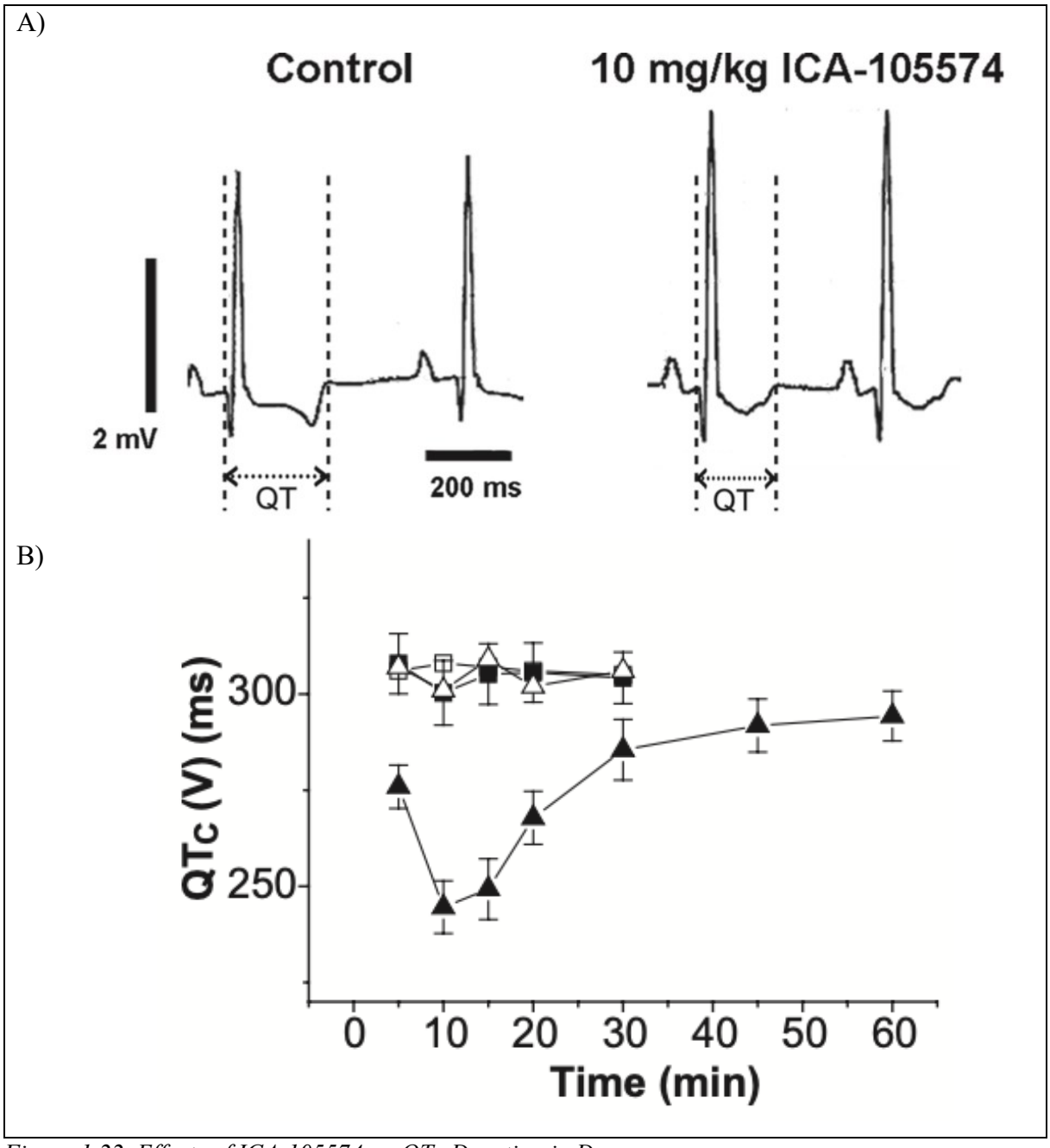

Figure 1.22. Effects of ICA-105574 on QTc Duration in Dogs.

Figure from Asayama et al[70].

More recently, in a human-induced pluripotent stem cell-derived cardiomyocyte (hiPSC-CM) model of LQT2 (expression defective *KCNH2*$^{p.A422T/WT}$) ICA-105574 reversed pharmacologically-induced prolonged repolarization in a concentration-dependent manner at a dose of 10 µM[71] (Figure 1.23).

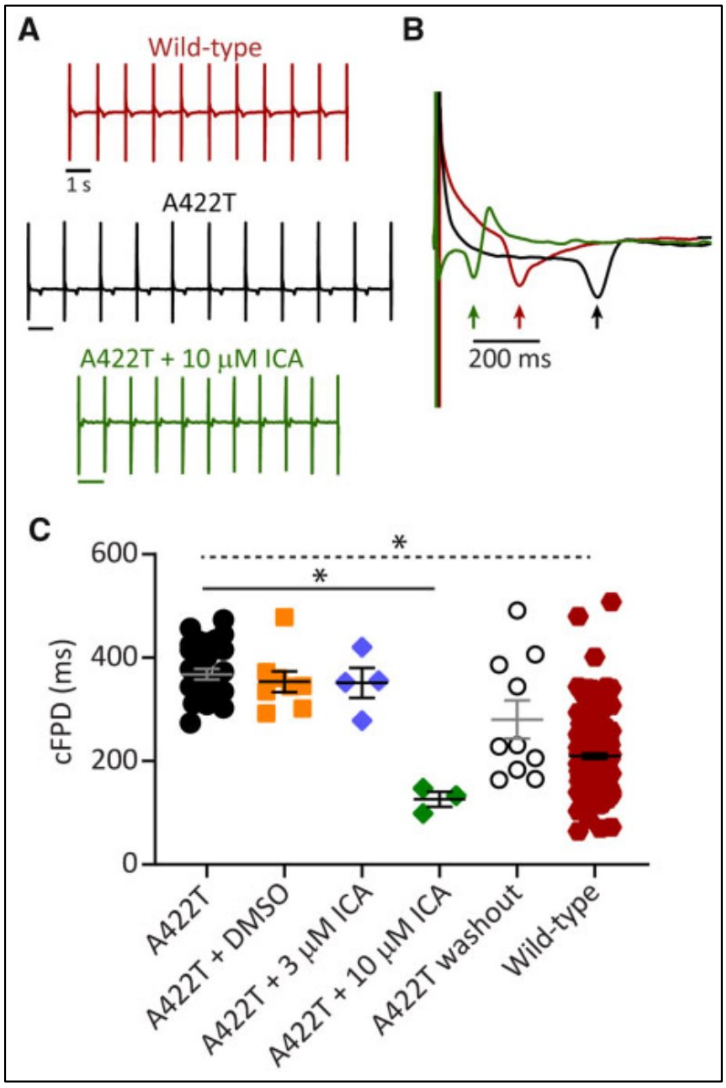

Figure 1.23. Effect of ICA-105574 in hIPSC-CM carrying p.A422T on KCNH2.

Panel A: Train of 10 consecutive field potentials recorded from monolayers of WT hIPSC-CM (red), mutated hIPSC-CM (black), and mutated hIPSC-CM treated with ICA-105574

Panel B: Averaged field potentials.

Panel C: Heart rate-corrected field duration potentials.

Figure and caption adapted from Perry M et al[71].

The work of Perry and colleagues is particularly valuable as it focused on the mechanisms underlying the repolarization overcorrection, which represents the largest issue with this novel class of antiarrhythmics.

Both *in vitro* and *in silico* data provided by Perry and colleagues that the overcorrection of repolarization induced by HERG1 channel agonist ICA-105574 occurs as a result of a temporal redistribution of the peak IKr to much earlier in the plateau phase of the action potential, which results in early repolarization (Figure 1.24).

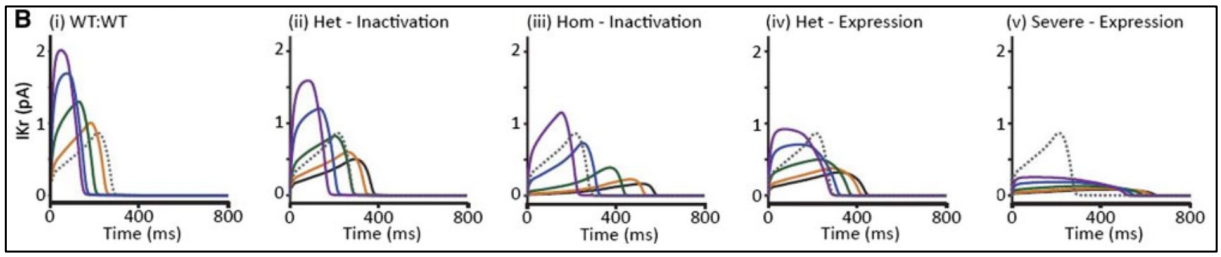

Figure 1.24. In silico Analysis of the Effects of ICA-105574 on IKr Temporal Redistribution.

IKr current averaged over 10 simulated beats in fully wild-type conformation (WT:WT) (i); in the presence of heterozygous (ii) or homozygous (iii) inactivation enhanced mutations [modelled as a -70 mV shift in the voltage dependence of inactivation in 50% (one allele) or 100% (both alleles) of channels, respectively]; or in the presence of a heterozygous expression defective mutation with moderate (iv, modelled as 100% reduction in one allele and 20% reduction in second allele) or severe (v, modelled as 100% reduction in one allele and 80% reduction in second allele) dominant-negative effects.

Progressively higher concentrations of ICA-105574 were modelled as shifts in the voltage dependence of inactivation of +10 mV (orange line), +30 mV (blue line), +60 mV (green line), and +90 mV (purple line).

Figure and caption adapted from Perry M et al[71].

1.9 Summary

Long QT Syndrome (LQTS) is a common inherited arrhythmogenic condition, characterized by prolongation of ventricular repolarization, which predisposes young and otherwise healthy individuals to sudden cardiac death[1].

The clinical management of LQTS was designed in the 1970s, in absence of insights explaining the prolongation of the QTc interval. Starting from the observation that patients affected by LQTS develop life-threatening arrhythmias during stress and/or strong emotion, treatment with beta-blockers was suggested. Despite the quantum leaps in our understanding of the pathophysiology of LQTS, the mainstay of treatment remains the use of beta-blockers[1]. However, the use of beta-blockers, preferentially nadolol[34], has been shown to reduce, but not abolish, the arrhythmic risk[34,40].

In 1996, Prof. Priori demonstrated that the use of the antiarrhythmic drug mexiletine, a sodium channel blocker, can counteract the gain-of-function mutations in the *SCN5A* gene which cause LQT3. *In vitro* studies performed by Prof. Priori showed that Anthopleurin-A, that slows the inactivation of the INa, induced a marked prolongation of the cardiac action potential, which was subsequently reverted upon the administration of mexiletine[42]. Twenty years later, our group demonstrated that mexiletine not only shortens and often normalizes the QTc interval, but also provides a clinically relevant reduction of the number of patients with arrhythmic events, the number of events per patient, and the annual event rate at follow-up[43]. As of today, mexiletine is considered the standard-of-care for patients with LQT3[1].

Our unpublished data on patients with LQT2 show that the use of mexiletine, a sodium channel blocker, has a similarly protective effect also in patients with LQT2, who harbor a mutation on *KCNH2* encoding for human ether-à-go-go" (HERG1) channel, a potassium-selective channel which conducts the rapid component of the delayed rectifier potassium current (I_{kr}). Therefore, we hypothesized that modulation of repolarizing currents aimed at abbreviating the QT interval may represent a potentially viable effective strategy to treat *all forms* of LQTS.

An exciting but uninvestigated therapeutic strategy are represented by HERG1 activators[65], a novel class of antiarrhythmic drugs, which act as activators of the delayed rectifier potassium current (I_{kr}), one of the main contributors to ventricular repolarization[6]. In particular, this thesis investigated the efficacy and safety of action potential duration normalization of ICA-105574, the most potent compound belonging to the class of HERG1 activators in the most severe forms of LQTS.

Experimental Section

2 BACKGROUND OF THE CURRENT WORK

In this document, I will report the results of the work we have been performing, under the leadership of Prof. Silvia G. Priori, within the framework of the European Research Council Grant "EU-Rhythmy" ERC-ADG-2014-ID:669387-2015-2021 (https://eurhythmy.eu/), the Spanish Ministerio de Economía y Competitividad Grant PID2020-113484RB-I00, and the Fondazione Telethon Grant GGP19134.

I shall report the results of the two phases of our efforts to investigate the efficacy and safety of action potential duration normalization using HERG1 channel agonists as a novel therapeutic strategy for the most malignant forms of Long QT Syndrome, using whole animal *in vivo* preclinical models.

Specifically, in the **Phase One**, we have been testing ICA-105574, a compound of a novel HERG1 channel agonist class, in three drug-induced models of Long QT Syndrome to investigate its ability to abbreviate the QT interval safely and efficaciously.

Aware of the fact that guinea pig models permit to study just the surface electrocardiogram and considering the availability of a first of its kind, large mammal knock-in model of Long QT Syndrome type 8, in **the Phase Two**, we investigated, using state-of-the-art electroanatomical mapping, the drug effects on the duration and dispersion of ventricular repolarization.

3 AIMS

The goal of the present study, which has been conducted in the framework of the European Research Council Grant "EU-Rhythmy" ERC-ADG-2014-ID:669387-2015-2021 (https://eurhythmy.eu/), the Spanish Ministerio de Economía y Competitividad Grant PID2020-113484RB-I00, and the Fondazione Telethon Grant GGP19134, is to respond to the urgent unmet need of patients affected by the most malignant forms of Long QT Syndrome (i.e., Long QT Syndrome type 8, Long QT Syndrome type 3, and Long QT Syndrome type 2).

Specifically, the aims of the study are:

- to develop and characterize *in vivo* drug-induced models of three different types of Long QT Syndrome (Long QT Syndrome type 2, Long QT Syndrome type 3, and Long QT Syndrome type 8),
- to characterize the first large mammal *knock-in* model of Long QT Syndrome (Long QT Syndrome type 8),
- to investigate the efficacy and safety of action potential duration normalization as a novel therapeutic strategy for Long QT Syndrome.

4 MATERIALS AND METHODS

4.1 Definitions

In the study, the following clinical definitions were included:

- Aborted cardiac arrest (ACA): an unexpected cardiocirculatory arrest, occurring within 1 hour of onset of acute symptoms, which is reversed by successful resuscitation maneuvers (e.g., defibrillation)[3];
- Idiopathic ventricular fibrillation (IVF): clinical investigations are negative in a patient surviving an episode of ventricular fibrillation;
- Life-threatening arrhythmic event (LAE): a composite end-point with either (*1*) cardiac arrest resuscitated by reanimation maneuvers (defibrillation by an external defibrillator or an implantable one); (*2*) documented arrhythmic syncope defined as sudden loss of consciousness with loss of postural tone, followed by spontaneous regain of consciousness due to a documented sustained ventricular arrhythmia, in absence of other justifying causes (i.e., orthostatic syncope or vasovagal stimulation), or (*3*) sudden cardiac death (SCD)[34,73–75];
- Non-sustained ventricular tachycardia (NSVT): three or more consecutive ventricular beats at a rate of >120 beats per minute (bpm), lasting for <30 s[76];
- Sinus rhythm: a rhythm that originates from the sinus node, such that (*1*) the impulse depolarizing the atria originates from the sinus node, (*2*) atrial frequency is comprised between 60 and 100 beats per minute (bpm), (*3*) P wave morphology is constant in all 12 electrocardiographic derivations, and (*4*) the P-P intervals are relatively constant[77];
- Sudden cardiac death (SCD): non-traumatic, unexpected fatal event occurring within 1 hour of the onset of symptoms in an apparently healthy subject; when a congenital, or acquired, potentially fatal cardiac condition was known to be present during life; OR autopsy has identified a cardiac or vascular anomaly as the probable cause of the event; OR no obvious extra-cardiac causes have been identified by post-mortem examination and therefore an arrhythmic event is a likely cause of death[3];
- QTc interval: defined mathematically as proposed by Bazett[30]:

$$QTc = \frac{QT}{\sqrt{RR}}$$

Additionally, the following electrophysiological definitions were used:

- Pacing threshold**:** Minimum amount of energy able to capture the local myocardium and elicit a ventricular beat. Measurement is performed by continuously pacing at a faster than spontaneous rate and by decreasing progressively the pacing energy until a pacing stimulus does not capture the myocardium.
- Ventricular effective refractory period (ERP): The shortest coupling interval from the preceding beat at which a stimulus can capture the myocardium.
- Local recovery time (LRT): Measure of the moment at which the local action potential returns to the baseline after completion of depolarization. This is defined as the maximal positive dV/dt of the unipolar electrogram recorded locally at the time of the surface ECG T wave (Figure 4.1).
- Total recovery time (TRT): the time range that corresponds to the latest LRT of the region of interest.

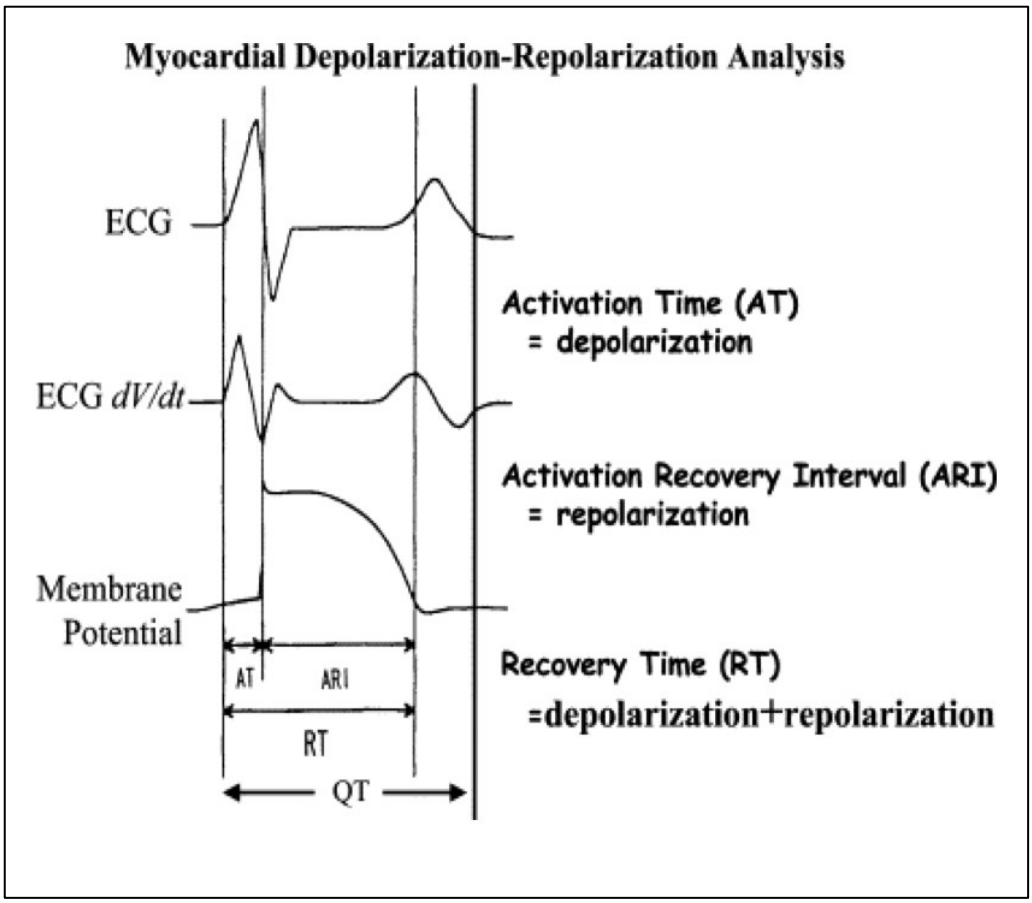

Figure 4.1. Electrophysiological intervals and their correspondence to electrocardiographic parameters and cellular action potential.

4.2 Study Approval

Guinea Pig Model

All animal protocols were approved by the University of Pavia Committee for animal welfare and by the Italian Ministry of Health and conform to the European Union Directive 2010/63/EU.

Swine Model

All animal protocols were approved by CNIC's internal ethical committee, the *Universidad Autónoma de Madrid* and the *Comunidad de Madrid* (PROEX 041/17) and conform to the European Union Directive 2010/63/EU.

4.3 Experimental Drug Synthesis

3-nitro-N-(4-phenoxyphenyl) benzamide (ICA-105574) (Figure 4.2) was synthesized by Prof. Lentini from Department of Pharmacy at the University of Bari following a recently reported procedure of Zangerl-Plessl and colleagues[68] with only one modification - the use of HTBU (CAS number: 94790-37-1) in lieu of HATU (CAS number: 148893-10-1) as a coupling reagent.

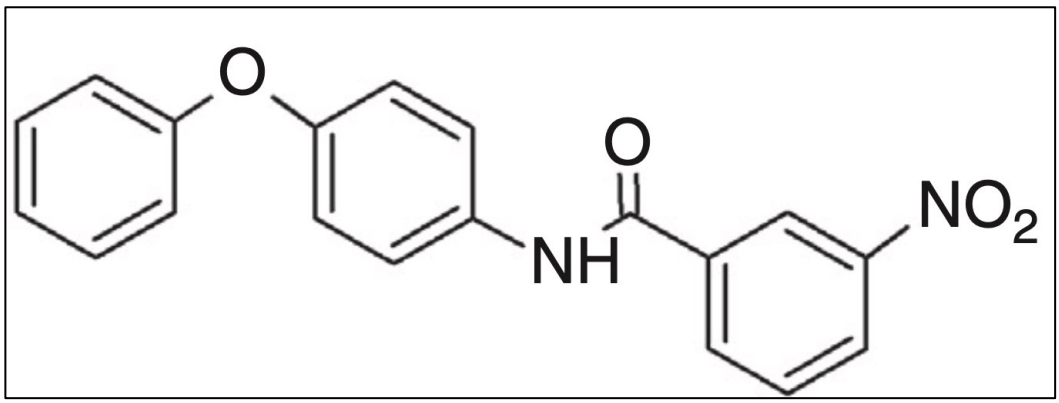

Figure 4.2. Chemical Structure of ICA-105574, a Novel HERG Channel Agonist

For the *in vivo* experiments, ICA-105574 was dissolved with 30% *N*, *N*-dimethylacetamide, 50% polyethylene glycol 400, and 20% water for injection up to 8 mg/mL.

4.4 Development of Drug-Induced Models of Long QT Syndrome

This part of our study is conducted at the IRCCS Istituti Clinici Scientifici Maugeri, located in Pavia, Italy (Figure 4.3), in collaboration with Marco Denegri, PhD; Elisa Tavazzani, PhD; Andrea Mazzanti, MD, PhD; and Alessandro Trancuccio, MD, PhD candidate; and under the supervision of Prof. Silvia G. Priori, MD, PhD.

Figure 4.3. IRCCS ICS Maugeri Pavia

In line with the recommendations for the European Medicines Agency guidelines[78] for the assessment of the delay of ventricular repolarization by pharmaceuticals, we have used guinea pigs (*Cavia porcellus*) as the animal species of choice for the development of our drug-induced models of LQTS. Hartley guinea pigs were acquired from the supplier (Charles River), weighing 180–400 g, and were kept in specific cages (Tecniplast) at our laboratory for a week after transfer to allow adjustment and acclimation to the indoor animal facility. The animals were housed in a controlled environment, with 12 hours light/dark cycle and room temperature at 25°C, with free access to water and food.

One week after transfer, surgery for telemeter implant was performed, as per previously published protocols[79]. Briefly, animals were placed in a specific isolated chamber for anesthesia

(VisualSonics Vevo Compact Anesthesia System; FUJIFILM VisualSonics, Inc., Toronto, ON, Canada). Anesthesia was induced and maintained with isoflurane inhalation (MAC 2%). Surgical area is depilated and accurately disinfected using Poviderm 10%-Iodopovidone (Farmec). A dorsal incision allowed for the subcutaneous insertion of a DSI PhysioTel Implantable Telemetry system (Data Sciences International, St. Paul, MN, USA) telemeter and the two derivations were implanted in the proximity of the upper limbs. The wound was closed using sterile surgical suture (Ethilon 4.0) and/or metallic clips, and local anesthetic cream was applied (EMLA®: Lidocaine 2.5% + Prilocaine 2.5%). Following the surgical procedure, the animals were repositioned in a cage for monitoring until awakening, which if necessary was stimulated with continuous flow of oxygen. In the first two days post-surgery, rimadyl 5 mg/ml diluted with saline solution was administered subcutaneously for pain control.

One week after the telemeter implant, baseline electrocardiograms were recorded for 30-45 minutes in resting conditions in conscious animals.

Considering that LQT2 is caused by loss-of-function mutations in the *HERG*-encoded $K_V11.1$ potassium channel[6], DL-sotalol, which is a well-known blocker of $K_V11.1$ potassium channel[80], has been used to develop drug-induced models of LQT2[79]. Therefore, we also selected DL-sotalol for our **drug-induced LQT2 model** [79]: the drug was orally administered in the form of tablets (Hexal AG, Holzkirchen, Germany) at the dose of 50 mg/kg in guinea pigs of both sexes, as per previously published protocols[79].

Considering that LQT3 is caused by gain-of-function mutations in the *SCN5A*-encoded $Na_V1.5$ sodium channel, which augment the late I_{Na} current, Anthopleurin-A, an inhibitor of the inactivation of INa current, has been previously used by our group to develop a drug-induced models of LQT3[42]. Therefore, also in this study we obtained the **drug-induced LQT3 model** by administering Anthopleurin-A[81] (Sigma-Aldrich, St. Louis, MO, USA) intraperitoneally at the dose of 20 μg/kg in guinea pigs of both sexes.

Considering that LQT8 is caused by gain-of-function mutations in the *CACNA1C*-encoded $Ca_V1.2$ calcium channel, Bay K8644, an enhancer of $Ca_V1.2$-conducted ICa current, has been used to develop drug-induced models of LQT8[82]. Briefly, Bay K8644 is a 1,4-dihydropyridine derivative used as a high-potency agonist for L-type Ca^{2+} channels ($Ca_v1.2$'s), and is the first inotropic agent shown to act specifically on these channels[83] by binding to transmembrane segments within the alpha subunit[84]. Bay K8644 increases the $Ca_v1.2$'s open probability and shifts its voltage-dependent activation and inactivation to more negative potentials[83,85,86]. The effects of Bay K8644 are complex to dissect, as (1) Bay K8644's effect strongly depends on holding potential, indicating binding to several channel states[85,86]; and (2)

Bay K8644 is commonly provided as a mixture of 2 enantiomers with opposing effects. S(-)-Bay K8644 has the highest affinity for $Ca_v1.2s$, 25 nM at physiological membrane potentials (10 times higher than the R(+) enantiomer[87]) and acts as an agonist, which explains the overall effects of Bay K8644[86]. On the other hand, R(+)-Bay K8644 is an antagonist that promotes channel inactivation more strongly than the S(-) enantiomer[86].

Therefore, we used Bay K8644 intraperitoneally at the dose of 50 µg/kg to mimic LQT8 and obtain a **drug-induced LQT8 model**[82,88] (Sigma-Aldrich, St. Louis, MO, USA) in guinea pigs of both sexes.

4.5 Engineering of a Knock-In Porcine Model of Long QT Syndrome

Our partners at Avantea (Cremona, Italy; www.avantea.it; Principal Investigator: Prof. Cesare Galli) generated a *knock-in* pig exploiting CRISPR/Cas9 system[89]. Briefly, porcine adult fibroblasts (PAFs) were derived from a skin biopsy of a Large White x Landrace hybrid boar with a previous successful record of somatic cell nuclear transfer (SCNT). Recipient sows used as surrogate mothers were also of Large White x Landrace hybrid breed.

The TS1 Knock-in large white pigs were generated following the general SOPs (cell culture, transfections, SCNT, recipient sows' synchronization, surgical Embryo Transfer, and post-implantation development) as per previously published protocols[90,91].

To ensure best quality of life for the animals, the colony of wild type (WT) and Timothy syndrome (TS1) pigs resided in a veterinarian-staffed farm in the countryside. A balanced diet was provided, and healthcare was carefully monitored. Breeding was coordinated by the veterinarians to ensure that the colony was preserved, and an adequate number of pigs was available to conduct the planned experiments. Animals were transported to our laboratory at CNIC 24-72 hours prior to the experiments to allow adjustment and acclimation to the indoor animal facility.

4.6 *In Vivo* Characterization of the Phenotype in Drug-Induced Models of Long QT Syndrome

This part of our study has been conducted at the IRCCS Istituti Clinici Scientifici Maugeri, located in Pavia, Italy, in collaboration with Marco Denegri, PhD; Elisa Tavazzani, PhD; Andrea Mazzanti, MD, PhD; and Alessandro Trancuccio, MD, PhD candidate; and under the supervision of Prof. Silvia G. Priori, MD, PhD.

4.6.1 Preliminary In Vivo Testing of HERG Channel Agonists in Drug-Induced Models

Prior to the induction of drug induced LQTS, baseline electrocardiograms were recorded for 30 minutes in resting conditions in conscious animals. Following the pharmacological induction, an electrocardiogram was recorded for 60 minutes to obtain a stable heart rate that would provide accurate measurement of the QT interval.

After 60 minutes of continuous electrocardiographic monitoring following the induction of drug-induced LQTS, the therapeutic drug (ICA-105574) was administered intravenously at the dosage of 15 mg/kg. The electrocardiogram was subsequently recorded for further 90 minutes.

Pre-set timepoints were determined to assess the effects of the drug, as follows: **baseline**, **30 minutes post-induction**, **60 minutes post-induction**, **ICA-105574 start**, **15 minutes post-ICA-105574**, **30 minutes post-ICA-105574**, and **60 minutes post-ICA-105574**. At each pre-set timepoint, three measurements of the main electrocardiographic parameters (heart rate, PR interval, QRS interval, QT interval) were obtained.

The quality of electrocardiographic recordings was evaluated by two independent operators (E.T. and M.D.) and converted into a PDF file using proprietary Ponemah software (Data Sciences International, St. Paul, MN, USA). At the end of the experiment, the animal was repositioned in a cage and monitored until complete recovery. The animals were periodically monitored for five days after the experiment and subjected to the obligatory veterinary control.

4.7 *In Vivo* Characterization of the Phenotype in a Knock-In Porcine Model of LQTS

This part of our study has been conducted at the Centro Nacional de Investigaciones Cardiovasculares Carlos III (CNIC), located in Madrid, Spain (Figure 4.4), in collaboration with Andreu Porta-Sánchez, MD, PhD; Andrea Mazzanti, MD, PhD; and Alessandro Trancuccio MD, PhD candidate; and under the supervision of Prof. Silvia G. Priori, MD, PhD (Figure 4.5). There, where I have been appointed visiting scientist since the beginning of my PhD project, we have been characterizing our novel knock-in porcine model using 12-lead electrocardiography (ECG), multiparametric cardiac magnetic resonance (CMR), and electrophysiology studies (EPS) using cardiac catheterization and electroanatomical mapping of electrical activity of the heart.

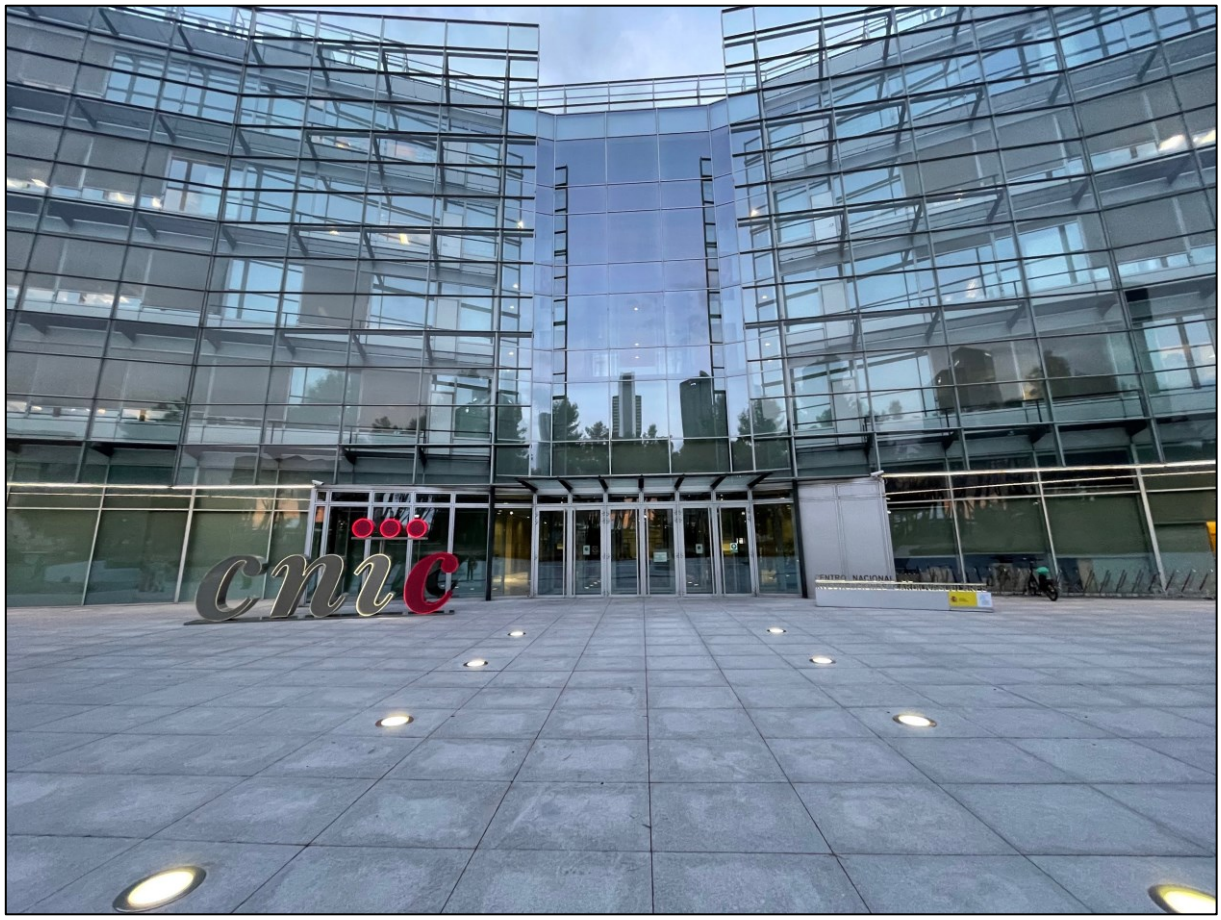

Figure 4.4. Main entrance to Centro Nacional de Investigaciones Cardiovasculares Carlos III in Madrid, Spain.

Figure 4.5. Professor Priori and the Molecular Cardiology Team at CNIC, Madrid

4.7.1 Anesthesia

After a 12-hour fasting period, animals received an intramuscular sedative injection of a 2mg/kg azaperone (Stresnil®) and 5 mg/kg tiletamine/zolazepam hydrochloride (Zoletil®) mix. For lengthy procedures, such as cardiac magnetic resonance (CMR) and electrophysiologic study (EPS), endotracheal intubation was performed, and general anesthesia was maintained with isoflurane inhalation (MAC 1.5%) in a Synchronized Intermittent Mandatory Ventilation mode, fixing 16 and 20 breaths/min with tidal volumes between 6-8 mL/kg. Veterinarians continuously monitored hemodynamic parameters, including body temperature, heart rate, oxygen saturation, and arterial blood pressure throughout the procedures.

4.7.2 Surface 12-lead Electrocardiogram

We recorded the surface electrocardiogram (ECG) at 1 kHz for at least 5 minutes (Mortara Instruments, Milwaukee, WI, USA) (paper speed 25 mm/s and voltage settings 10 mm/mV) in both TS1 and wild type (WT) animals as previously described[92].

The principal ECG parameters, including but not limited to heart rate, PR interval, QRS interval and QT interval were measured using manual calipers at a 100 mm/s sweep speed. The QT interval duration was measured at a stable heart rate between 50 and 100 beats per minute in lead DII or V5[93] and corrected for the heart rate using the Bazett formula[30].

4.7.3 Implantable Loop Recorder

Using the sedation protocol described and under sterile conditions, the left parasternal region was infiltrated with local anesthesia (1% Bupivacaine, Braun), and an incision was performed to insert an implantable loop recorder (Medtronic Reveal LINQ, St Paul, Minneapolis, MN (USA) or St Jude Medical CONFIRM Rx, St Paul, Minneapolis, MN (USA)) in the intramuscular space. The wound was closed with self-absorbable sutures, and monitoring parameters were activated to record significant bradyarrhythmia or tachyarrhythmia. After the insertion, the device was interrogated to ensure that optimal sensing was obtained. During follow-up, the devices were interrogated periodically and whenever sudden unexpected cardiac death occurred.

4.7.4 Cardiac Magnetic Resonance

Cardiac magnetic resonance (CMR) studies were performed as described previously[94], to investigate our animal model for the presence of the structural malformations known to occur in some of the TS1 patients (i.e., patent ductus arteriosus, patent foramen ovale, ventricular septal defects, and Tetralogy of Fallot).

In anticipation of the need to obtain competence in reading and interpreting CMR, during the first year of my PhD programme, Prof. Priori and I envisioned that I would benefit of joining the CMR unit at the Centro Cardiologico Monzino (CCM) in Milan, Italy (Figure 4.6), to train for six months as a research fellow at the Department of Cardiac Imaging, directed by Dr. Gianluca Pontone, an internationally recognized expert in the field. At the end of the fellowship, I had acquired the skills to interpret independently CMR examinations.

Using the sedation protocol described CMR studies were acquired using a 3 Tesla Philips Achieva Tx whole-body scanner (Philips Healthcare, Eindhoven, The Netherlands) equipped with a 32-element phased-array cardiac coil. Segmented cine steady-state free-precession (SSFP) sequence was performed to acquire 11–13 contiguous short axis slices on 30 fully acquired cardiac phases covering the heart from the base to the apex to evaluate the anatomy, the dimensions, volumetry and global and regional left ventricular (LV) and right ventricular (RV) function. Ventricular measurements were indexed to body surface area. Body surface area was calculated using the Kelly formula[95].

Acquired sequences were reconstructed using Circle cvi42 (Circle Cardiovascular Imaging Inc., Calgary, Canada; Figure 4.7). Briefly, systole and diastole were determined manually, in short axis stacks, and endocardial and epicardial borders were traced manually for the study of biventricular volumetry and function.

Figure 4.6. Entrance to Centro Cardiologico Monzino in Milan, Italy.

Tissue characterization has been performed using T1 mapping, T2 mapping and sequences for late gadolinium enhancement (LGE). Modified Look-Locker inversion recovery (MOLLI) sequences at midventricular level have been used for high-resolution T1 mapping, to assess for the presence of diffuse myocardial fibrosis and/or edema, acquired before and 10 min after contrast administration. Pre- and post-contrast T1 MOLLI sequences were analyzed as proposed by Rogers and colleagues[96]. Partition coefficient (λ) and extracellular volume (ECV) were calculated as follows:

$$\lambda = \frac{\frac{1}{T1_{myocardium\ pre-contrast}} - \frac{1}{T1_{myocardium\ post-contrast}}}{\frac{1}{T1_{blood\ pre-contrast}} - \frac{1}{T1_{blood\ post-contrast}}}$$

$$ECV = (1 - Hct) * \lambda$$

where Hct is hematocrit, as proposed by Flett and colleagues[97]. Blood samples were taken the day of CMR study, and complete blood count (CBC) with Hct was obtained.

Indexed intracellular and extracellular mass (IICM and IECM, respectively) were calculated as follows:

$$IICM = Indexed\ LV\ mass * \frac{(100 - ECV)}{100}$$

$$IIEM = Indexed\ LV\ mass * \frac{ECV}{100}$$

Gradient-spin-echo (GraSE) imaging was used for myocardial T2 mapping, to investigate the presence of edema. T2 mapping sequences were analyzed quantitatively, and qualitatively, for presence of local anomalies.

Late gadolinium enhancement (LGE) images using conventional phase sensitive inversion recovery (PSIR) were acquired 10–20 minutes after infusion of a bolus (2 mL/s) of 0.2 mmol/kg of gadobenate dimeglumine (MultiHance, Bracco, Rome, Italy). The optimal inversion time was selected to null the LV myocardial signal by using a Look-Locker sequence before LGE imaging. Presence of LGE was assessed visually in the entire short axis stack and in the corresponding long axes.

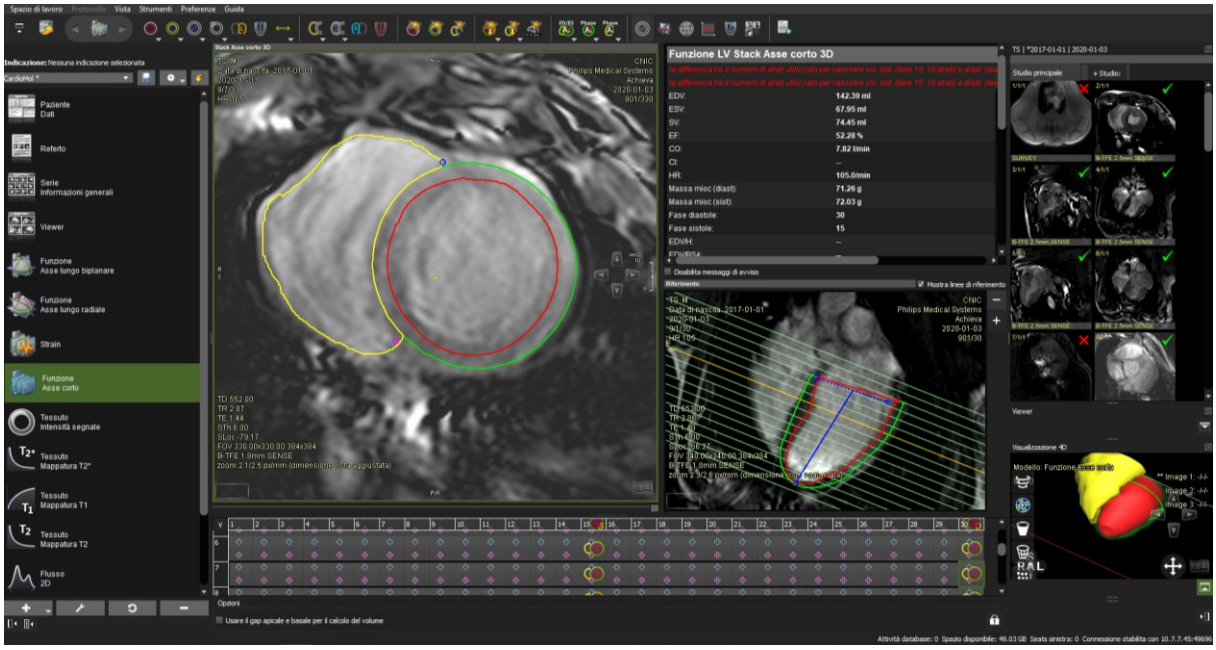

Figure 4.7. Circle cvi42 Interface for the Analysis of CMR

4.7.5 Hematology and Clinical Biochemistry

Blood samples were analyzed in an ADVIA 2120i hematology system (Siemens, Munich, Germany). Serum samples were analyzed in a Dimension RxL Max analyzer (Siemens, Munich, Germany).

4.7.6 Histology

Whole hearts were fixed using formalin solution by the Histology Department of CNIC, Madrid. The specimens were paraffin-embedded, sectioned and stained with hematoxylin and eosin (H&E) and picrosirius red staining. H&E-stained slides were analyzed qualitatively for the morphological characteristics; picrosirius red-stained slides were analyzed qualitatively for collagen fibers I and III of myocardium.

4.7.7 Assessment of Isolated Ventricular Cardiomyocyte

Single cell study was performed by Demetrio J. Santiago, PhD from our laboratory at CNIC, Madrid, Spain, to characterize the morphology of the ventricular cardiomyocytes.

Ventricular myocytes from WT and TS1 piglets (WT n=11, and TS1 n=6; aged 1 month and weighting between 5 and 8 kg) were isolated with the Langendorff method, according to standard methods. Isolated cardiac myocytes from WT and TS1 piglets (n=21 to n=25 cells per animal) were observed at 40X magnification and their dimensions were measured.

In order to determine the intrinsic electrical properties of single cells, membrane capacitance was measured using the voltage-clamp method.

4.7.8 Invasive Electrophysiological Characterization of Knock-In Porcine Model of LQTS

For this part of the study, we used TS1 pigs and WT littermates, of both genders, weighing between 60 and 80 kilograms, between six and eight months of age. In Figure 4.8 the set-up of the electrophysiological laboratory where the studies have been performed is shown.

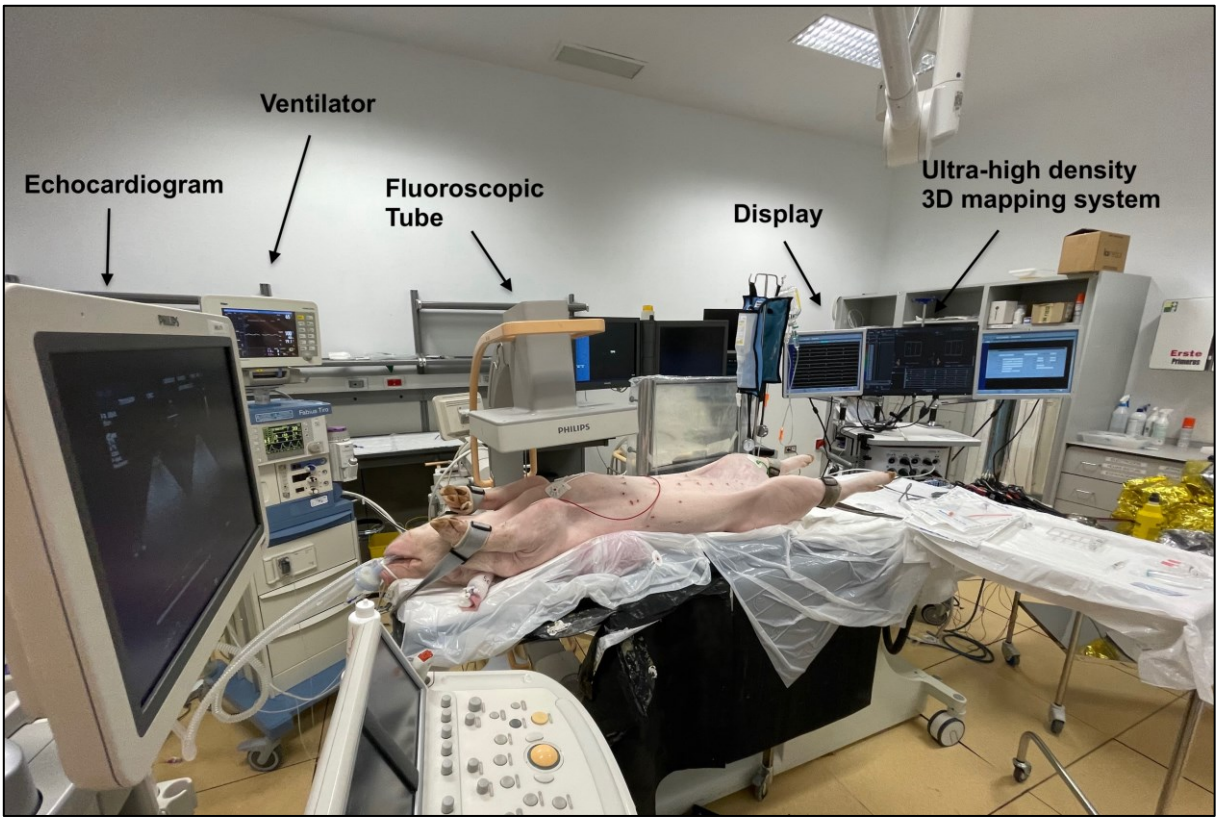

Figure 4.8. Advanced Electrophysiological Laboratory Set-up at CNIC, Madrid

4.7.8.1 Cardiac catheterization, monitoring and electrophysiological testing

The inguinal region was infiltrated with 1% bupivacaine and, ultrasound-guided percutaneous femoral venous and arterial accesses were performed using the Seldinger technique[98]. Invasive blood pressure monitoring was continuously performed via a pressurized line in a 5 Fr sheath in the femoral artery. An esophageal temperature probe was positioned to ensure accurate temperature control. Infrared light for warming and emergency blankets were used to avoid body temperature changes during electrophysiology study. Defibrillator pads were positioned on the chest of the animals.

Under fluoroscopic guidance, a 6 Fr pentapolar diagnostic catheter (Bard EP, Lowell, MA, USA) was placed in the right ventricular (RV) free wall to allow pacing and to act as an intracardiac activation reference. The proximal electrode was positioned in the inferior vena cava and served as an indifferent unipolar electrode.

To ensure stability during the testing, a deflectable catheter was used for RV pacing and the position was tested periodically in fluoroscopy to ensure no macroscopic dislodgement was present. Signals were filtered and amplified via a digital amplifier (Lab System Pro, Boston Scientific, Lowell, MA). All electrophysiological signals were filtered at 0.5-500 Hz for unipolar signals and 30-250 Hz for bipolar signals. Repeated QT and RR measurements were obtained throughout the EP study before the first beat of the start of each pacing protocol.

4.7.8.2 Endo-Epicardial Ultra-High Density Sequential Electroanatomical Mapping

Assessment of the patterns of ventricular repolarization (local repolarization time, LRT) during extra stimulation from the right ventricle with a large number of mapping points was performed with the Rhythmia HDx mapping system 3.0 (Boston Scientific, Marlborough, Massachusetts, USA). An IntellaMap Orion catheter (Boston Scientific, Marlborough, MA (USA)) with 64 printed electrodes distributed equally in 8 rows in a steerable basket catheter was used as a roving catheter to acquire sequentially the electroanatomical mapping points in all chambers[99]. The fill threshold for projecting data points into the surface mapped was 2 mm.

To ensure that all animals were studied under the same pacing protocol, a first extra stimulus (S2) was delivered as close as possible to the refractory period (VERP+30ms) during spontaneous sinus rhythm to obtain an S2 map. This was followed by adding a second extra stimulus (S3) coupled as close as possible to the VERP (VERP+30ms) and the acquisition of S3 maps. This was done with a third extra stimulus (S4) delivered as close as possible to the VERP (+30 ms) to obtain an S4 map. S4 maps were obtained for all animals. The three surfaces (LV endocardium, RV endocardium, Epicardium) were mapped sequentially for each condition.

Our group, in collaboration with the Research and Development team of Boston Scientific Germany (Düsseldorf, Germany), has developed a technique for the annotation of repolarization (Figure 4.9). Briefly, the annotated unipolar signals were inverted (Figure 4.9) using a custom-made MATLAB-based software developed in-house. Inverted unipolar signals were then re-imported into the proprietary software of Boston Scientific, and the mapping window was moved onto the T wave and adjusted as needed.

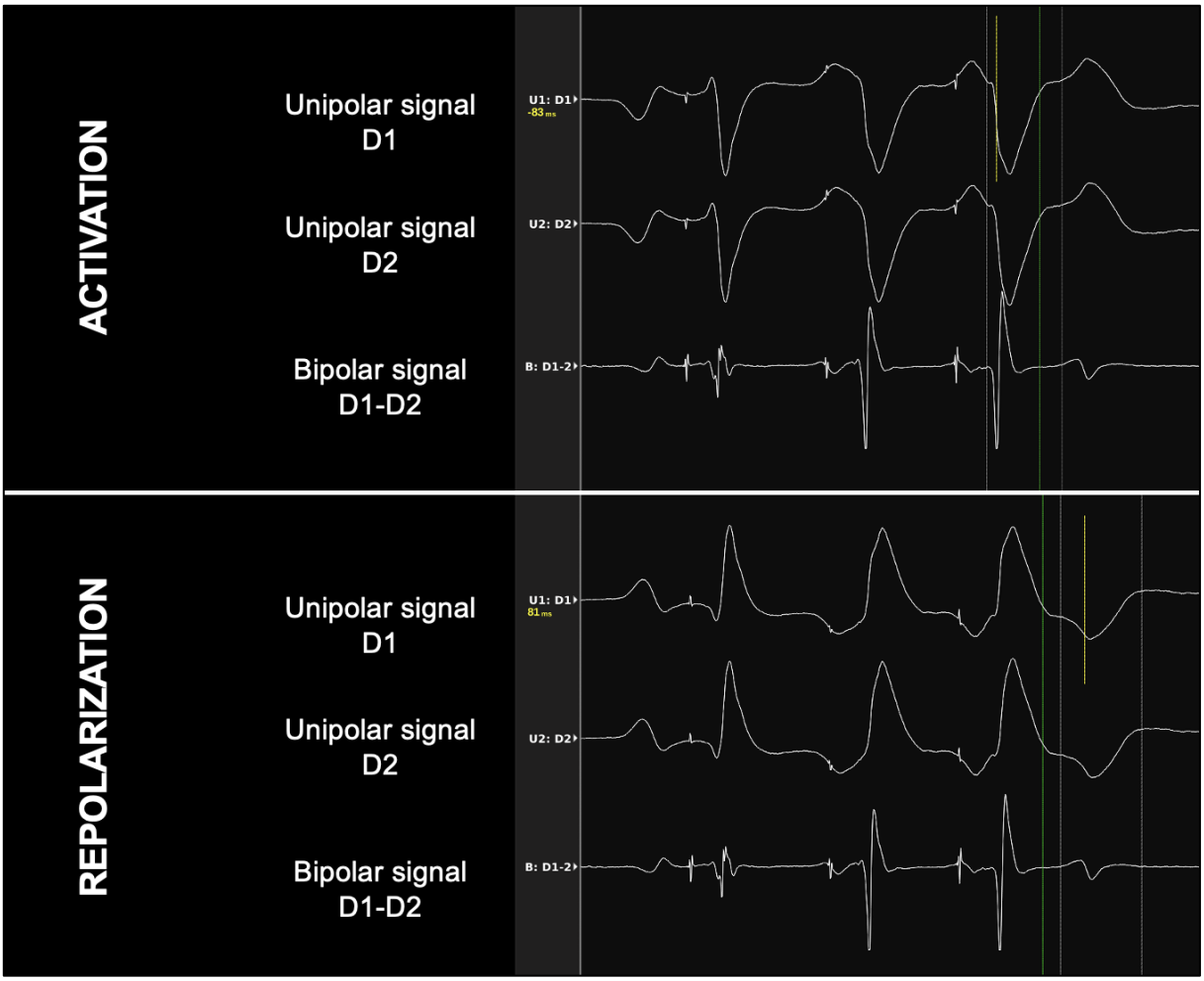

Figure 4.9. Example of Inversion of Unipolar Signals

The automatic annotation algorithm was then run on the T wave to create the LRT map based on the -dV/dt of the inverted unipolar signal (an equivalent of the +dV/dt of the raw acquired signal; Figure 4.9 and Figure 4.10), corresponding to the Wyatt method[100].

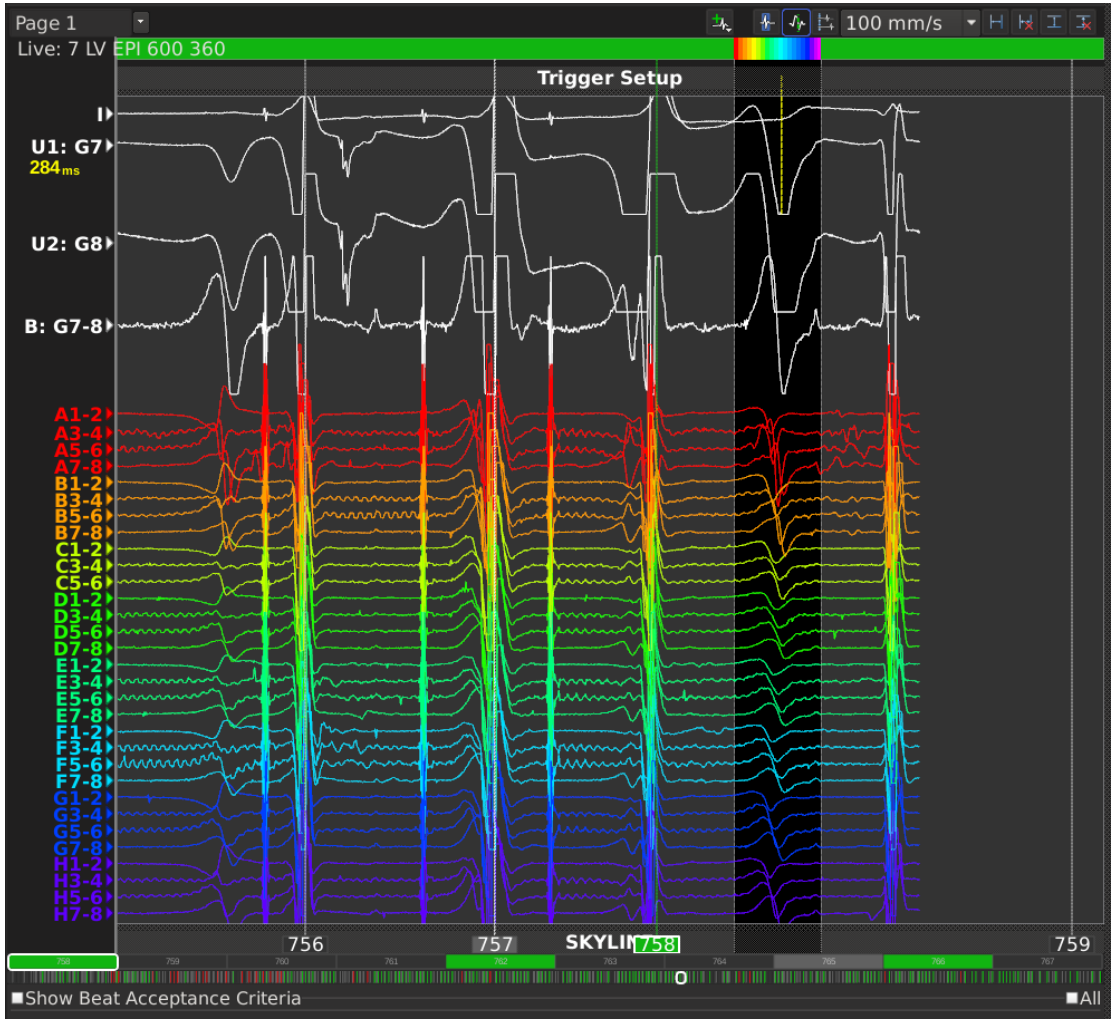

Figure 4.10. Example of automatic annotation of LRT, using proprietary software, with the use of -dV/dt of the inverted unipolar EGM signal during the surface ECG QRS complex occurrence.

The automatically annotated points for LRT maps were manually reviewed with a gain of 1 mV/mm and at a sweep speed of 200 mm/s. Corrections to annotations were limited to isolated outliers to reduce arbitrary measures and ensure reproducibility. A fiducial timing reference for each map was used to ensure all three chambers mapped were referenced to the same timing annotation. All annotations were then referenced to the RV pacing spike to ensure comparability between animals (time 0 ms). Once the maps were finished, the export tool in the Rhythmia system was used. Annotations were then exported and collated for analysis with custom software written in MATLAB (MathWorks Inc., Natick, MA (USA)).

We computed the 3D map of the distribution of the LRT values over the LV and RV endocardial and epicardial surfaces by using the MATLAB patch() function (The MathWorks, Natick, MA).

Spatiotemporal gradients calculation

We calculated the spatial gradient of LRT on the triangulated mesh of each surface. We computed at each vertex of the surface p the absolute value of the parameter difference quotient over each edge E_{pq} meeting at p:
$D_{pq} = |LRT(p) – LRT(q)|/|p-q|$. We then define the LRT gradient GradLRT(p) at vertex p as the maximum of these difference quotients: $GradLRT(p) = \max_q D_{pq}$.

4.7.9 Drug Administration and In Vivo Assessment of Drug Effects

ICA-105574 was administered intravenously with slow infusion (1 mg/min) at the dosage of 12 mg/kg, similarly to the dose used in dogs by Asayama and colleagues[70], under continuous electrocardiographic monitoring of the main parameters (heart rate, PR interval, QRS interval, QT interval), as well as monitoring of clinical parameters (oxygen saturation, blood pressure, temperature).

QT interval was measured every minute during the administration of the drug and, for statistical purposes, QTc measurements 10 minutes after the end of administration were considered. At the end of the infusion, endo-epicardial high density sequential electroanatomical mapping (RHYTHMIA HDx) was repeated according to the same protocol described above.

4.8 Statistical Analyses

Statistical analysis was performed using RStudio Version 4.1.1 (Boston, MA, USA).

Continuous data were reported as mean ± standard deviation (SD), or median and interquartile range (IQR), as appropriate. Normality testing was performed with the Shapiro-Wilk test. Comparisons of continuous data were performed using appropriate unpaired (Student's t-test or Mann-Whitney U test) or paired tests (paired Student's t-test or Wilcoxon signed-rank test), as appropriate.

Two-sided p value of <0.05 was considered statistically significant in all analyses.

4.8.1 Methodological Considerations

Phase One: Drug-Induced Models

Considering the availability of high quality prolonged electrocardiographic recordings in guinea pigs and aiming to assess the trend of QTc change, we decided to perform multiple measurements of the QTc interval at pre-specified timepoints (defined previously). To this end, we fitted a **mixed effects linear regression model** was fitted to account for repeated measurements from the same animals at pre-specified timepoints.

Briefly, mixed effects linear regression models are a set of novel, powerful statistical tools that permit the extension of linear regression to data with a hierarchical structure[101]. Importantly, mixed effects linear regression is able to handle both data with a single level of grouping (e.g., repeated measures collected over time for a single individual, where the grouping is represented at the individual level) and multihierarchical models (e.g., students' test results, where grouping is represented at the individual level, classroom level, year level, school level, school district level, state level, national level)[101]. Mixed effects linear regression is well-suited to serial observations on the same unit: it may be reasonable to assume that the outcome variable is linear within the same unit, but that the linearity of one unit may be different from another unit[102]. Therefore, in the assessment of repeated measurements from the same animals at pre-specified timepoints, which are assumed to have a linear behavior intra-animal, but non-identical linearity inter-animal, the use of a mixed effects linear regression appears logical.

Phase Two: Knock-In Model

In wild-type pigs, the occurrence of sudden cardiac death (SCD) is not an expected event. On the other hand, considering that LQTS is characterized by the unpredictable occurrence of SCD, pig model of LQTS is expected to experience SCD. Conventional methods used for survival analysis[103] are inadequate for analysis in which in one group no events occur. Specifically, in the absence of events in one group, the hazard rate in that group is 0, and the between-group hazard ratio is infinite, resulting in the model converging on $\beta = \infty$ [104].

Different approaches have been proposed to deal with this peculiar situation, but the most validated approach[105] is the adoption of the **Firth method** to reduce the bias of maximum likelihood estimates[106].

4.8.2 Statistical Analysis in Phase One: Drug-Induced Models

For the preliminary assessment of the effects of HERG1 channel agonists in different drug-induced models, a mixed effects linear regression model was fitted using the *lmer* function of the *lme4* package for R. The QTc was inserted as the only outcome variable, and pre-set timepoints (described earlier) as the explanatory covariate. In all related analyses, p values were calculated using Kenward-Roger method of standard errors and degrees of freedom[107]. Graphical representation of the model was made using *ggplot2* function of the *tidyverse* package for R.

4.8.3 Statistical Analysis in Phase Two: Knock-In Model

To quantify the risk of the TS1 pigs of suffering a spontaneous sudden cardiac death (SCD) during their daily life at the farm**,** we used *Surv* function of the *survival* package for R to fit a Kaplan-Meier estimator of SCD-free survival function with follow-up as a timescale. Time to SCD was defined as the time between birth and the occurrence of SCD. Groups were compared using the log-rank test.

Multivariable Firth penalized method[106] for Cox proportional hazards model[103] using *coxphf* function of the *coxphf* package for R was used to evaluate the effects of genotype and gender on the risk of suffering sudden cardiac death at follow-up.

For the in vivo assessment of the effects of HERG1 channel agonists in TS1 pigs, a simple linear regression model was fitted, with QTc as the outcome variable and pre-specified timepoints as the explanatory covariate. Graphical representation of the model was made using *ggplot2* function of the *tidyverse* package for R.

For comparison of data obtained during electrophysiological studies, a nested t-test was used. For baseline analysis, an independent samples nested t-test was used; while for the analysis of ICA-105574 effect, a paired samples nested t-test was used. Graphical representations of the model were made using *ggpaired* function of the *ggpubr* package for R.

5 RESULTS

5.1 PHASE ONE: Preliminary Testing of HERG1 Channel Agonists in Drug-Induced Models of Long QT Syndrome

In the first phase of the appraisal of the efficacy and safety of ICA-105574, a novel HERG1 channel agonist, we used three different drug-induced models of Long QT Syndrome: type 2, type 3, and type 8. We developed and characterized the three models, and after having ascertained that the models reproducibly manifested QT interval prolongation, we tested ICA-105574.

5.1.1 Development and Characterization of Drug-Induced Models of LQTS

As a first step, we recorded a baseline electrocardiogram for 30 minutes in resting conditions in all guinea pigs utilized for the experiments. Following the baseline recording, induction drug was administered. Specifically, DL-sotalol for the induction of LQT2, Anthopleurin-A for the induction of LQT3, Bay K8644 for the induction of LQT8 were administered (for more details please refer to the section Methods, subsection Development of Drug-Induced Models of LQTS).

5.1.1.1 Development and Characterization of Drug-Induced Model of LQT2

After intraperitoneal administration of DL-Sotalol at a dose of 50 mg/kg, the drug effects on principal electrocardiographic parameters were assessed.

As expected, at 60 minutes after the administration of DL-sotalol, RR interval lengthened (Table 5.1 and 5.2) and a modest prolongation of atrioventricular conduction was observed (Table 5.1 and 5.3), in the absence of relevant effects on intraventricular conduction (Table 5.4)

Importantly, a pronounced and statistically significant prolongation of the QTc interval was consistently obtained in all guinea pigs (Tables 5.1, 5.5; Figures 5.1 and 5.2). Specifically, the overall effect of DL-sotalol appears to be very strong, as corroborated by narrow confidence intervals at each timepoint (Table 5.5; Figure 5.2). Inter-animal variance appears to be rather low, as testified by ICC of 0.191.

Despite marked QTc prolongation, during the prolonged electrocardiographic registration no spontaneous arrhythmic events were observed.

N=7 animals	RR, ms (median, IQR)	ΔRR, ms (%)	PR, ms (median, IQR)	ΔPR, ms (%)	QRS, ms (median, IQR)	ΔQRS, ms (%)	QTcB, ms (median, IQR)	ΔQTcB, ms (%)
Baseline	194, 191-209	Ref.	57, 57-60	Ref.	34, 34-39	Ref.	253, 249-258	Ref.
Sotalol 30 minutes	246, 226-254	+52 (+27%)	57, 57-60	0 (0%)	34, 31-37	0 (0%)	287, 280-292	+34 (+13%)
Sotalol 60 minutes	263, 251-271	+69 (+36%)	62, 57-63	+5 (+9%)	34, 34-36	0 (0%)	296, 290-297	+43 (+17%)

Table 5.1. Summary of the Principal Electrocardiographic Parameters at Baseline and After Induction of LQT2.

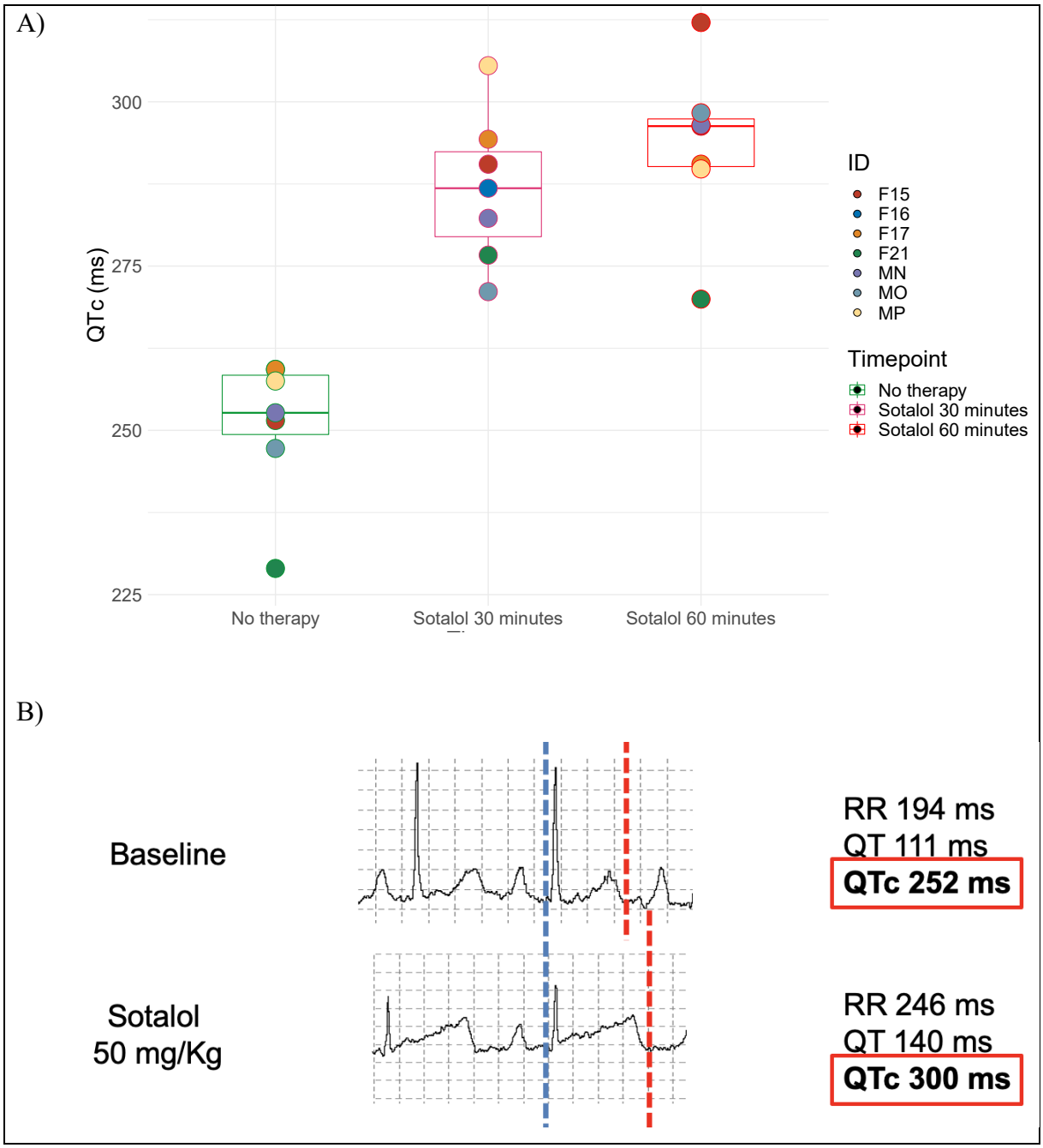

Figure 5.1. Effect of Sotalol on the QTc Interval in Guinea Pigs

Panel A: Boxplot of median QTc values per animal at different timepoints. Each colored dot represents an animal.

Panel B: Electrocardiographic example of sotalol effect on the QTc interval. Blue line shows the beginning of the Q wave, whereas the red line shows the end of the T wave. The distance from the blue line to the red line is the QT interval. Correction of the QT interval for the preceding RR interval, as described by Bazett[30], yields the QTc interval.

N=7 animals	RR, ms (median, IQR)	ΔRR, ms (%)	p-value
Baseline	194, 191-209	Ref.	Ref.
Sotalol 30 minutes	246, 226-254	+52 (+27%)	***<0.001***
Sotalol 60 minutes	263, 251-271	+69 (+36%)	***<0.001***

Table 5.2. Mixed Effects Linear Regression Assessing the Effect of Sotalol on RR interval in Guinea Pigs

N=7 animals	PR, ms (median, IQR)	ΔPR, ms (%)	p-value
Baseline	57, 57-60	Ref.	Ref.
Sotalol 30 minutes	57, 57-60	0 (0%)	0.497
Sotalol 60 minutes	62, 57-63	+5 (+9%)	0.247

Table 5.3. Mixed Effects Linear Regression Assessing the Effect of Sotalol on PR interval in Guinea Pigs

N=7 animals	QRS, ms (median, IQR)	ΔQRS, ms (%)	p-value
Baseline	34, 34-39	Ref.	Ref.
Sotalol 30 minutes	34, 31-37	0 (0%)	0.564
Sotalol 60 minutes	34, 34-36	0 (0%)	0.935

Table 5.4. Mixed Effects Linear Regression Assessing the Effect of Sotalol on QRS interval in Guinea Pigs

N=7 animals	QTcB, ms (median, IQR)	ΔQTcB, ms (%)	p-value
Baseline	253, 249-258	Ref.	Ref.
Sotalol 30 minutes	287, 280-292	+34 (+13%)	***<0.001***
Sotalol 60 minutes	296, 290-297	+43 (+17%)	***<0.001***

Table 5.5. Mixed Effects Linear Regression Assessing the Effect of Sotalol on QTc interval in Guinea Pigs

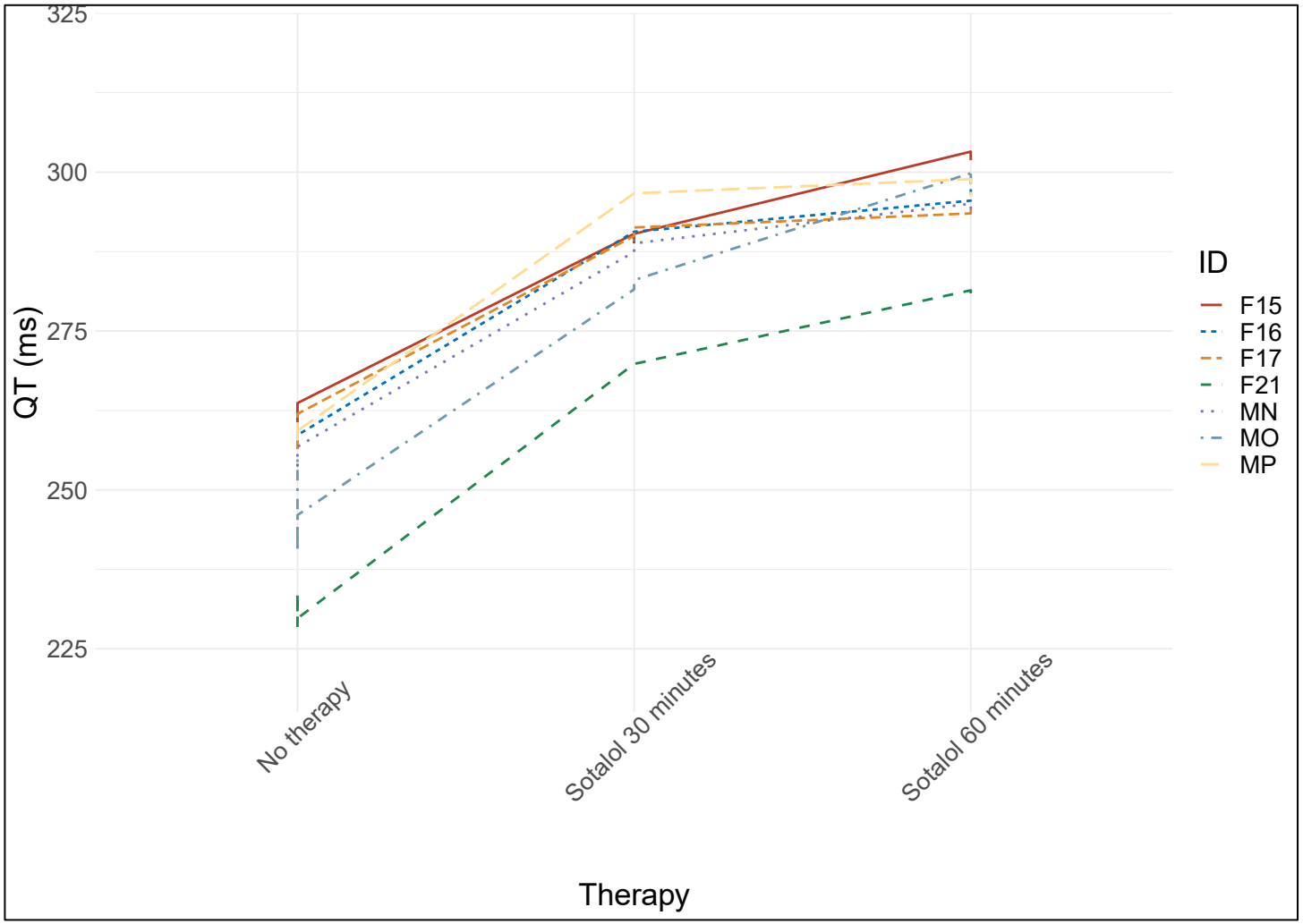

Figure 5.2. Mixed Effects Linear Regression Model Assessing the Effect of Sotalol on the QTc Interval in Guinea Pigs

Dots, which are color coded, represent measurements from an individual animal. Colored lines represent the model fit superimposed on the raw data for each individual animal.

5.1.1.2 Development and Characterization of Drug-Induced Model of LQT3

After intraperitoneal administration of Anthopleurin-A at a dose of 20 μg/kg, the drug effects on principal electrocardiographic parameters were assessed.

At 60 minutes after the administration of Anthopleurin-A, RR interval shortened (Tables 5.6 and 5.7), and a shortening of atrioventricular conduction was observed (Tables 5.6 and 5.8), without relevant effects on intraventricular conduction (Tables 5.6 and 5.9).

Importantly, a pronounced and statistically significant prolongation of the QTc interval was consistently obtained in all guinea pigs (Tables 5.6 and 5.10; Figure 5.3). Specifically, the overall effect of Anthopleurin-A appears to be very strong, as corroborated by narrow confidence intervals at each timepoint (Table 5.10; Figure 5.4). Inter-animal variance appears to be low, as testified by ICC of 0.308.

Despite marked QTc prolongation, during the prolonged electrocardiographic registration no spontaneous arrhythmic events were observed.

N=6 animals	RR, ms (median, IQR)	ΔRR, ms (%)	PR, ms (median, IQR)	ΔPR, ms (%)	QRS, ms (median, IQR)	ΔQRS, ms (%)	QTcB, ms (median, IQR)	ΔQTcB, ms (%)
Baseline	200, 192-214	Ref.	61, 60-69	Ref.	36, 32-40	Ref.	262, 252-263	Ref.
APA 30 minutes	180, 177-189	-20 (-10%)	55, 55-56	-6 (-10%)	38, 36-38	+2 (+6%)	290, 284-295	+28 (+11%)
APA 60 minutes	192, 182-197	-8 (-4%)	56, 55-61	-5 (-8%)	37, 33-38	+1 (+3%)	296, 293-297	+34 (+13%)

Table 5.6. Principal Electrocardiographic Parameters at Baseline and After Induction of LQT3.

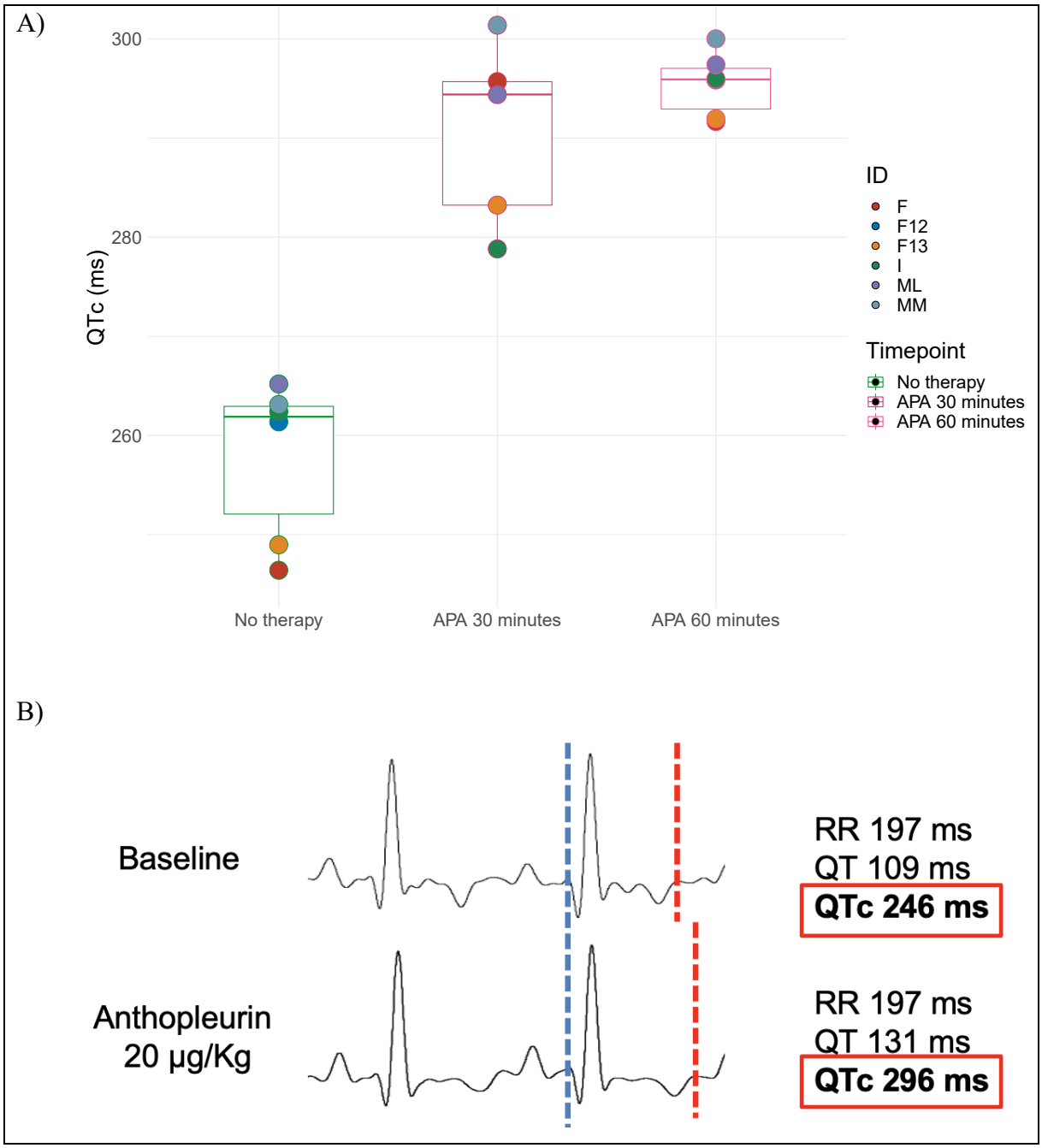

Figure 5.3. Effect of Anthopleurin-A on the QTc Interval in Guinea Pigs

Panel A: Boxplot of median QTc values per animal at different timepoints. Each colored dot represents an animal.

Panel B: Electrocardiographic example of Anthopleurin-A effect on the QTc interval. Blue line shows the beginning of the Q wave, whereas the red line shows the end of the T wave. The distance from the blue line to the red line is the QT interval. Correction of the QT interval for the preceding RR interval, as described by Bazett[30], yields the QTc interval.

N=6 animals	RR, ms (median, IQR)	ΔRR, ms (%)	p-value
Baseline	200, 192-214	Ref.	Ref.
APA 30 minutes	180, 177-189	-20 (-10%)	***<0.001***
APA 60 minutes	192, 182-197	-8 (-4%)	***<0.001***

Table 5.7. Mixed Effects Linear Regression Assessing the Effect of Anthopleurin-A on RR interval in Guinea Pigs

N=6 animals	PR, ms (median, IQR)	ΔPR, ms (%)	p-value
Baseline	61, 60-69	Ref.	Ref.
APA 30 minutes	55, 55-56	-6 (-10%)	***<0.001***
APA 60 minutes	56, 55-61	-5 (-8%)	***<0.001***

Table 5.8. Mixed Effects Linear Regression Assessing the Effect of Anthopleurin-A on PR interval in Guinea Pigs

N=6 animals	QRS, ms (median, IQR)	ΔQRS, ms (%)	p-value
Baseline	36, 32-40	Ref.	Ref.
APA 30 minutes	38, 36-38	+2 (+6%)	0.929
APA 60 minutes	37, 33-38	+1 (+3%)	0.206

Table 5.9. Mixed Effects Linear Regression Assessing the Effect of Anthopleurin-A on QRS interval in Guinea Pigs

N=6 animals	QTcB, ms (median, IQR)	ΔQTcB, ms (%)	p-value
Baseline	262, 252-263	Ref.	Ref.
APA 30 minutes	290, 284-295	+28 (+11%)	***<0.001***
APA 60 minutes	296, 293-297	+34 (+13%)	***<0.001***

Table 5.10. Mixed Effects Linear Regression Assessing the Effect of Anthopleurin-A on QTc interval in Guinea Pigs

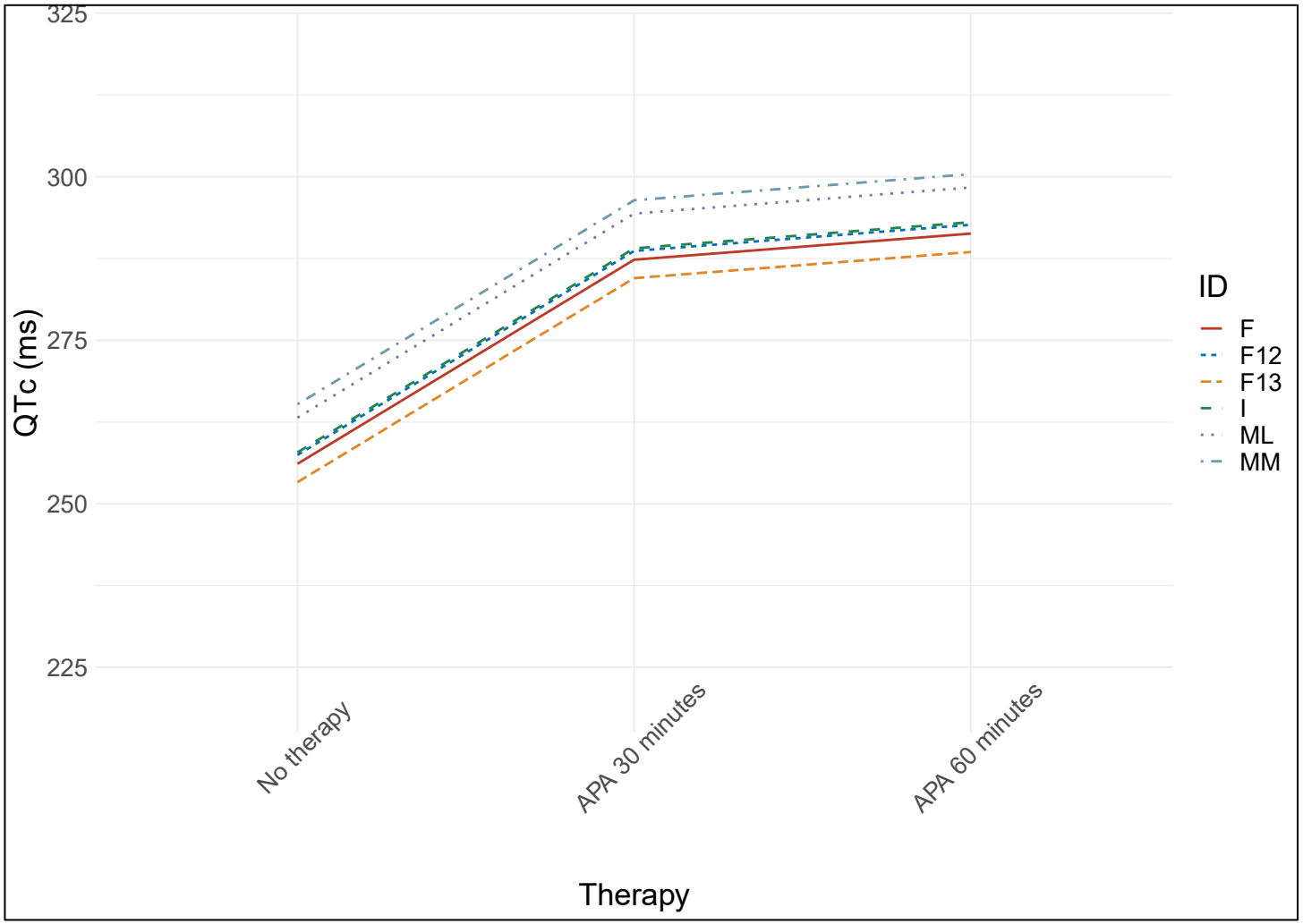

Figure 5.4. Mixed Effects Linear Regression Model Assessing the Effect of Anthopleurin-A on the QTc Interval in Guinea Pigs

Dots, which are color coded, represent measurements from an individual animal. Colored lines represent the model fit superimposed on the raw data for each individual animal.

5.1.1.3 Development and Characterization of Drug-Induced Model of LQT8

After intraperitoneal administration of Bay K8664 at a dose of 50 μg/kg, the drug effects on principal electrocardiographic parameters were assessed (Tables 5.11-5.15).
Importantly, a pronounced and statistically significant prolongation of the QTc interval was consistently obtained in all guinea pigs (Tables 5.11 and 5.15; Figure 5.5). Specifically, the overall effect of Bay K8644 appears to be very strong, as corroborated by narrow confidence intervals at each timepoint (Table 5.15; Figure 5.6). Inter-animal variance appears to be very low, as testified by ICC of 0.166.

Relevantly, despite marked QTc prolongation, during the extended electrocardiographic registration no spontaneous arrhythmic events were observed.

N=6 animals	RR, ms (median, IQR)	ΔRR, ms (%)	PR, ms (median, IQR)	ΔPR, ms (%)	QRS, ms (median, IQR)	ΔQRS, ms (%)	QTcB, ms (median, IQR)	ΔQTcB, ms (%)
Baseline	206, 184-206	Ref.	57, 57-57	Ref.	23, 23-23	Ref.	245, 236-245	Ref.
Bay K8644 30 minutes	189, 174-194	-17 (-8%)	57, 57-57	0 (0%)	23, 23-23	0 (0%)	274, 270-280	+29 (+12%)
Bay K8644 60 minutes	214, 197-231	+8 (+4%)	57, 53-57	0 (0%)	23, 23-23	0 (0%)	286, 279-296	+41 (+17%)

Table 5.11. Principal Electrocardiographic Parameters at Baseline and After Induction of LQT8.

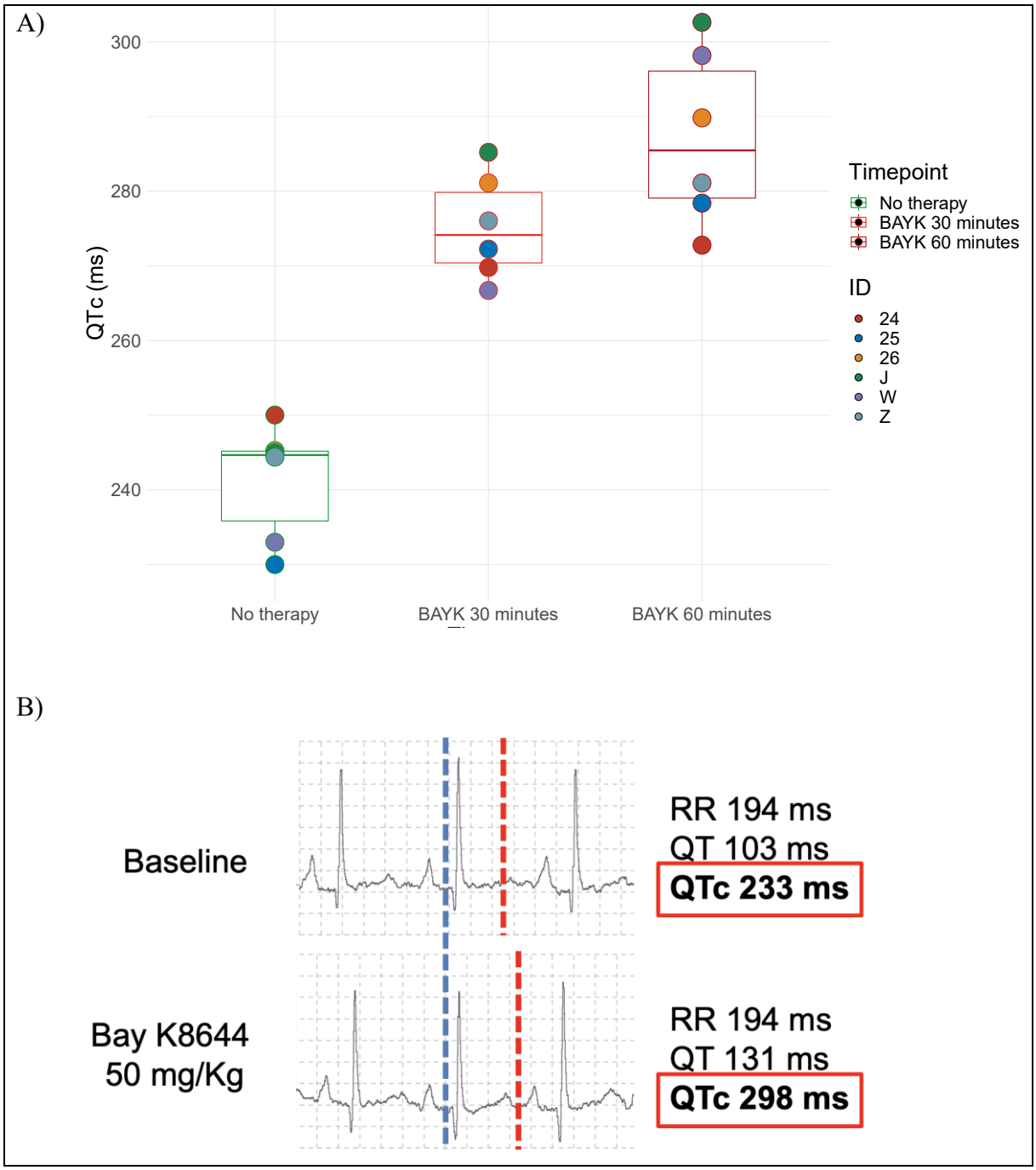

Figure 5.5. Effect of Bay K8644 on the QTc Interval in Guinea Pigs

Panel A: Boxplot of median QTc values per animal at different timepoints. Each colored dot represents an animal.

Panel B: Electrocardiographic example of Bay K8644 effect on the QTc interval. Blue line shows the beginning of the Q wave, whereas the red line shows the end of the T wave. The distance from the blue line to the red line is the QT interval. Correction of the QT interval for the preceding RR interval, as described by Bazett[30], yields the QTc interval.

N=6 animals	RR, ms (median, IQR)	ΔRR, ms (%)	p-value
Baseline	206, 184-206	Ref.	Ref.
Bay K8644 30 minutes	189, 174-194	-17 (-8%)	0.057
Bay K8644 60 minutes	214, 197-231	+8 (+4%)	***0.001***

Table 5.12. Mixed Effects Linear Regression Assessing the Effect of Bay K8644 on RR interval in Guinea Pigs

N=6 animals	PR, ms (median, IQR)	ΔPR, ms (%)	p-value
Baseline	57, 57-57	Ref.	Ref.
Bay K8644 30 minutes	57, 57-57	0 (0%)	-
Bay K8644 60 minutes	57, 53-57	0 (0%)	-

Table 5.13. Mixed Effects Linear Regression Assessing the Effect of Bay K8644 on PR interval in Guinea Pigs

N=6 animals	QRS, ms (median, IQR)	ΔQRS, ms (%)	p-value
Baseline	23, 23-23	Ref.	Ref.
Bay K8644 30 minutes	23, 23-23	0 (0%)	-
Bay K8644 60 minutes	23, 23-23	0 (0%)	-

Table 5.14. Mixed Effects Linear Regression Assessing the Effect of Bay K8644 on QRS interval in Guinea Pigs

N=6 animals	QTcB, ms (median, IQR)	ΔQTcB, ms (%)	p-value
Baseline	245, 236-245	Ref.	Ref.
Bay K8644 30 minutes	274, 270-280	+29 (+12%)	***<0.001***
Bay K8644 60 minutes	286, 279-296	+41 (+17%)	***<0.001***

Table 5.15. Mixed Effects Linear Regression Assessing the Effect of Bay K8644 on QTc interval in Guinea Pigs

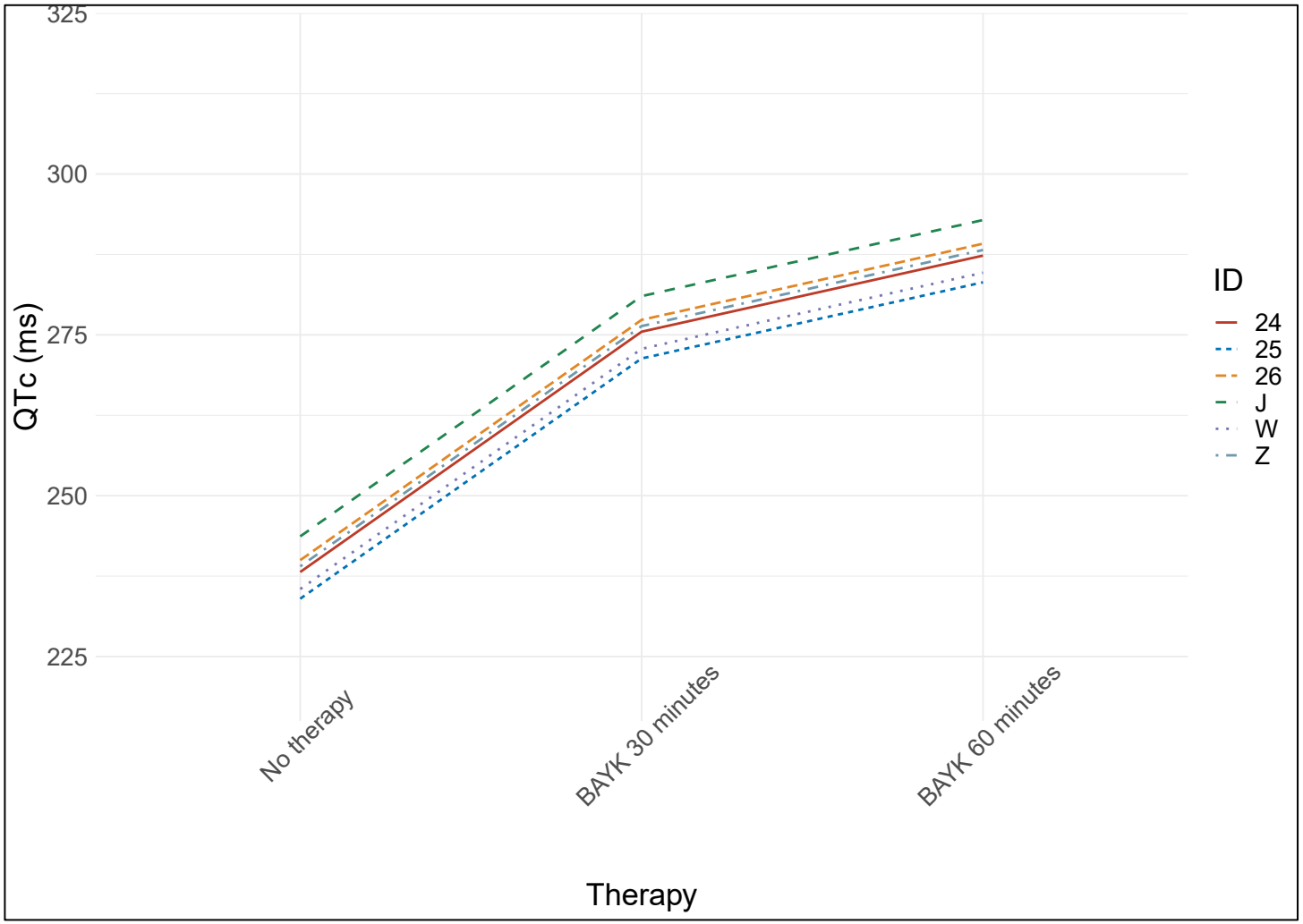

Figure 5.6. Mixed Effects Linear Regression Model Assessing the Effect of Bay K8644 on the QTc Interval in Guinea Pigs

Dots, which are color coded, represent measurements from an individual animal. Colored lines represent the model fit superimposed on the raw data for each individual animal.

5.1.1.4 Summary of Drug-Induced Long QT Syndrome Models

To summarize, we successfully and reproducibly developed three different models of Long QT Syndrome (Figure 5.7).

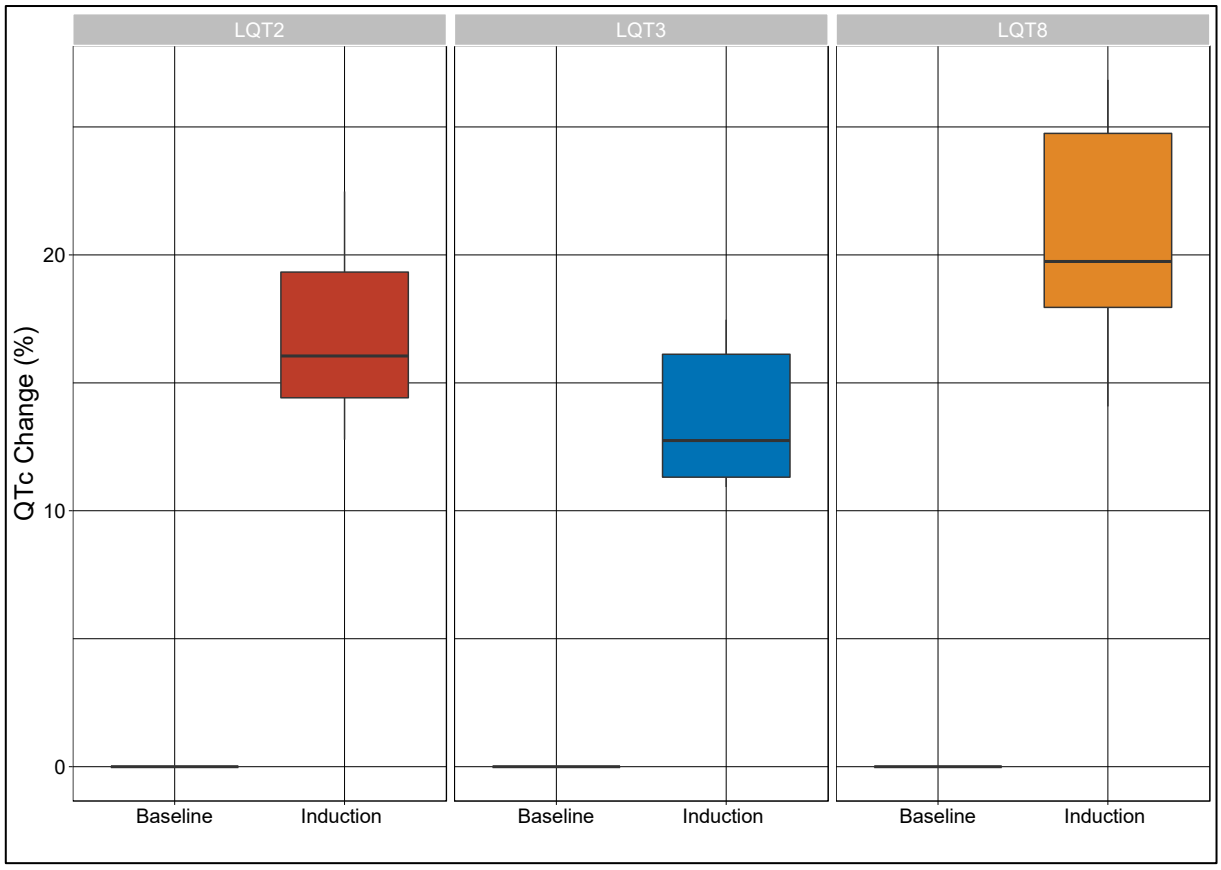

Figure 5.7. Summary of the Percentual Change in QTc in Three Drug-Induced Models of LQTS.

On average, the QTc interval lengthened by 17±4 %, 14±3 %, and 21±5 % in LQT2, LQT3, and LQT8, respectively (Figure 5.7).

5.1.2 Preliminary In Vivo Testing of HERG1 Channel Agonists in Drug-Induced Models of Long QT Syndrome

Following the demonstration of successful induction of LQTS in three drug-induced models of LQTS, a single intraperitoneal dose of ICA-105574 at 15 mg/kg was administered (for more details please refer to the section Methods, subsection Preliminary *In Vivo* Testing of HERG Channel Agonists in Drug-Induced Models of LQTS).

5.1.2.1 HERG1 Channel Agonists in Drug-Induced Model of LQT2

After intraperitoneal administration of ICA-105574 at a dose of 15 mg/kg, the drug effects on principal electrocardiographic parameters were assessed.

Immediately upon drug administration, RR interval shortened modestly (Tables 5.16 and 5.17), but this effect was transient and by 15 minutes after administration, and the RR interval continued lengthening throughout the registration, likely attributable to Class II effect of DL-Sotalol used. No other biologically significant effects on the principal electrocardiographic parameters were observed (Tables 5.16, 5.18, 5.19).

Importantly, a pronounced and statistically significant shortening of the QTc interval was consistently obtained in all guinea pigs (Tables 5.16 and 5.20; Figure 5.8). Specifically, the overall effect of ICA-105574 appears to be strong, as corroborated by relatively narrow confidence intervals at each timepoint (Table 5.20; Figure 5.9). Inter-animal variance appears to be low and has been estimated to be in the order of 18% (ICC=0.180).
Relevantly, despite marked QTc shortening induced by ICA-105574, during the prolonged electrocardiographic registration no proarrhythmic events were observed.

The pharmacological effect of ICA-105574 waned rather quickly, with QTc interval lengthening 30 minutes after drug administration (Table 5.20; Figure 5.9).

N=7 animals	RR, ms (median, IQR)	ΔRR, ms (%)	PR, ms (median, IQR)	ΔPR, ms (%)	QRS, ms (median, IQR)	ΔQRS, ms (%)	QTcB, ms (median, IQR)	ΔQTcB, ms (%)
Sotalol 60 minutes	263, 251-271	Ref.	62, 57-63	Ref.	34, 34-36	Ref.	296, 290-297	Ref.
ICA-105574 start	257, 242-263	-6 (-3%)	57, 57-66	-5 (-8%)	34, 34-34	0 (0%)	256, 252-257	-40 (-14%)
ICA-105574 15 minutes	269, 260-286	+6 (+3%)	57, 57-63	-5 (-8%)	34, 31-36	0 (0%)	289, 287-294	-7 (-3%)
ICA-105574 30 minutes	297, 280-297	+34 (+13%)	62, 57-63	0 (0%)	34, 31-36	0 (0%)	295, 289-300	-1 (-0.3%)
ICA-105574 60 minutes	293, 289-297	+30 (+11%)	63, 60-63	+1 (0%)	34, 31-34	0 (0%)	296, 292-299	0 (0%)

Table 5.16. Principal Electrocardiographic Parameters After Induction of LQT2 and After Administration of ICA-105574.

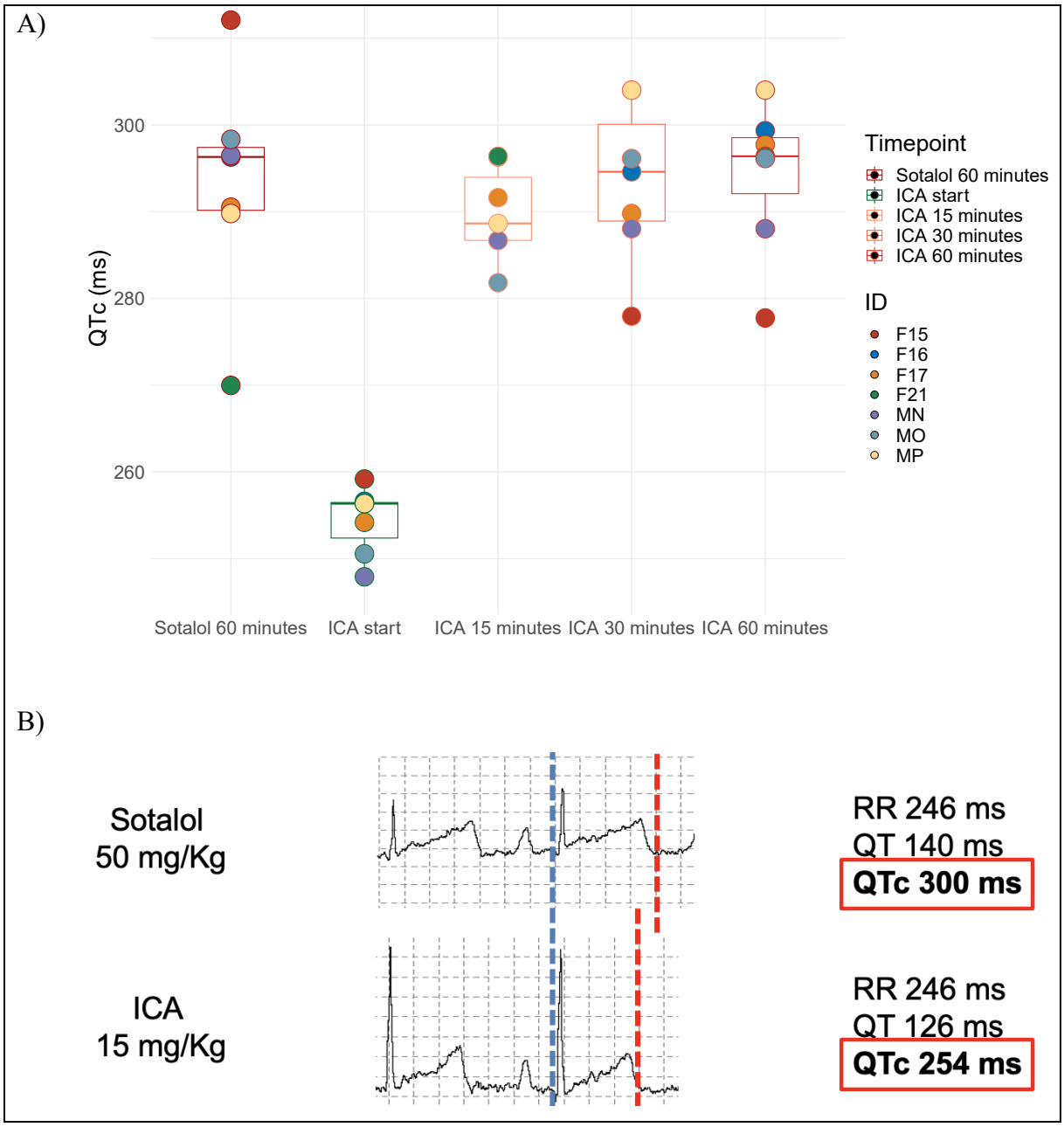

Figure 5.8. Effect of ICA-105574 on the QTc Interval in a Drug-Induced Guinea Pig Model of LQT2

Panel A: Boxplot of median QTc values per animal at different timepoints. Each colored dot represents an animal.

Panel B: Electrocardiographic example of ICA-105574 effect on the QTc interval in a drug-induced model of LQT2. Blue line shows the beginning of the Q wave, whereas the red line shows the end of the T wave. The distance from the blue line to the red line is the QT interval. Correction of the QT interval for the preceding RR interval, as described by Bazett[30], yields the QTc interval.

N=7 animals	RR, ms (median, IQR)	ΔRR, ms (%)	p-value
Sotalol 60 minutes	263, 251-271	Ref.	Ref.
ICA-105574 start	257, 242-263	-6 (-3%)	***0.003***
ICA-105574 15 minutes	269, 260-286	+6 (+3%)	0.183
ICA-105574 30 minutes	297, 280-297	+34 (+13%)	***<0.001***
ICA-105574 60 minutes	293, 289-297	+30 (+11%)	***<0.001***

Table 5.17. Mixed Effects Linear Regression Assessing the Effect of ICA-105574 on RR interval a Drug-Induced Guinea Pig Model of LQT2

N=7 animals	PR, ms (median, IQR)	ΔPR, ms (%)	p-value
Sotalol 60 minutes	62, 57-63	Ref.	Ref.
ICA-105574 start	57, 57-66	-5 (-8%)	0.643
ICA-105574 15 minutes	57, 57-63	-5 (-8%)	0.628
ICA-105574 30 minutes	62, 57-63	0 (0%)	0.467
ICA-105574 60 minutes	63, 60-63	+1 (0%)	0.227

Table 5.18. Mixed Effects Linear Regression Assessing the Effect of ICA-105574 on PR interval a Drug-Induced Guinea Pig Model of LQT2

N=7 animals	QRS, ms (median, IQR)	ΔQRS, ms (%)	p-value
Sotalol 60 minutes	34, 31-36	Ref.	Ref.
ICA-105574 start	34, 34-34	0 (0%)	-
ICA-105574 15 minutes	34, 31-36	0 (0%)	-
ICA-105574 30 minutes	34, 31-36	0 (0%)	-
ICA-105574 60 minutes	34, 31-34	0 (0%)	-

Table 5.19. Mixed Effects Linear Regression Assessing the Effect of ICA-105574 on QRS interval a Drug-Induced Guinea Pig Model of LQT2

N=7 animals	QTcB, ms (median, IQR)	ΔQTcB, ms (%)	p-value
Sotalol 60 minutes	296, 290-297	Ref.	Ref.
ICA-105574 start	256, 252-257	-40 (-14%)	***<0.001***
ICA-105574 15 minutes	289, 287-294	-7 (-3%)	0.060
ICA-105574 30 minutes	295, 289-300	-1 (-0.3%)	0.907
ICA-105574 60 minutes	296, 292-299	0 (0%)	0.912

Table 5.20. Mixed Effects Linear Regression Assessing the Effect of ICA-105574 on QTcB interval a Drug-Induced Guinea Pig Model of LQT2

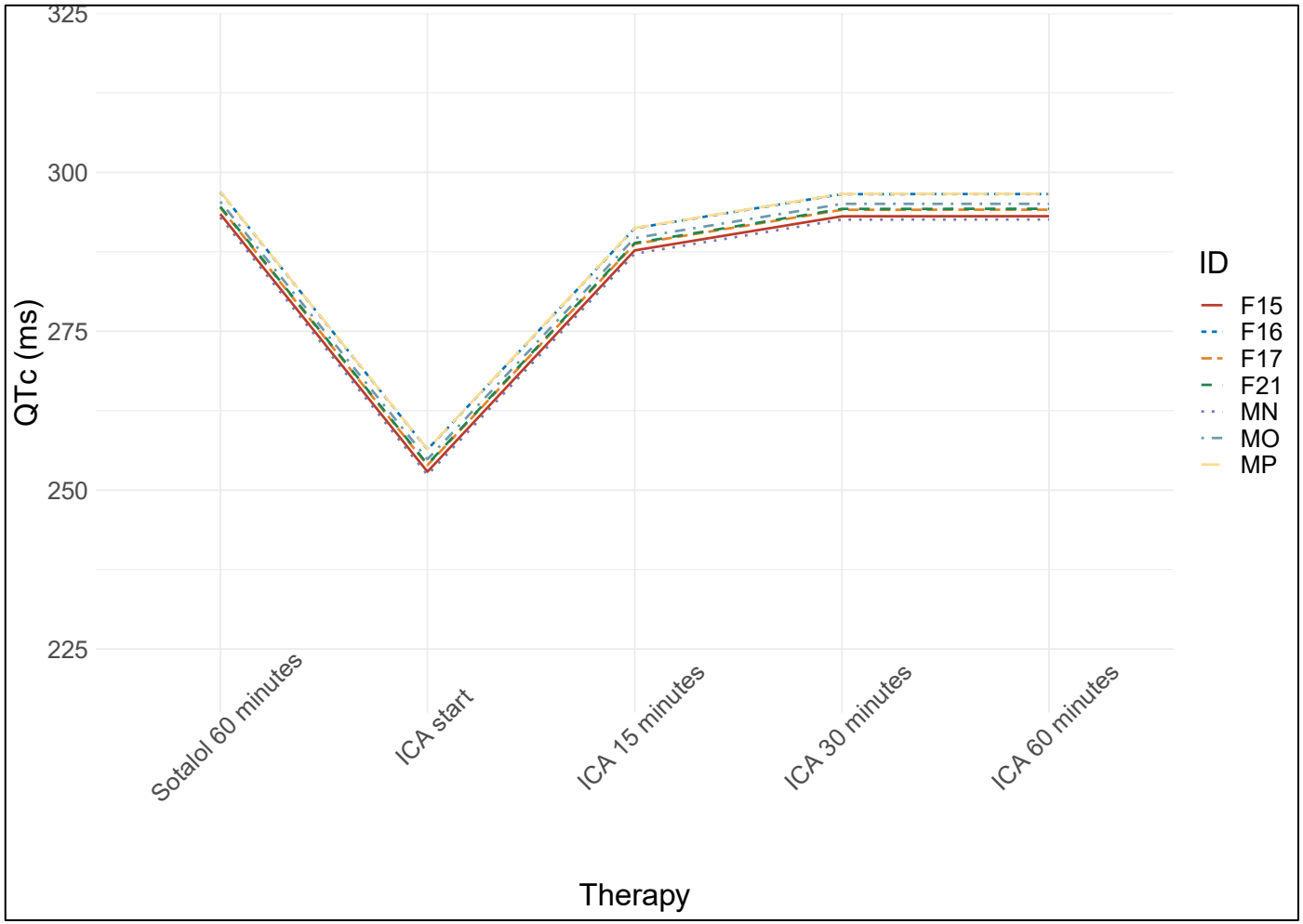

Figure 5.9. Mixed Effects Linear Regression Model Assessing the Effect of ICA-105574 on the QTc Interval in a Drug-Induced Model of LQT2.

Dots, which are color coded, represent measurements from an individual animal. Colored lines represent the model fit superimposed on the raw data for each individual animal.

Moreover, as shown in Table 5.21 and Figures 5.10 and 5.11, ICA-105574 was able to completely normalize the QTc interval in our drug-induced model of LQT2.

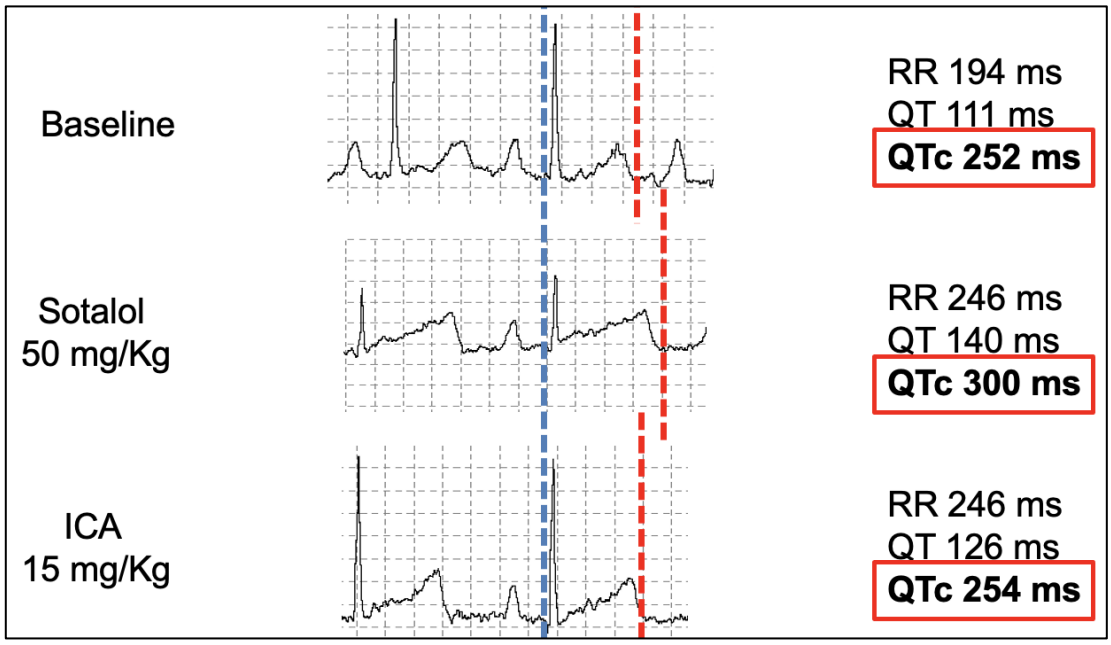

Figure 5.10. ICA-105574 Mediates QTc Interval Normalization in a Drug-Induced Guinea Pig Model of LQT2

N=7 animals	QTcB, ms (median, IQR)	ΔQTcB, ms (%)	p-value
Baseline	253, 249-258	Ref.	Ref.
Sotalol 60 minutes	296, 290-297	+43 (+17%)	***<0.001***
ICA-105574 start	256, 252-257	+3 (+2%)	0.420

Table 5.21. Mixed Effects Linear Regression Assessing the Ability of ICA-105574 to Normalize QTcB interval to Baseline Values in a Drug-Induced Model of LQT2

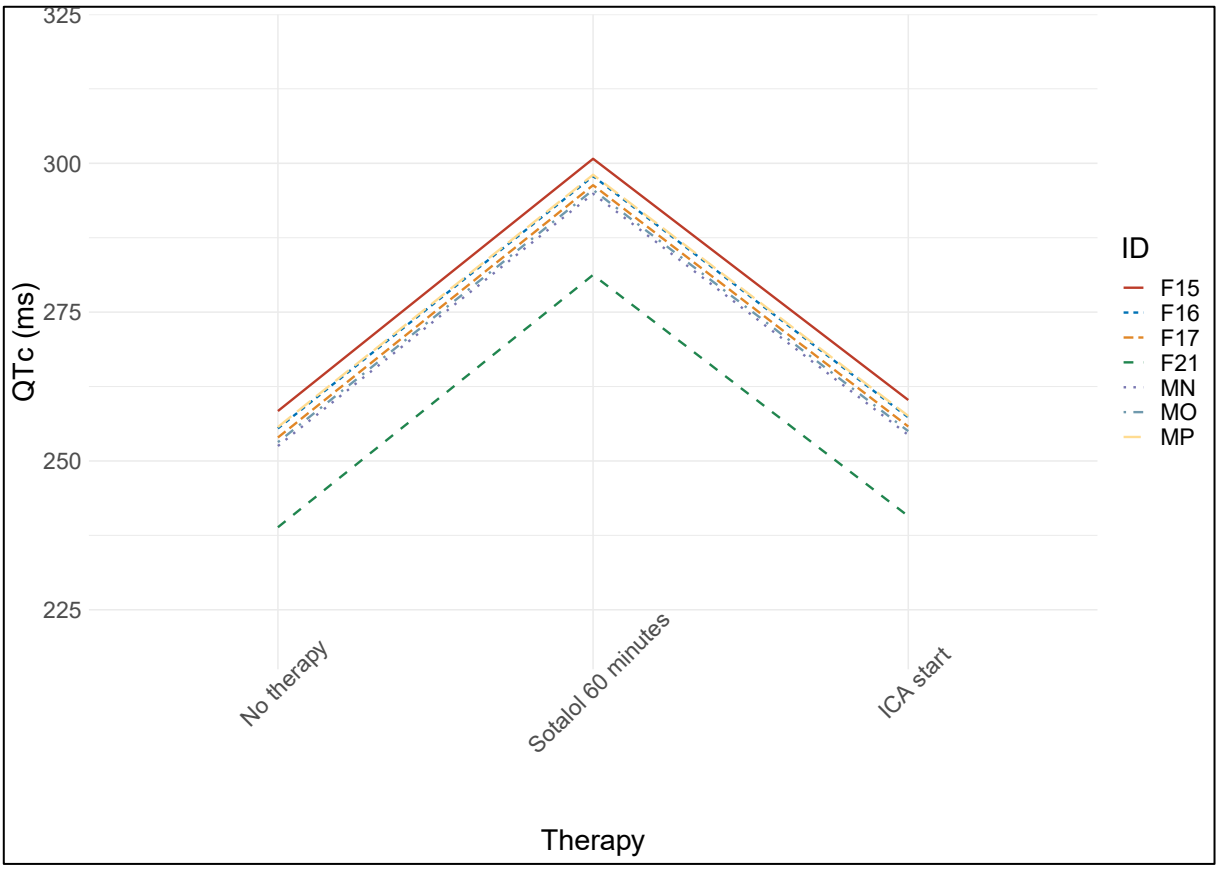

Figure 5.11. Mixed Effects Linear Regression Model Assessing the Effect of ICA-105574 to Normalize the QTc Interval in a Drug-Induced Model of LQT2

Dots, which are color coded, represent measurements from an individual animal. Colored lines represent the model fit superimposed on the raw data for each individual animal.

5.1.2.2 HERG1 Channel Agonists in Drug-Induced Model of LQT3

After intraperitoneal administration of ICA-105574 at a dose of 15 mg/kg, the drug effects on principal electrocardiographic parameters were assessed.

Immediately upon drug administration, RR interval lengthened modestly (Tables 5.22 and 5.23), but this effect was transient and by 15 minutes after administration, the RR interval was back to baseline values. No other biologically significant effects on the principal electrocardiographic parameters were observed (Tables 5.22, 5.24, 5.25).

Importantly, a pronounced and statistically significant shortening of the QTc interval was consistently obtained in all guinea pigs (Tables 5.22 and 5.26; Figure 5.12). Specifically, at parity of RR interval and gender, the overall effect of ICA-105574 appears to be strong, as corroborated by relatively narrow confidence intervals at each timepoint (Table 5.26; Figure 5.13). Inter-animal variance appears to be low and has been estimated to be in the order of 47% (ICC=0.470).

Relevantly, despite marked QTc shortening induced by ICA-105574, during the prolonged electrocardiographic registration no proarrhythmic events were observed.

N=6 animals	RR, ms (median, IQR)	ΔRR, ms (%)	PR, ms (median, IQR)	ΔPR, ms (%)	QRS, ms (median, IQR)	ΔQRS, ms (%)	QTcB, ms (median, IQR)	ΔQTcB, ms (%)
APA 60 minutes	192, 182-197	Ref.	56, 55-61	Ref.	37, 33-38	Ref.	296, 293-297	Ref.
ICA-105574 start	216, 193-245	+24 (+13%)	56, 55-60	0 (0%)	38, 36-38	+1 (+3%)	254, 250-266	-42 (-14%)
ICA-105574 15 minutes	184, 168-190	-8 (-4%)	56, 51-56	0 (0%)	37, 34-38	0 (0%)	260, 258-265	-36 (-12%)
ICA-105574 30 minutes	201, 189-212	+9 (+5%)	54, 50-56	-2 (-4%)	37, 34-38	0 (0%)	263, 257-270	-33 (-11%)
ICA-105574 60 minutes	207, 185-226	+15 (+8%)	56, 55-56	0 (0%)	37, 34-38	0 (0%)	294, 290-298	-2 (-1%)

Table 5.22. Principal Electrocardiographic Parameters After Induction of LQT3 and After Administration of ICA-105574.

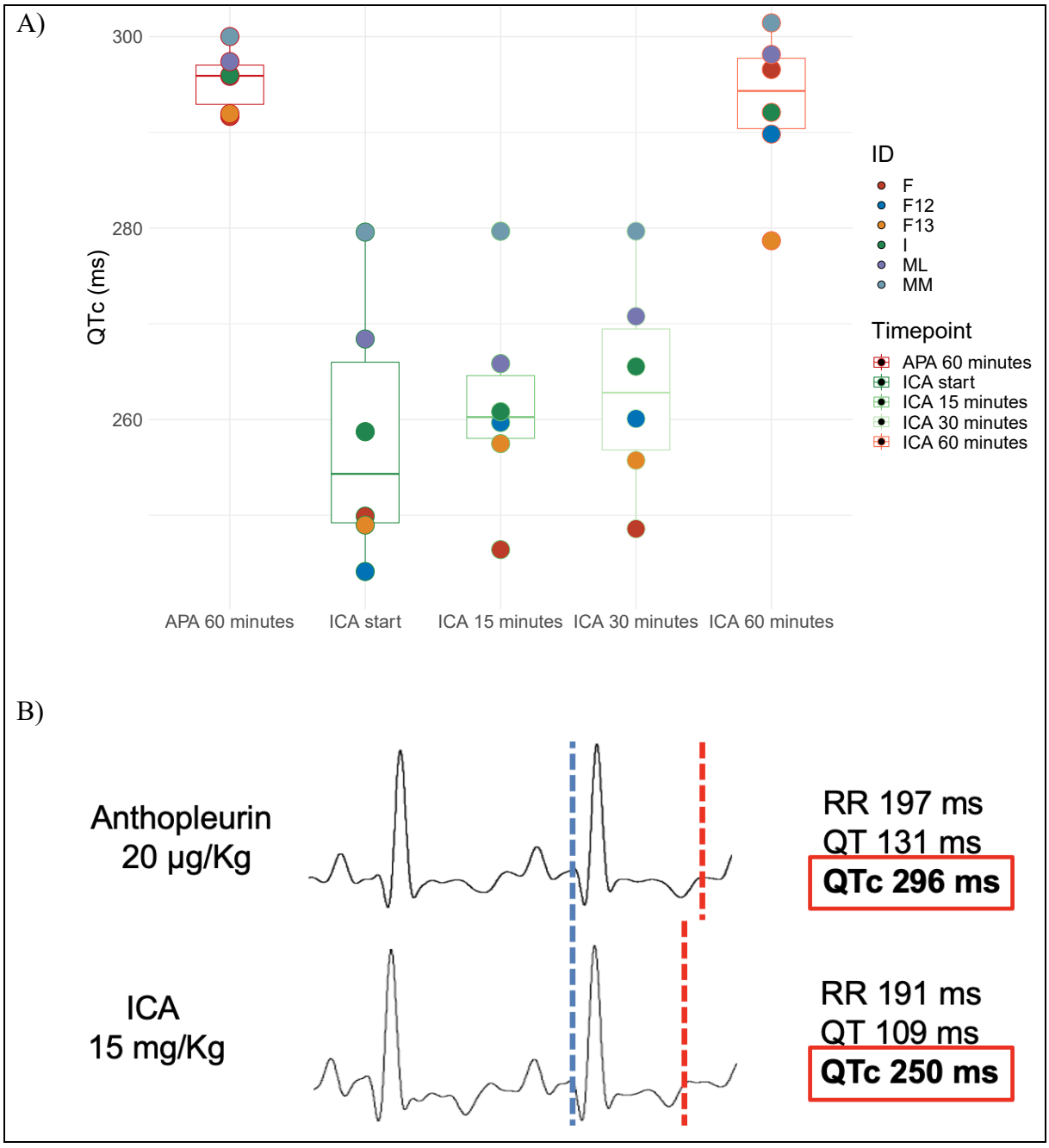

Figure 5.12. Effect of ICA-105574 on the QTc Interval in a Drug-Induced Guinea Pig Model of LQT3

Panel A: Boxplot of median QTc values per animal at different timepoints. Each colored dot represents an animal.

Panel B: Electrocardiographic example of ICA-105574 effect on the QTc interval in a drug-induced model of LQT3. Blue line shows the beginning of the Q wave, whereas the red line shows the end of the T wave. The distance from the blue line to the red line is the QT interval. Correction of the QT interval for the preceding RR interval, as described by Bazett[30], yields the QTc interval.

N=6 animals	RR, ms (median, IQR)	ΔRR, ms (%)	p-value
APA 60 minutes	192, 182-197	Ref.	Ref.
ICA-105574 start	216, 193-245	+24 (+13%)	***<0.001***
ICA-105574 15 minutes	184, 168-190	-8 (-4%)	0.123
ICA-105574 30 minutes	201, 189-212	+9 (+5%)	0.052
ICA-105574 60 minutes	207, 185-226	+15 (+8%)	0.051

Table 5.23. Mixed Effects Linear Regression Assessing the Effect of ICA-105574 on RR interval a Drug-Induced Guinea Pig Model of LQT3

N=6 animals	PR, ms (median, IQR)	ΔPR, ms (%)	p-value
APA 60 minutes	56, 55-61	Ref.	Ref.
ICA-105574 start	56, 55-60	0 (0%)	0.550
ICA-105574 15 minutes	56, 51-56	0 (0%)	0.550
ICA-105574 30 minutes	54, 50-56	-2 (-4%)	0.075
ICA-105574 60 minutes	56, 55-56	0 (0%)	0.141

Table 5.24. Mixed Effects Linear Regression Assessing the Effect of ICA-105574 on PR interval a Drug-Induced Guinea Pig Model of LQT3

N=6 animals	QRS, ms (median, IQR)	ΔQRS, ms (%)	p-value
APA 60 minutes	37, 33-38	Ref.	Ref.
ICA-105574 start	38, 36-38	+1 (+3%)	***0.030***
ICA-105574 15 minutes	37, 34-38	0 (0%)	0.678
ICA-105574 30 minutes	37, 34-38	0 (0%)	0.464
ICA-105574 60 minutes	37, 34-38	0 (0%)	0.125

Table 5.25. Mixed Effects Linear Regression Assessing the Effect of ICA-105574 on QRS interval a Drug-Induced Guinea Pig Model of LQT3

N=6 animals	QTcB, ms (median, IQR)	ΔQTcB, ms (%)	p-value
APA 60 minutes	296, 293-297	Ref.	Ref.
ICA-105574 start	254, 250-266	-42 (-14%)	***<0.001***
ICA-105574 15 minutes	260, 258-265	-36 (-12%)	***<0.001***
ICA-105574 30 minutes	263, 257-270	-33 (-11%)	***<0.001***
ICA-105574 60 minutes	294, 290-298	-2 (-1%)	0.364

Table 5.26. Mixed Effects Linear Regression Assessing the Effect of ICA-105574 on QTcB interval a Drug-Induced Guinea Pig Model of LQT3

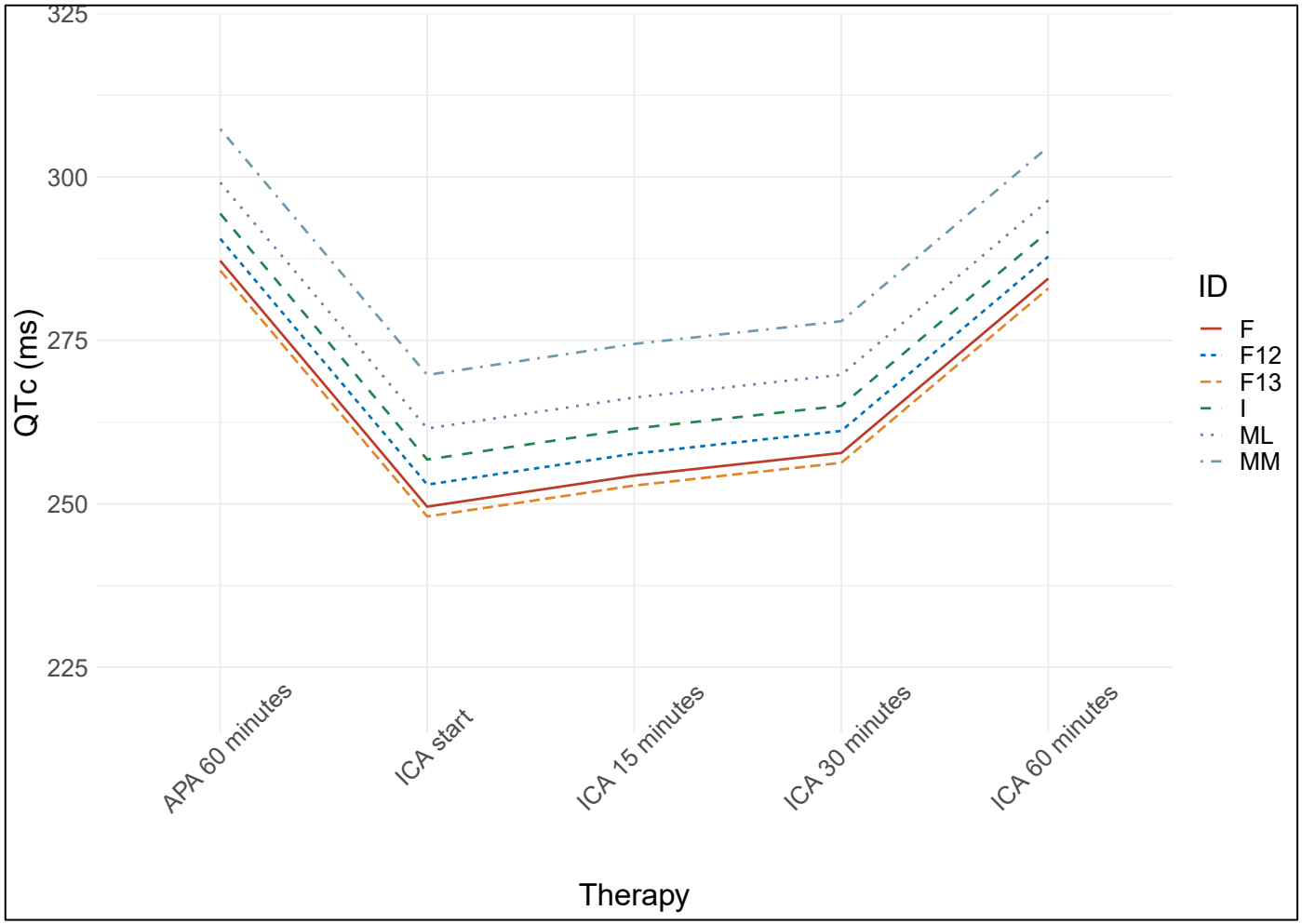

Figure 5.13. Mixed Effects Linear Regression Model Assessing the Effect of ICA-105574 on the QTc Interval in a Drug-Induced Model of LQT3

Dots, which are color coded, represent measurements from an individual animal. Colored lines represent the model fit superimposed on the raw data for each individual animal.

Moreover, as shown in Table 5.27 and Figures 5.14 and 5.15, ICA-105574 was able to completely normalize the QTc interval in our drug-induced model of LQT3.

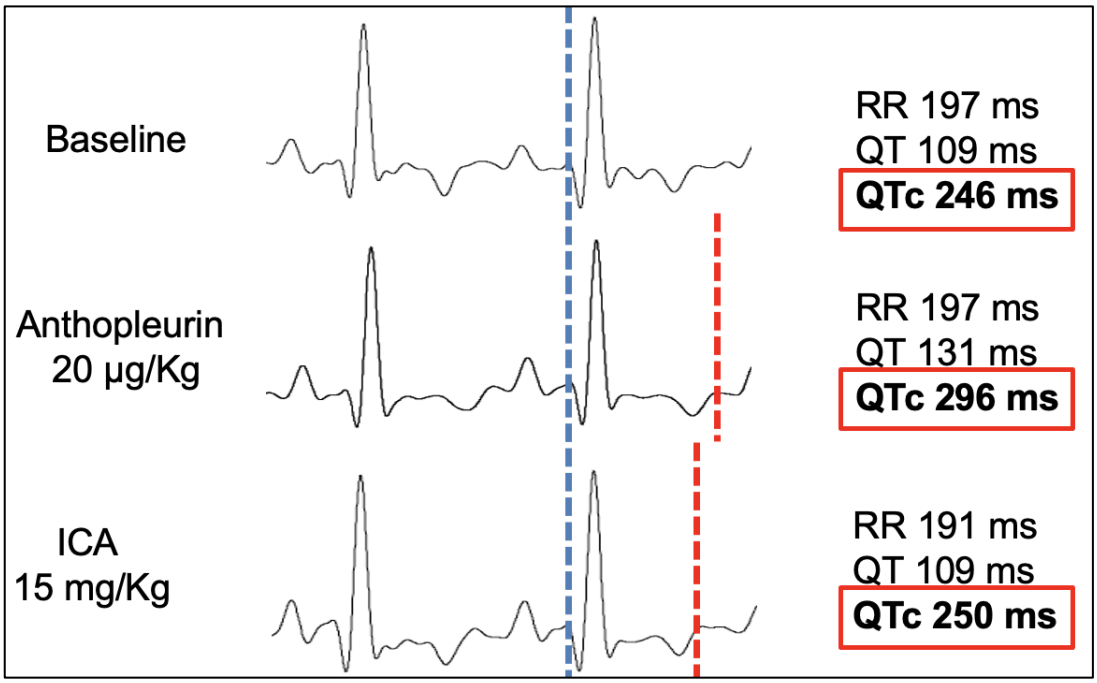

Figure 5.14. ICA-105574 Mediates QTc Interval Normalization in a Drug-Induced Guinea Pig Model of LQT3

N=6 animals	QTcB, ms (median, IQR)	ΔQTcB, ms (%)	p-value
Baseline	262, 252-263	Ref.	Ref.
APA 60 minutes	296, 293-297	+35 (+14%)	***<0.001***
ICA-105574 start	254, 250-266	-2 (-1%)	0.334

Table 5.27. Mixed Effects Linear Regression Assessing the Ability of ICA-105574 to Normalize QTcB interval to Baseline Values in a Drug-Induced Model of LQT3

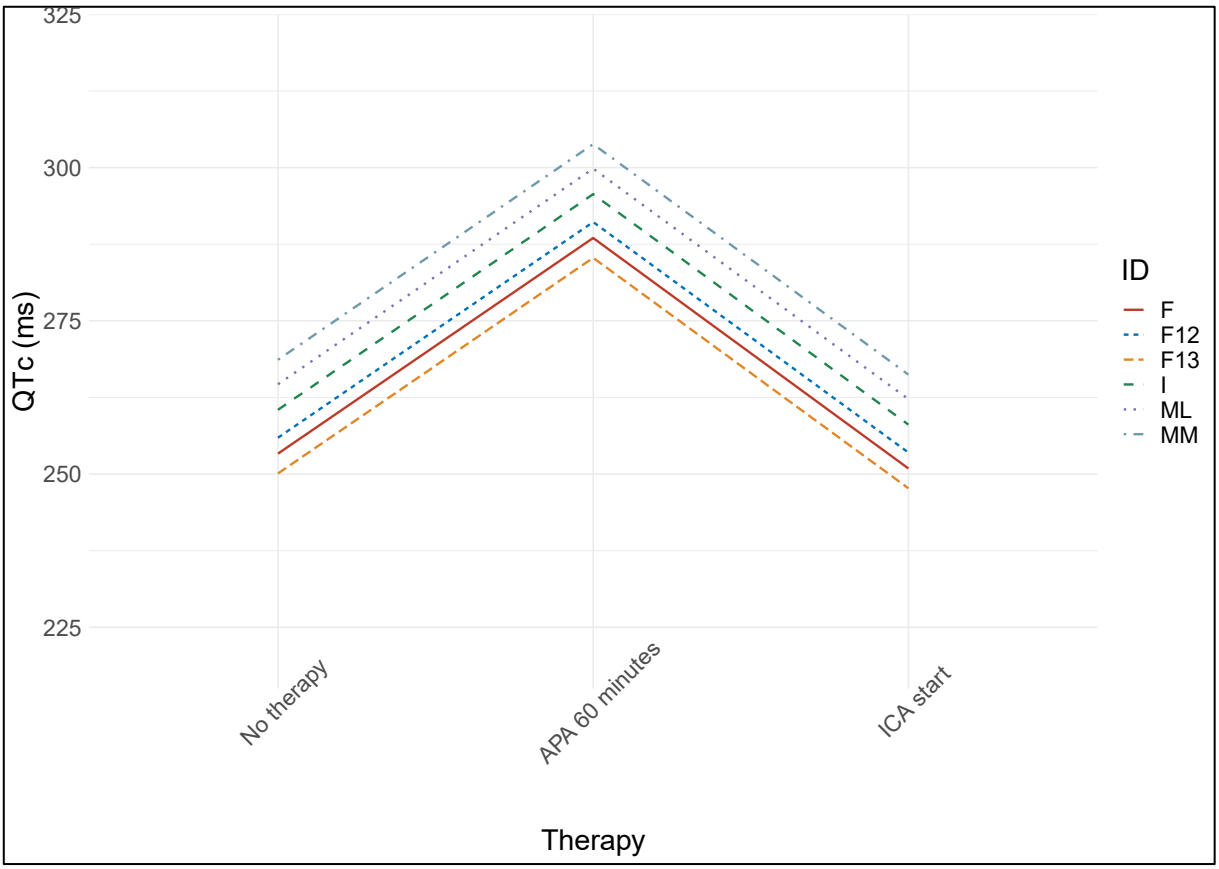

Figure 5.15. Mixed Effects Linear Regression Model Assessing the Effect of ICA-105574 to Normalize the QTc Interval in a Drug-Induced Model of LQT3.

Dots, which are color coded, represent measurements from an individual animal. Colored lines represent the model fit superimposed on the raw data for each individual animal.

5.1.2.3 HERG1 Channel Agonists in Drug-Induced Model of LQT8

After intraperitoneal administration of ICA-105574 at a dose of 15 mg/kg, the drug effects on principal electrocardiographic parameters were assessed.

No biologically significant effects on the principal electrocardiographic parameters, excluding the QT and QTc interval, were observed (Tables 5.28-5.31).

Importantly, a pronounced and statistically significant shortening of the QTc interval was consistently obtained in all guinea pigs (Tables 5.28 and 5.32; Figure 5.16). Specifically, the overall effect of ICA-105574 appears to be strong, as corroborated by relatively narrow confidence intervals at each timepoint (Table 5.32; Figure 5.17). Inter-animal variance appears to be relatively low and has been estimated to be in the order of 31% (ICC=0.314).
Relevantly, despite marked QTc shortening induced by ICA-105574, during the prolonged electrocardiographic registration no proarrhythmic events were observed.

The pharmacological effects of the drug were most pronounced immediately after the drug administration and 15 minutes after. At 30 and 60 minutes we observed a gradual waning of the drug effect (Table 5.32; Figure 5.17).

N=6 animals	RR, ms (median, IQR)	ΔRR, ms (%)	PR, ms (median, IQR)	ΔPR, ms (%)	QRS, ms (median, IQR)	ΔQRS, ms (%)	QTcB, ms (median, IQR)	ΔQTcB, ms (%)
Bay K8644 45 minutes	214, 197-231	Ref.	57, 53-57	Ref.	23, 23-23	Ref.	286, 279-296	Ref.
ICA-105574 start	217, 209-226	+3 (+1%)	57, 57-61	0 (0%)	23, 23-23	0 (0%)	238, 232-239	-48 (-17%)
ICA-105574 15 minutes	171, 171-176	-43 (-20%)	57, 53-57	0 (0%)	23, 23-23	0 (0%)	246, 237-248	-40 (-14%)
ICA-105574 30 minutes	193, 186-203	-21 (-10%)	57, 57-57	0 (0%)	23, 23-23	0 (0%)	281, 275-284	-5 (-2%)
ICA-105574 60 minutes	206, 197-223	-8 (-4%)	57, 57-57	0 (0%)	23, 23-23	0 (0%)	279, 267-284	-7 (-2)

Table 5.28. Principal Electrocardiographic Parameters After Induction of LQT8 and After Administration of ICA-105574.

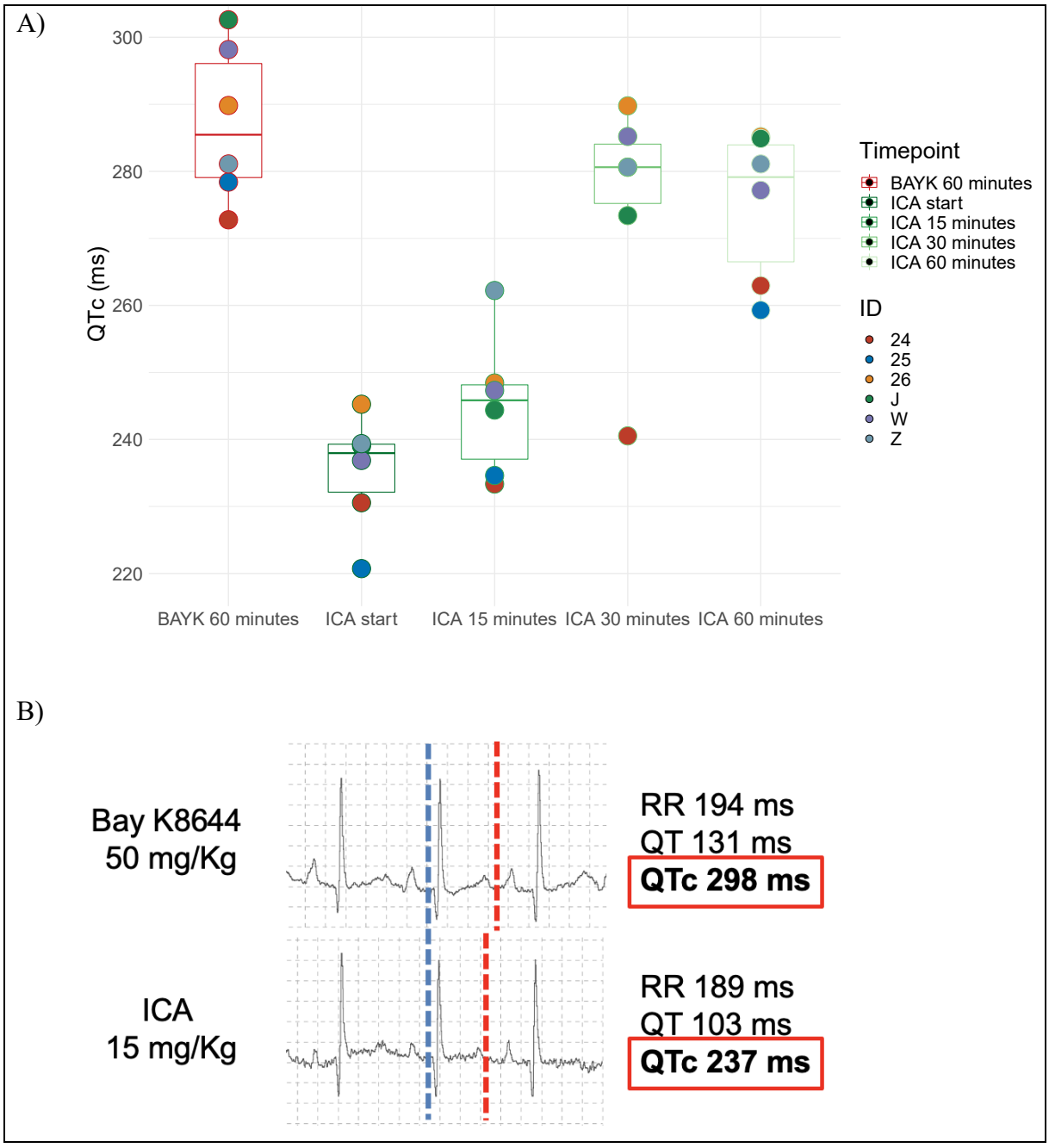

Figure 5.16. Effect of ICA-105574 on the QTc Interval in a Drug-Induced Guinea Pig Model of LQT8

Panel A: Boxplot of median QTc values per animal at different timepoints. Each colored dot represents an animal.

Panel B: Electrocardiographic example of ICA-105574 effect on the QTc interval in a drug-induced model of LQT8. Blue line shows the beginning of the Q wave, whereas the red line shows the end of the T wave. The distance from the blue line to the red line is the QT interval. Correction of the QT interval for the preceding RR interval, as described by Bazett[30], yields the QTc interval.

N=6 animals	RR, ms (median, IQR)	ΔRR, ms (%)	p-value
Bay K8644 45 minutes	214, 197-231	Ref.	Ref.
ICA-105574 start	217, 209-226	+3 (+1%)	1.000
ICA-105574 15 minutes	171, 171-176	-43 (-20%)	***<0.001***
ICA-105574 30 minutes	193, 186-203	-21 (-10%)	***<0.001***
ICA-105574 60 minutes	206, 197-223	-8 (-4%)	***<0.001***

Table 5.29. Mixed Effects Linear Regression Assessing the Effect of ICA-105574 on RR interval in a Drug-Induced Guinea Pig Model of LQT8

N=6 animals	PR, ms (median, IQR)	ΔPR, ms (%)	p-value
Bay K8644 45 minutes	57, 53-57	Ref.	Ref.
ICA-105574 start	57, 57-61	0 (0%)	-
ICA-105574 15 minutes	57, 53-57	0 (0%)	-
ICA-105574 30 minutes	57, 57-57	0 (0%)	-
ICA-105574 60 minutes	57, 57-57	0 (0%)	-

Table 5.30. Mixed Effects Linear Regression Assessing the Effect of ICA-105574 on PR interval in a Drug-Induced Guinea Pig Model of LQT8

N=6 animals	QRS, ms (median, IQR)	ΔQRS, ms (%)	p-value
Bay K8644 45 minutes	23, 23-23	Ref.	Ref.
ICA-105574 start	23, 23-23	0 (0%)	-
ICA-105574 15 minutes	23, 23-23	0 (0%)	-
ICA-105574 30 minutes	23, 23-23	0 (0%)	-
ICA-105574 60 minutes	23, 23-23	0 (0%)	-

Table 5.31. Mixed Effects Linear Regression Assessing the Effect of ICA-105574 on QRS interval in a Drug-Induced Guinea Pig Model of LQT8

N=6 animals	QTcB, ms (median, IQR)	ΔQTcB, ms (%)	p-value
Bay K8644 45 minutes	286, 279-296	Ref.	Ref.
ICA-105574 start	238, 232-239	-48 (-17%)	***<0.001***
ICA-105574 15 minutes	246, 237-248	-40 (-14%)	***<0.001***
ICA-105574 30 minutes	281, 275-284	-5 (-2%)	***<0.001***
ICA-105574 60 minutes	279, 267-284	-7 (-2)	***<0.001***

Table 5.32. Mixed Effects Linear Regression Assessing the Effect of ICA-105574 on QTcB interval in a Drug-Induced Guinea Pig Model of LQT8

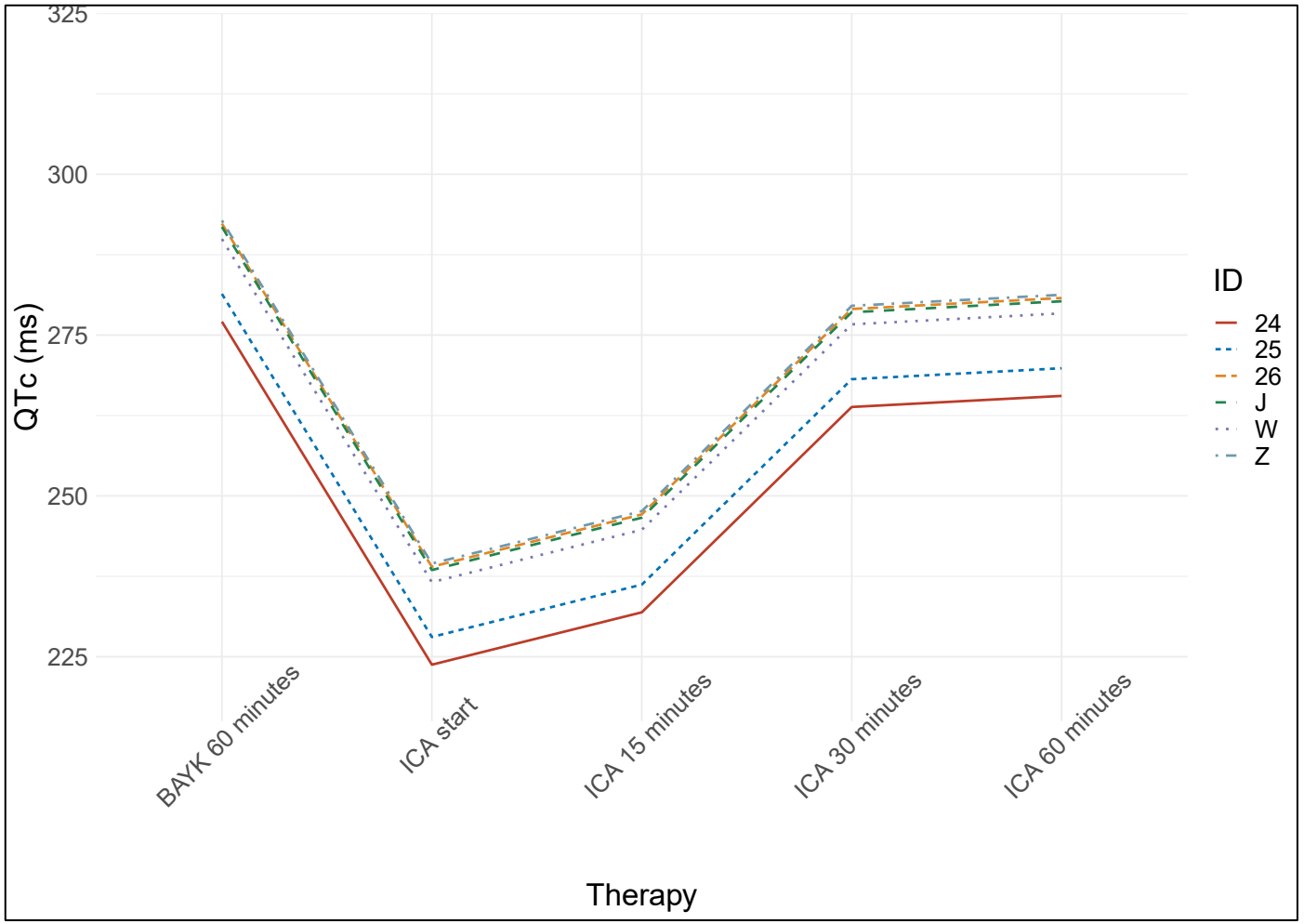

Figure 5.17. Mixed Effects Linear Regression Model Assessing the Effect of ICA-105574 on the QTc Interval in a Drug-Induced Model of LQT8.

Dots, which are color coded, represent measurements from an individual animal. Colored lines represent the model fit superimposed on the raw data for each individual animal.

Moreover, as shown in Table 5.33 and Figures 5.18 and 5.19, ICA-105574 was able to completely normalize the QTc interval in our drug-induced model of LQT8.

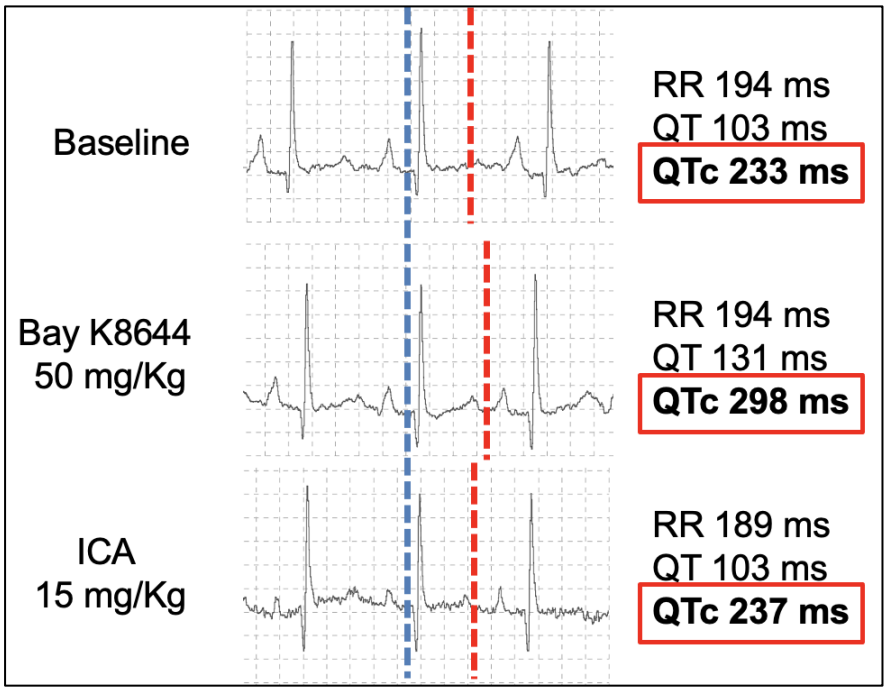

Figure 5.18. ICA-105574 Mediates QTc Interval Normalization in a Drug-Induced Guinea Pig Model of LQT8

N=6 animals	QTcB, ms (median, IQR)	ΔQTcB, ms (%)	p-value
Baseline	245, 236-245	Ref.	Ref.
Bay K8644 45 minutes	286, 279-296	+49 (+21%)	***<0.001***
ICA-105574 start	238, 232-239	-4 (-2%)	0.131

Table 5.33. Mixed Effects Linear Regression Assessing the Ability of ICA-105574 to Normalize QTcB interval to Baseline Values in a Drug-Induced Model of LQT8

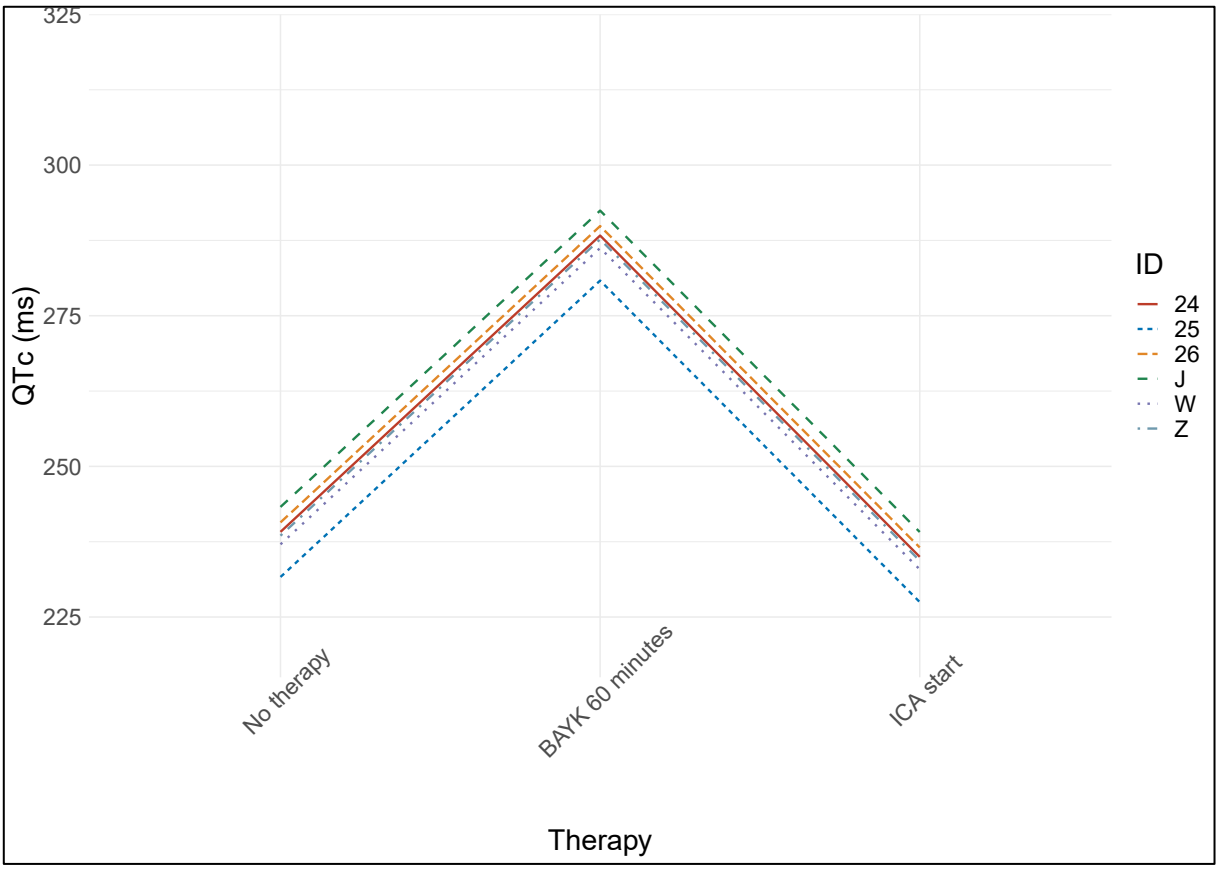

Figure 5.19. Mixed Effects Linear Regression Model Assessing the Effect of ICA-105574 to Normalize the QTc Interval in a Drug-Induced Model of LQT8.

Dots, which are color coded, represent measurements from an individual animal. Colored lines represent the model fit superimposed on the raw data for each individual animal.

5.1.2.4 Summary of Drug-Induced Long QT Syndrome Models

To summarize, we successfully tested ICA-105574 in three different models of Long QT Syndrome (Figure 5.20).

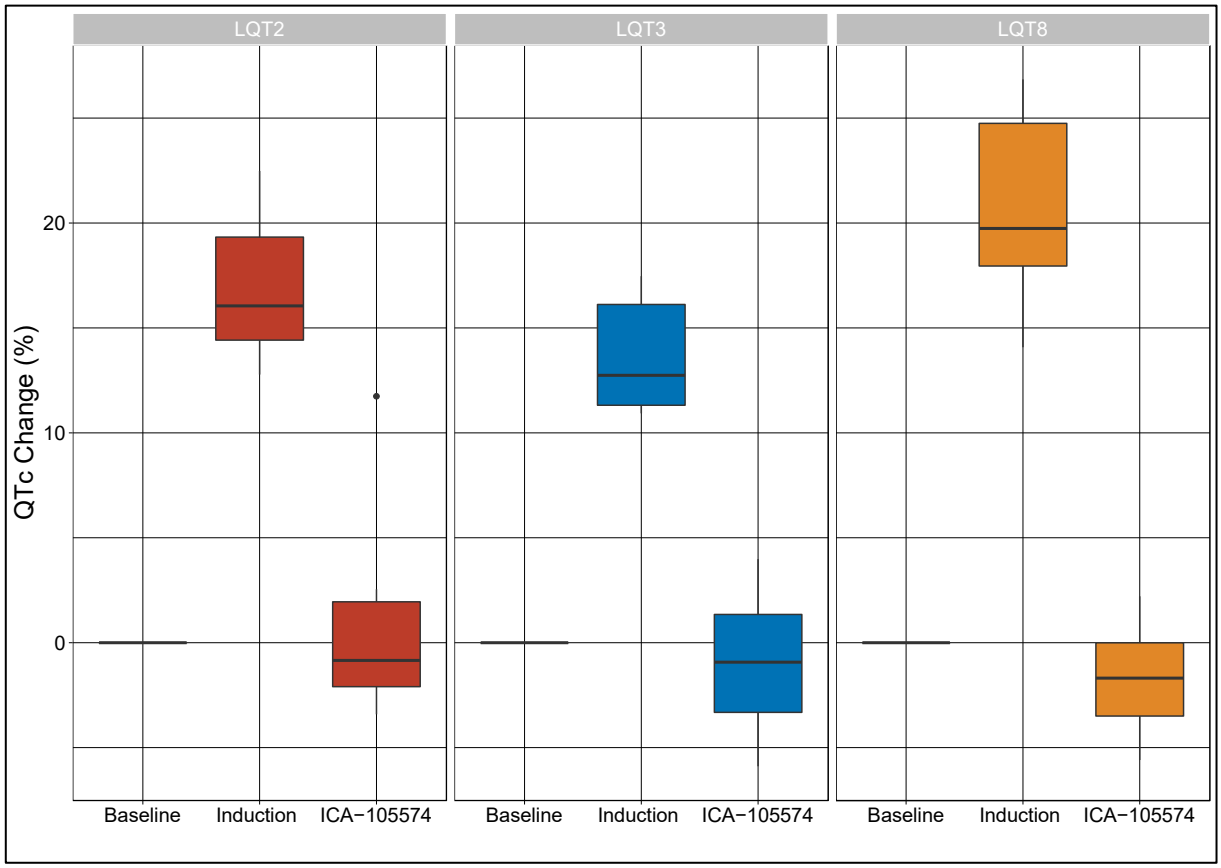

Figure 5.20. Summary of the Percentual Change in QTc with ICA-105574 in Three Drug-Induced Models of LQTS.

On average, upon ICA-105574 administration the QTc interval shortened by 14±4 %, 13±4 %, and 19±3 % in LQT2, LQT3, and LQT8, respectively, as compared to induction values (Figure 5.20). Relevantly, QT interval after ICA-105574 was not different as compared to baseline (LQT2: 1±5%; LQT3: -1±4%; LQT8: -2%±3%: p=ns for all).

Page intentionally left blank.

5.2 PHASE TWO: HERG1 Channel Agonist Testing in a Large Mammal Knock-in Model of LQTS

In Phase One, we have shown in three different drug-induced models that ICA-105574, a novel HERG1 channel agonist, can efficaciously and safely shorten and normalize the QT interval.

Although drug-induced models, using sotalol used to reproduce LQT2[108] and anthopleurin-A to mimic LQT3[12] have been pivotal in advancing the knowledge on LQTS-related arrhythmogenesis, they have limitations[109], such as the lack of specificity at the high concentrations of the drug used and the all-or-none effect that does not replicate the coexistence of normal and abnormal proteins in the cells from heterozygous carriers, as is the case of the vast majority of patients with LQTS.

We exploited the opportunity to study *in vivo* the effects and safety of ICA-105574 using the first successful knock-in large mammal model of a cardiac channelopathy. The study of swine models has been a valuable asset in cardiac electrophysiology to help bridge the translation gap from basic research to humans[110]. Due to the similarities in anatomy and electrophysiological properties between pigs and humans[111,112], our porcine model of TS1 allows for studying the pharmacological effects of ICA-105574 in physiological conditions and using clinical-grade equipment, including electroanatomical mapping.

Having in mind the aforementioned, in Phase Two, we have first characterized *in vivo* the phenotype of our novel knock-in model of LQT8 (TS1 pig). Following the baseline characterization, we investigated the effects of ICA-105574 on the QTc interval, but also its effect on dispersion of repolarization, which has been shown to be crucial for arrhythmogenesis. Considering the above-mentioned limitations of drug-induced models of LQTS, assessment of dispersion of repolarization and its hypothetical modifications is only possible in a large mammal model, which renders the Phase Two of the study fundamental and indispensable for a robust assessment of efficacy and safety of ICA-105574, an exponent of a novel class of antiarrhythmics.

5.2.1 In Vivo Characterization of Knock-in Model of LQT8

5.2.1.1 12-Lead Electrocardiogram

Over the past years, we have been extensively characterizing our novel TS1 knock-in pig model. A fundamental aspect of in vivo characterization is represented by the 12-lead electrocardiogram.

In N=55 pigs studied at CNIC (TS1 N=28 [51%] and wild-type [WT] N=27 [49%]), at 10.8 months [IQR: 9.8-11.2] of age, a resting ECG was recorded, as described in Section Methods, subsection In Vivo Characterization of Knock-in Model of LQT8. Importantly, the 12-lead electrocardiogram (ECG) showed significant QTc interval prolongation in TS1 pigs (586 ms [IQR: 558-615 ms]) *vs*. WT (482 ms [IQR: 469-500 ms]; p<0.001) controls (Table 5.34, Figures 5.21 and 5.22). Relevantly, the shortest QTc interval recorded in TS1 pigs was longer than the longest QTc interval recorded in WT pigs (Figure 5.22). To further investigate this, a receiver operator characteristic curve was fitted, which allowed to identify that a cut-off of 523 ms was 93% sensible and 100% specific for identifying the genotype of the pig (AUC=1).

Lastly, TS1 pigs tended to be slightly more bradycardic than their WT littermates (820 ms [IQR: 735-935 ms] *vs*. 774 ms [680-850 ms]; p=0.025) (Table 5.34).

Variable	WT (N=27)	TS1 (N=28)	p-value
Male gender (N [%])	18 (67)	17 (61)	0.646
Age (months), median [IQR]	10.6 [9.5-11.4]	10.9 [9.8-11.2]	0.381
Weight (kg), median [IQR]	54 [50-60]	48 [45-51]	***<0.001***
Temperature (C°), median [IQR]	37.3 [36.9-37.7]	37.4 [36.9-37.6]	0.839
PR (ms), median [IQR]	150 [129-169]	160 [150-172]	0.262
QRS (ms), median [IQR]	80 [75-81]	89 [80-99]	***0.006***
RR (ms), median [IQR]	774 [680-850]	820 [735-935]	***0.025***
QT (ms), median [IQR]	440 [380-450]	550 [495-580]	***<0.001***
QTc (ms), median [IQR]	482 [469-500]	586 [558-615]	***<0.001***

Table 5.34. Main electrocardiographic parameters in WT pigs as compared to TS1 pigs.

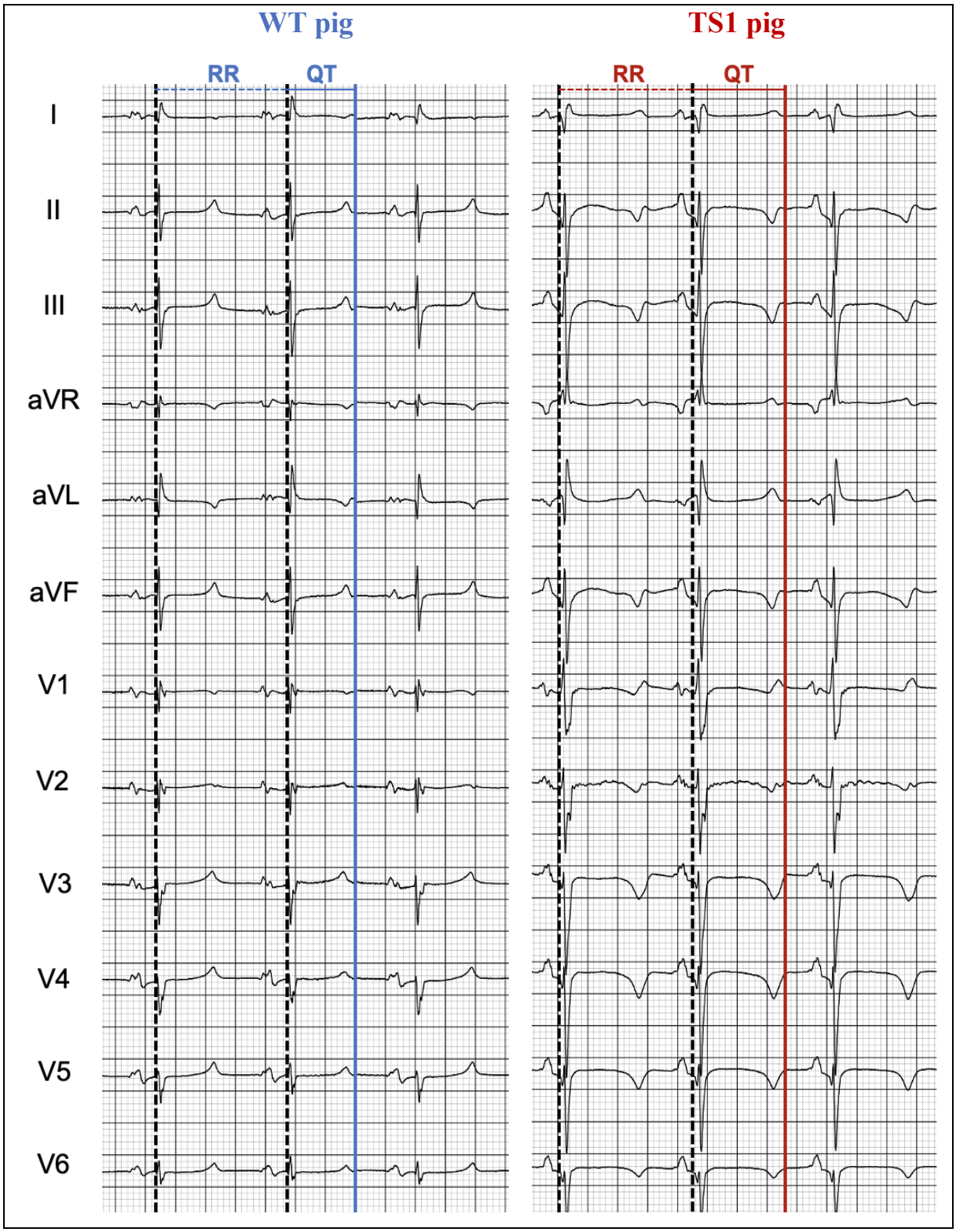

Figure 5.21. 12-lead electrocardiogram in WT pigs vs. TS1 pigs.

The distance between the dotted line and the colored full line (blue in WT, red in TS1) represents the QT interval. The distance between two vertical dotted black lines represents the RR, which was used to correct the QT interval, using the Bazett formula[30].

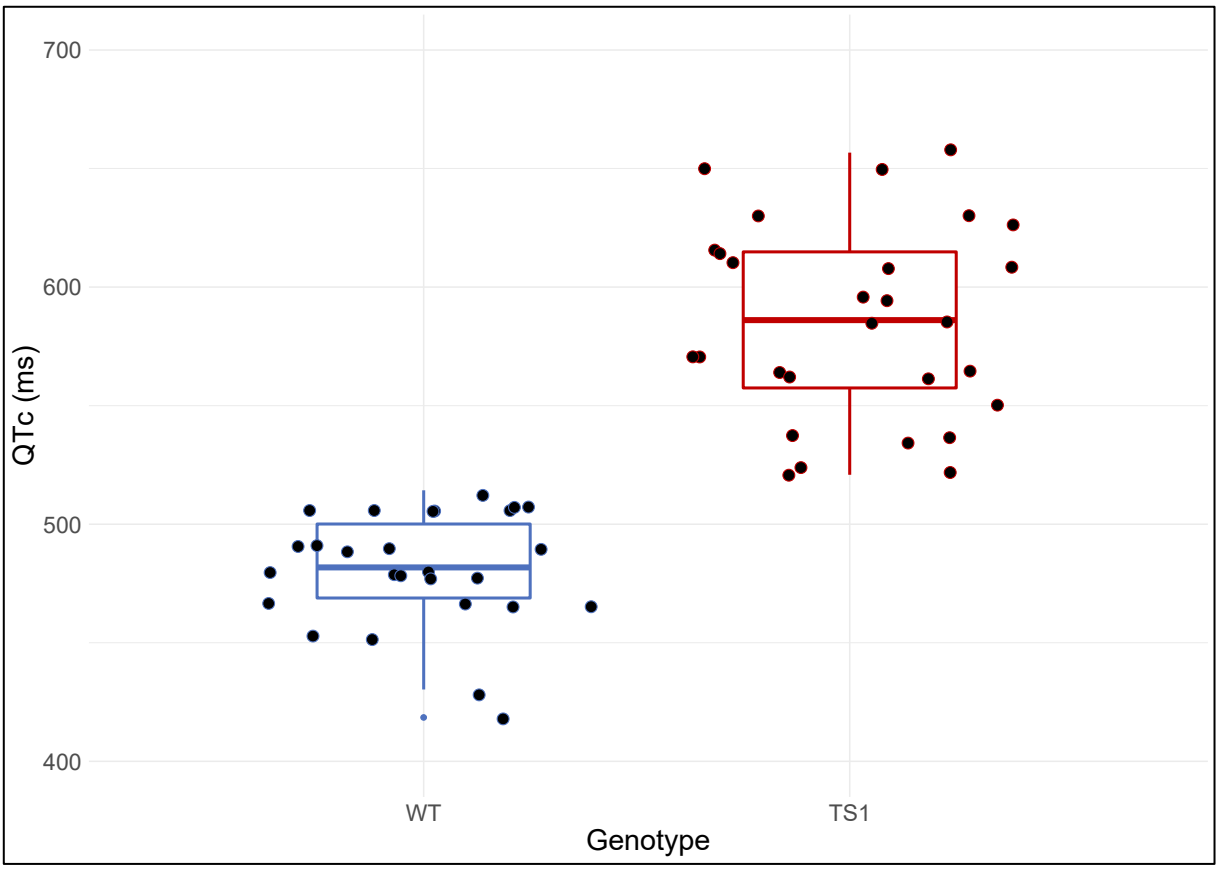

Figure 5.22. Boxplot Summarizing the QTc Intervals in WT and TS1 pigs

TS1 pigs (in red) show a significantly longer QTc interval as compared to their age- and sex-matched WT littermates (in blue).

5.2.1.2 Survival Analysis

After ascertaining that our TS1 pig model presents electrocardiographic alterations compatible with human disease (i.e., QTc interval prolongation), our focus shifted to the assessment of survival of TS1 pigs as compared to their WT littermates.

Importantly, TS1 pigs displayed high mortality *in utero* and after birth (Figure 5.23), consistent with human lethality. As shown in Figure 5.23 the cumulative probability of suffering sudden cardiac death at 1 year of follow-up was 34.0% (95% Confidence Interval, CI: 21.0%-44.8%) in TS1 pigs as compared to 0% (95% CI: 0.0%-0.0%) in WT pigs (p<0.001). Relevantly, pig's gender (Figure 5.24) was shown to play a role in survival: the cumulative probability of suffering sudden cardiac death at 1 year of follow-up was 27.6% (95% CI: 14.5%-38.7) in male pigs as compared to 9.5% (95% CI: 1.4%-16.9) in female pigs (p=0.008).

Multivariable Cox analysis modified with Firth's penalized partial likelihood approach confirmed that male gender (Hazard Ratio, HR: 2.8; 95% CI: 1.3-6.2; p=0.005) and TS1 genotype (HR: 55.4, 95% CI: 7.8-7020.7; p<0.0001) were independent and robust predictors for the occurrence of sudden cardiac death at follow-up (Table 5.35).

	N	Events / p-m	Rate x 100 p-m (95% CI)	HR (95% CI)	p-value
Genotype					
WT	261	0/3455	0.0 (0.0-0.1)	Ref.	
TS1	159	34/2863	1.2 (0.1-1.7)	55.4 (7.8-7020.7)	***<0.0001***
Gender					
Female	203	9/3043	0.3 (0.1-0.6)	Ref.	
Male	217	25/3275	0.8 (0.5-1.1)	2.8 (1.3-6.2)	***0.005***

Table 5.35. Predictors for the occurrence of SCD according to multivariable Cox regression in our pig colony

The outcome is the occurrence of sudden cardiac death. Abbreviations: WT, wild type; TS1, Timothy syndrome; p-m, person-months; CI, confidence intervals.

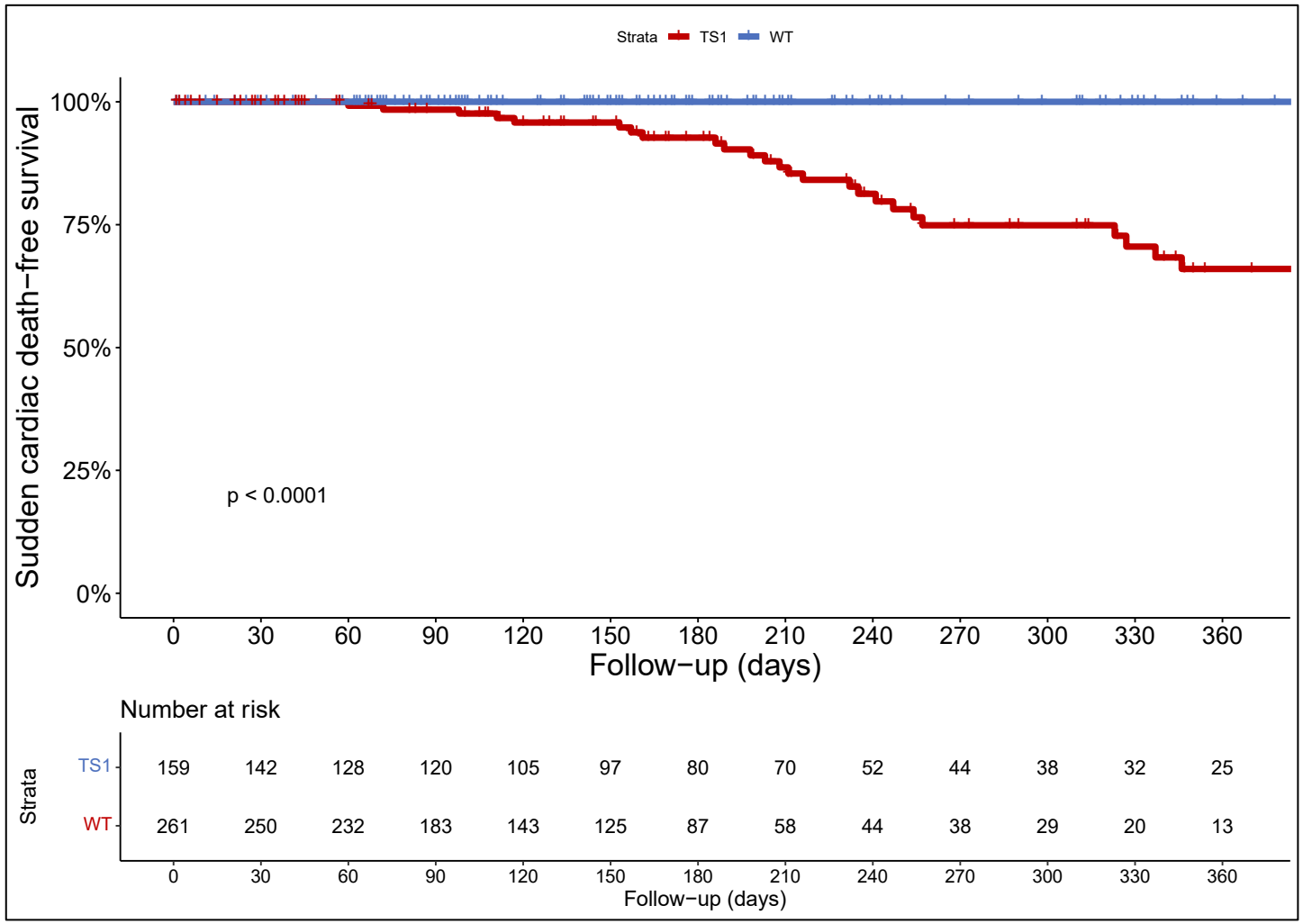

Figure 5.23. Kaplan-Meyer estimate of cumulative survival free from the sudden cardiac death in WT pigs and TS1 pigs.

The cumulative probability of experiencing sudden cardiac death was 1.6% (95% CI: 0.0%-3.7%), 7.3% (95% CI: 2.2%-12.0%), 25.1% (95% CI: 14.7%-34.2) and 34.0% (95% CI: 21.0%-44.8%) at 3, 6, 9, and 12 months of follow up in TS1 pigs. No WT pigs died suddenly.

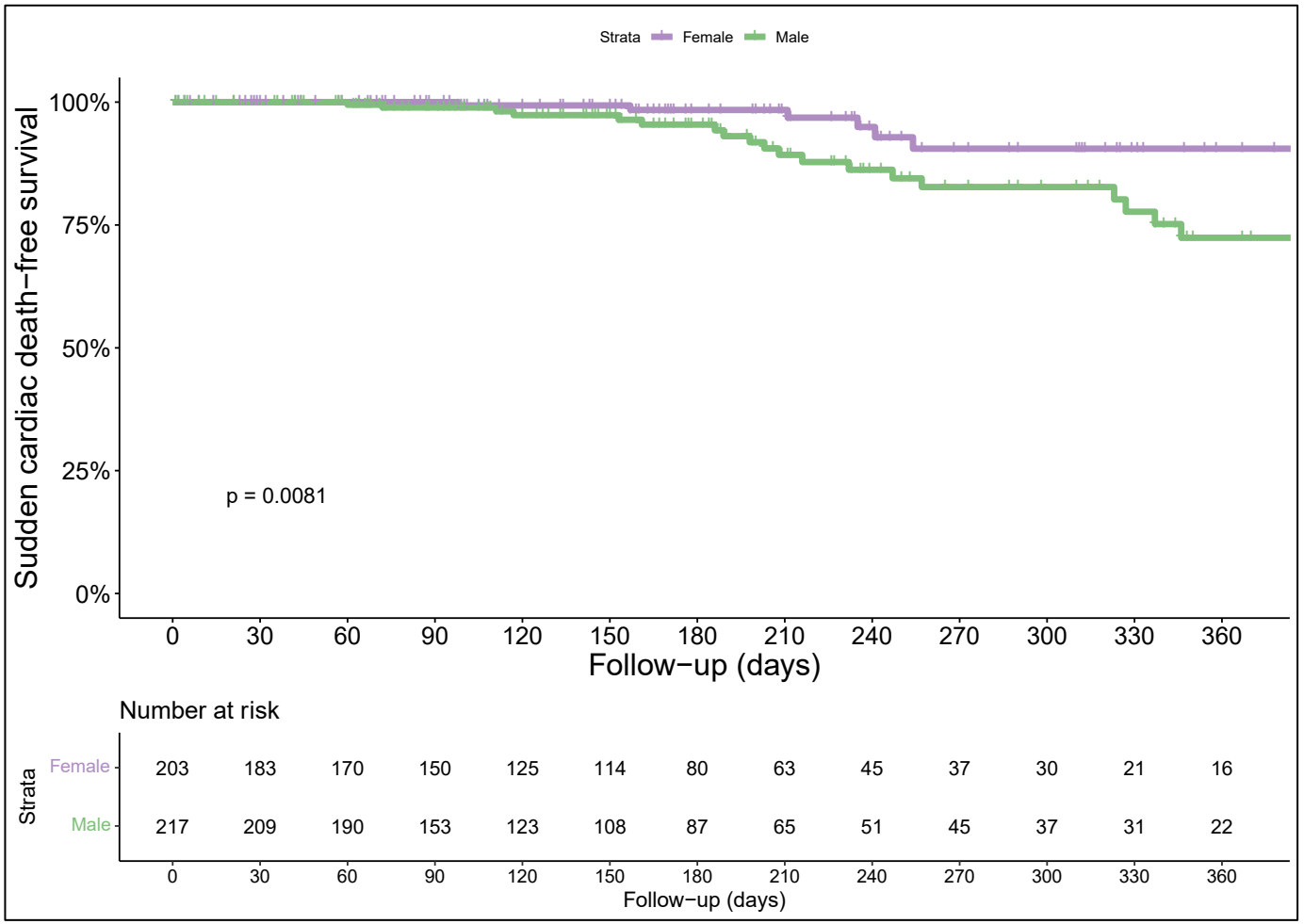

Figure 5.24. Kaplan-Meyer estimate of cumulative survival free from the sudden cardiac death in male and female pigs.

The cumulative probability of experiencing sudden cardiac death was 0.0% (95% CI: 0.0%-0.0%), 1.6% (95% CI: 0.0%-3.8%), 9.5% (95% CI: 1.4%-16.9) and 9.5% (95% CI: 1.4%-16.9) in female pigs and 1.1% (95% CI: 0.0%-2.6%), 4.6% (95% CI: 0.8%-8.2%), 17.3% (95% CI: 8.3%-25.4) and 27.6% (95% CI: 14.5%-38.7) in male pigs at 3,6, 9, and 12 months of follow up, respectively.

To establish that the cause of sudden cardiac death was the occurrence of ventricular fibrillation (VF), N=30 randomly selected TS1 pigs were implanted with subcutaneous loop recorders. As shown in Figures 5.25 and 5.26, we have documented the occurrence of polymorphic ventricular tachycardia degenerating into ventricular fibrillation (VF) in 11/30 (37%) as the cause of sudden death.

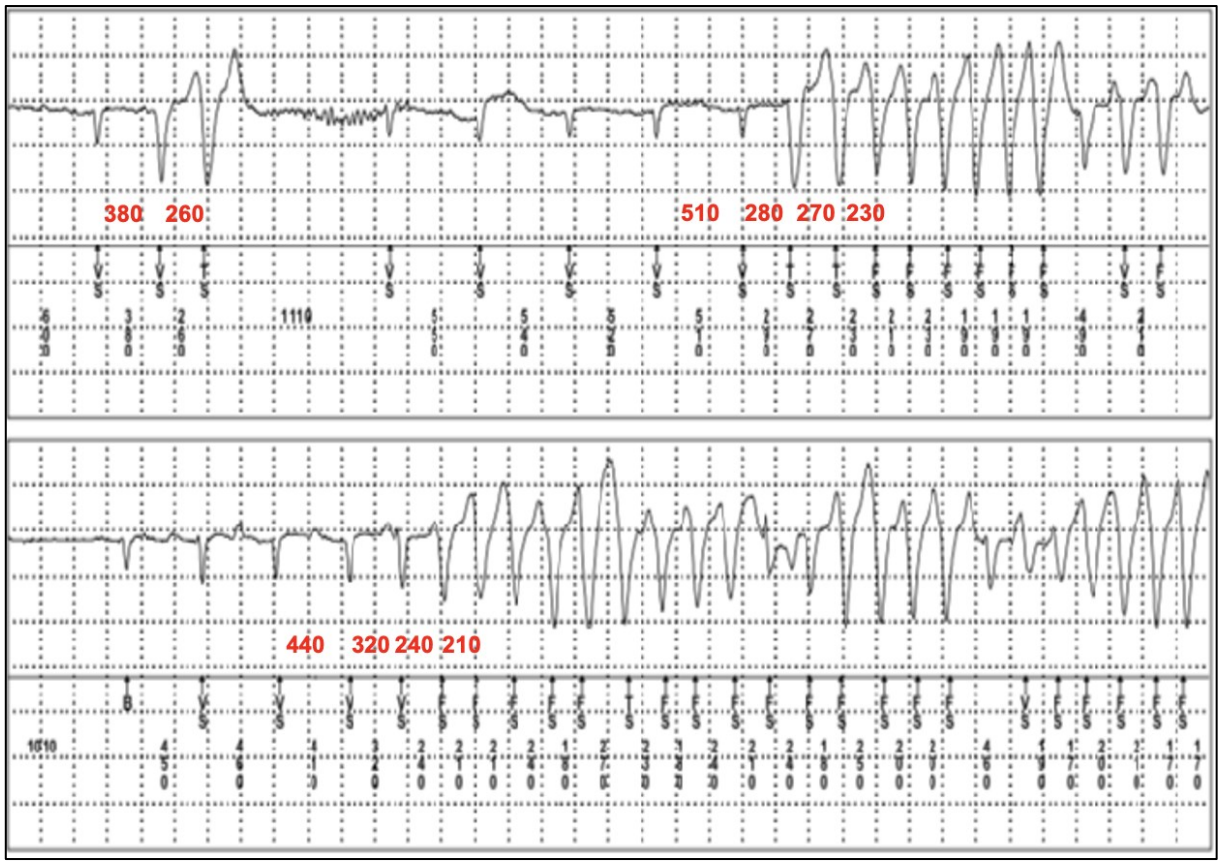

Figure 5.25. Post-mortem interrogation of the subcutaneous implantable loop recorder demonstrating VF as the cause of death

After experiencing sudden cardiac death, the interrogation of the subcutaneous implantable loop recorder showed the occurrence of a ventricular couplet, followed by a brief run of non-sustained ventricular tachycardia, and lastly the onset of polymorphic ventricular tachycardia degenerating into ventricular fibrillation (not shown in this recording). In red, the coupling intervals of ventricular beats are shown.

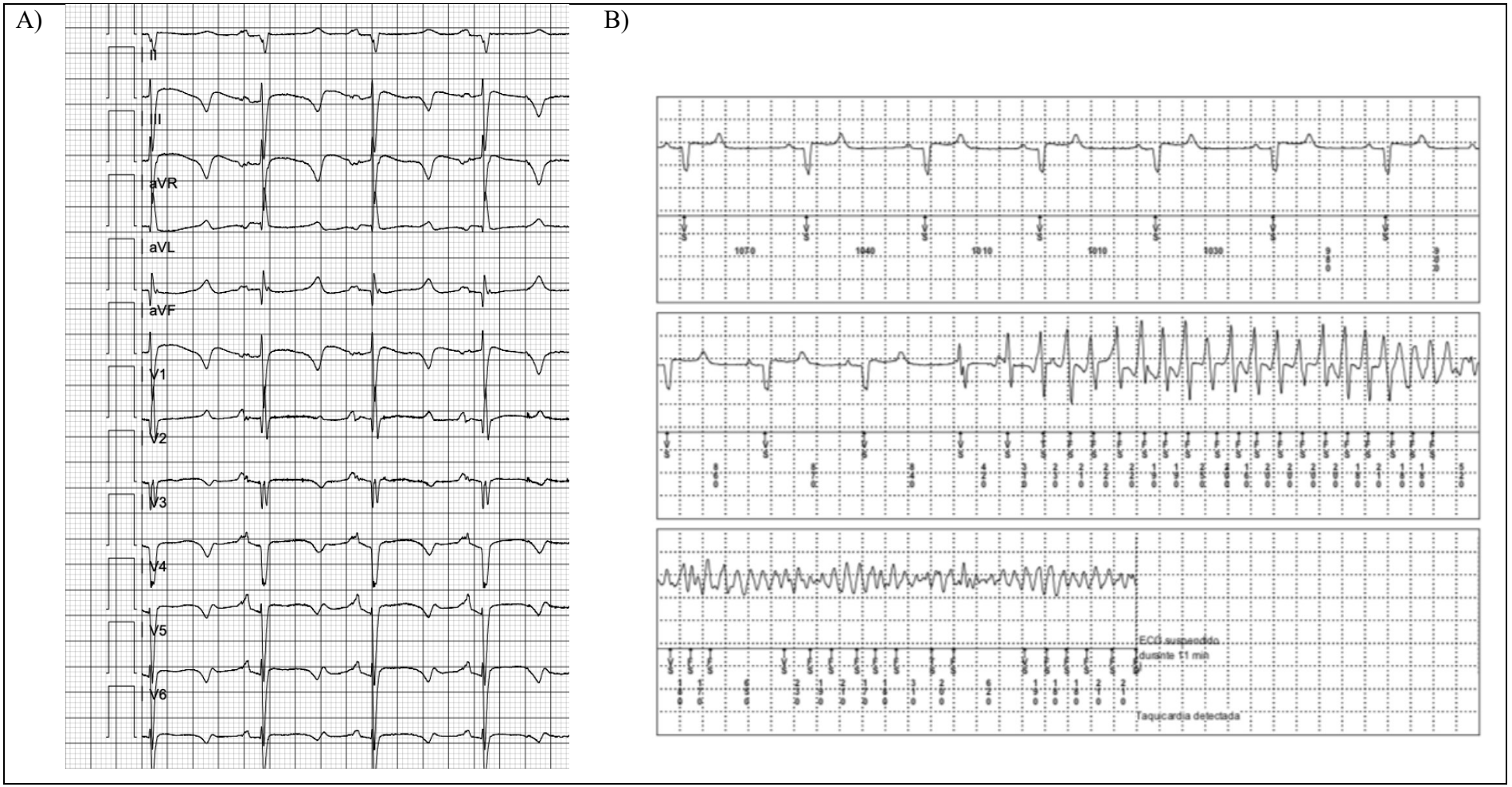

Figure 5.26. Ventricular Fibrillation as the Cause of Death in a TS1 pig.

In this female TS1 pig, electrocardiogram showed a marked QTc prolongation (Panel A; QTc 540 ms). Several days later, the animal suffered a sudden cardiac death, and post-mortem implantable loop recorder interrogation showed the onset of polymorphic ventricular tachycardia rapidly degenerating into ventricular fibrillation.

5.2.1.3 Structural Characterization using Cardiac Magnetic Resonance

The study population undergoing multiparametric cardiac magnetic resonance (CMR) consisted of n=20 animals, n=10 WT animals and 10 TS1 animals. The animals studied were comparable in terms of age (WT 4.8±0.7 months *vs*. TS1 5.5±2.0 months; p=0.737), body weight (WT animals weighting 63±10 *vs*. TS1 animals weighing 57±15 kg; p=0.343) and BSA (1.11±0.11 in WT group vs. 1.04±0.17 in TS1 group, p=0.316). One exam (n=1 TS1 animal) was not of sufficient quality and therefore was excluded from the present analysis.

Firstly, normal reference values for our laboratory were established, as described in the Section Methods, subsection In Vivo Characterization of the Phenotype in a Knock-In Model of Long QT Syndrome. The results are shown in Table 5.36.

Parameter	Lower reference limit	Upper reference limit
Left Ventricle		
LV EDV - BSA indexed (ml/m^2)	100	167
LV ESV - BSA indexed (ml/m^2)	35	77
LV SV - BSA indexed (ml/m^2)	57	98
LV EF (%)	50	67
LV CO - BSA indexed (l/min/m^2)	3.30	8.47
LV mass - BSA indexed (g/m^2)	66	89
Right Ventricle		
RV EDV - BSA indexed (ml/m^2)	72	152
RV ESV - BSA indexed (ml/m^2)	17	57
RV SV - BSA indexed (ml/m^2)	53	97
RV EF (%)	59	75
RV CO - BSA indexed (l/min/m^2)	3.24	8.16
Tissue Characterization Parameters		
Native T1 relaxation time (ms)	995	1143
Partition coefficient (λ)	0.33	0.39
ECV (%)	22.0	28.8
Indexed myocardial mass (g/m^2)	48	68
Indexed ECV mass (g/m^2)	16	23
T2 relaxation time (ms)	40	48

Table 5.36. Normal Reference Values for CMR Parameters in Our Cohort of WT Pigs

TS1 pigs demonstrated normal biventricular dimensions and volumetry (LVEDVi=131±23 ml/m^2 *vs*. 133±14 ml/m^2 in WT, p=0.810; RVEDVi=54±13 ml/m^2 *vs*. 56±9 ml/m^2, p=0.895; Table 5.37 and Figure 5.27), with only one pig demonstrating mild LV dilatation. Importantly, **all TS1 pigs presented normal segmental and global systolic biventricular function** (LVEF=59±4% vs. 58±3% in WT, p=0.592; RVEF=68±4% vs. 67±3% in WT, p=0.641; Table 5.37).

Parameter	WT (n=10)	TS1 (n=9)	p-value
Left Ventricle			
LV EDV - BSA indexed (ml/m^2)	133±14	131±23	0.810
LV ESV - BSA indexed (ml/m^2)	56±9	54±13	0.717
LV SV - BSA indexed (ml/m^2)	78±7	77±11	0.861
LV EF (%)	58±3	59±4	0.592
LV CO - BSA indexed (l/min/m^2)	5.89±0.88	4.88±0.90	***0.025***
LV mass - BSA indexed (g/m^2)	78±5	92±11	***0.002***
Right Ventricle			
RV EDV - BSA indexed (ml/m^2)	112±13	111±18	0.895
RV ESV - BSA indexed (ml/m^2)	37±7	35±9	0.752
RV SV - BSA indexed (ml/m^2)	75±7	75±11	0.979
RV EF (%)	67±3	68±4	0.641
RV CO - BSA indexed (l/min/m^2)	5.70±0.89	4.75±0.88	***0.031***

Table 5.37. Volumetric and Functional CMR Parameters in WT and TS1 Pigs

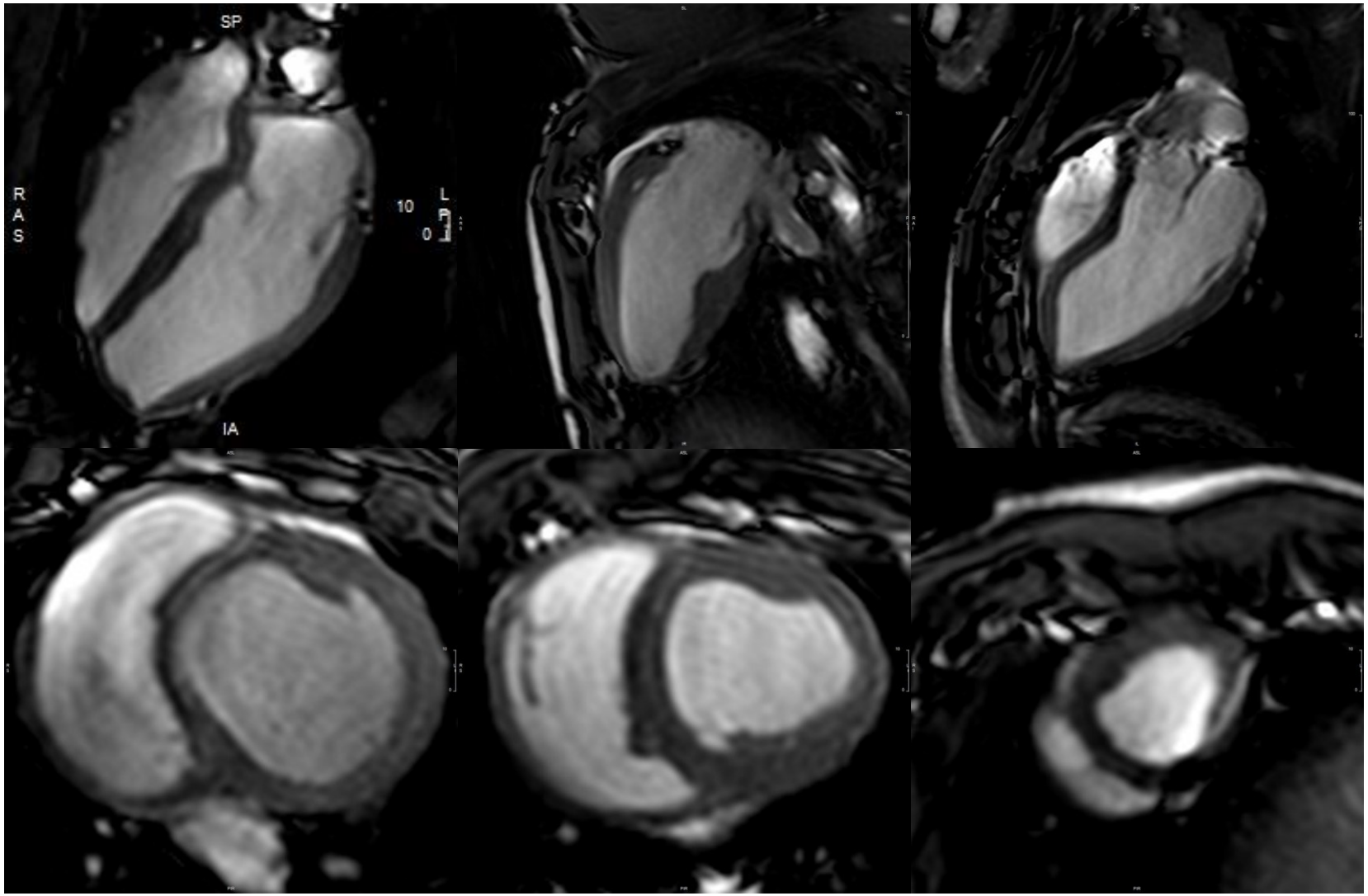

Figure 5.27. Segmented cine steady-state free-precession sequences showing three canonical long axis slices and three short axis slices in a TS1 pig.

Interestingly, TS1 animals had an average 15% increase in cardiac mass (92±11 g/m^2) compared to the WT animals (78±5 g/m^2, p=0.002; Table 5.37). Additionally, TS1 pigs had significantly greater linear measurements of wall thickness in all basal sections as compared to WT animals (Figure 5.28). There were no differences between segment thickness in TS1 animals (one-way ANOVA p=0.547), indicating that the observed hypertrophy is concentric.

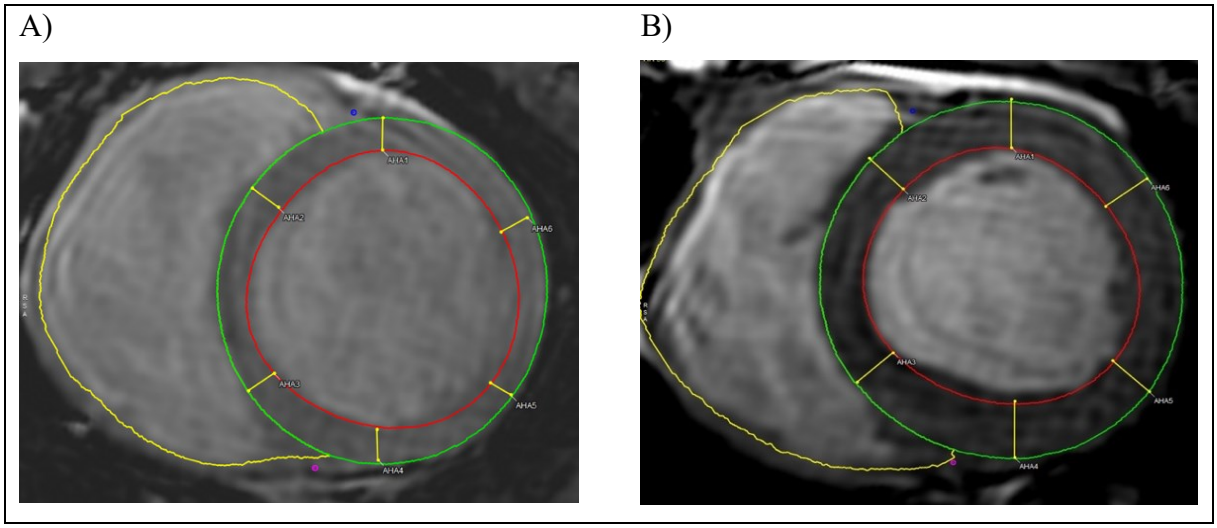

Figure 5.28. Cardiac Magnetic Resonance Imaging in WT and TS1 Pigs

Comparison of corresponding short-axis slices in end-diastole of a WT animal (panel A) and TS1 animal (panel B), with relevant linear measurements.

Half of TS1 animals (5/10, 50%) had a cardiac mass higher than the upper reference limit (URL), confirming the observation made by Splawski and colleagues in patients where 35% of individuals with TS1 presented mild cardiac hypertrophy[27].

Increased cardiac mass was independent of age (r=-0.20, p=0.581), gender (92±11 g/m^2 in males vs. 91±12 g/m^2, p=0.265) and QTc interval (r=0.05, p=0.892). Body weight was weakly associated to the absolute, non-indexed cardiac mass (r=0.69, p=0.03) in TS1 animals, but less than in WT animals (r=0.84, p=0.004).

Focusing on the tissue characterization, analysis of native T1 relaxation times showed that there were no significant differences between TS1 pigs as compared to WT animals (1092±43ms *vs*. 1070±34 ms, p=0.235; Table 5.38).
These findings suggest that no diffuse fibrosis or edema are present, as all TS1 pigs had normal native T1 relaxation times.

Parameter	WT (n=10)	TS1 (n=9)	p-value
Tissue Characterization			
Native T1 relaxation time (ms)	1070±34	1092±43	0.235
Partition coefficient (λ)	0.36±0.01	0.31±0.03	***<0.001***
ECV (%)	25.4±1.38	21.1±1.99	***<0.0001***
Indexed intracellular mass (g/m^2)	57.8±3.7	72.3±9.5	***<0.001***
Indexed ECV mass (g/m^2)	19.9±1.7	19.4±2.4	0.734
T2 relaxation time (ms)	44.23±1.57	44.84±1.23	0.359

Table 5.38. CMR Tissue Characterization Indices in WT and TS1

Interestingly, both the partition coefficient and ECV was significantly lower in the TS1 animals as compared to their WT counterparts (0.31±0.03 vs. 0.36±0.01, p<0.001; 21.1±2% *vs*. 25.4±1.4%, p<0.0001; Table 5.38). Strikingly, the finding of low ECV is reinforced by the finding that indexed intracellular mass (IICM) was significantly higher in TS pigs as compared to WT animals (72.3±9.5 vs. 57.8±3.7 g/m^2, p<0.001; Table 5.38).

T2 relaxation times were similar between the two groups (44.23±1.57 ms in WT vs. 44.84±1.23, p=0.359; Table 5.38), and there were no focal **alterations suggestive of myocardial edema** (Figure 5.29).

No WT nor TS1 animals had any evidence of late gadolinium enhancement suggestive for myocardial fibrosis (Figure 5.29).

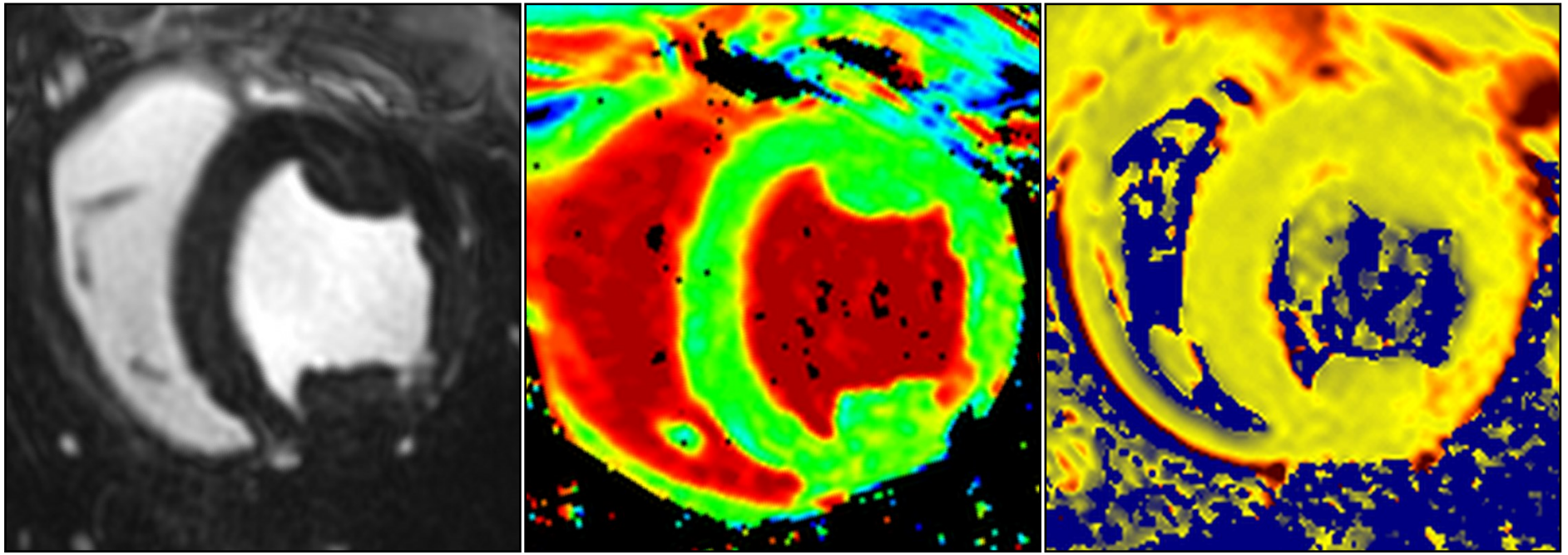

Figure 5.29. Tissue Characterization in TS1 Pig.

Tissue characterization studies did not identify late gadolinium enhancement (left panel) in any TS1 pigs studied. Relevantly, extracellular volume was mildly reduced in TS1 pigs (central panel), a finding compatible with a mild degree of intracellular hypertrophy. No evidence of myocardial edema could be identified using T2 mapping (right panel).

Considering that the sum of intracellular and extracellular mass is a constant, and since there is no evidence of myocardial edema nor of myocardial fibrosis, it is reasonable to hypothesize that the finding of increased intracellular mass is suggestive of a modest degree of intracellular (cardiomyocyte) hypertrophy in the absence of fibrosis.

To confirm this hypothesis, we performed **two** sets of experiments.

Firstly, the Histology Department of CNIC, Madrid performed the histological analysis on explanted hearts of TS1 pigs who died suddenly (Figure 5.30).

Classical hematoxylin and eosin stain (H&E) demonstrated normal morphology of the cardiomyocytes, with regular orientation and normal fiber array. Relevantly, H&E stain showed the absence of inflammatory infiltrate, corroborating the findings from CMR suggesting the absence of myocardial edema.

Picrosirius red staining, a histological stain aimed to identify and study collagen, did not identify any fibrosis on any studied samples. These findings confirm the normal morphology of the hearts of TS1 pigs and are completely concordant with the CMR results outlined above.

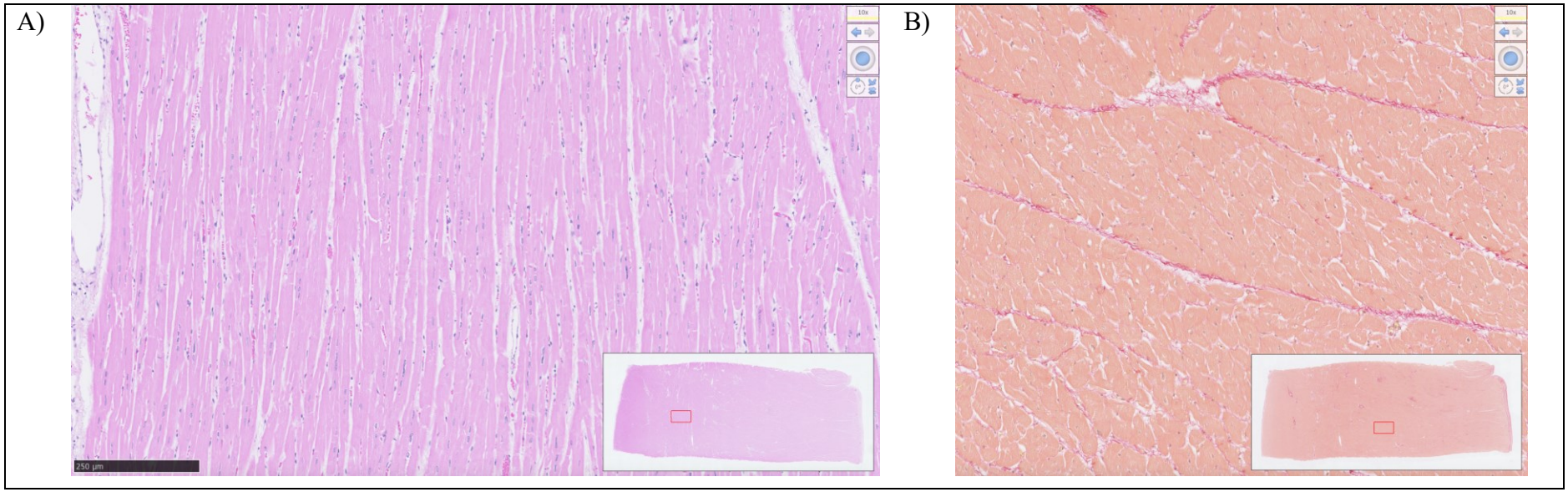

Figure 5.30. Histological samples of TS1 pig hearts.

Panel A: Hematoxylin and eosin stain showing regular fiber array and absence of inflammatory infiltrate.

Panel B: Picrosirius red stain showing absence of fibrosis (panel B).

Having confirmed that the extracellular matrix of the hearts of TS1 animals are not pathologically expanded, Demetrio Julian Santiago, PhD; from our laboratory at CNIC, Madrid studied the dimensions and capacitance of cardiomyocytes deriving from both WT and TS1 animals.

Interestingly, in terms of cellular dimensions, TS1 isolated ventricular cardiomyocytes (median length 13.3 μm [IQR: 11.3-15.7 μm]) were 10% wider than WT animals (median length 11.3 μm [IQR: 9.5-14.0 μm]); p=0.034, Figure 5.31 and Figure 5.32), but were of comparable length (p=0.653, Figure 5.31 and Figure 5.32). These findings were confirmed both by a cell-driven analysis and animal-driven analysis (Figure 5.32).

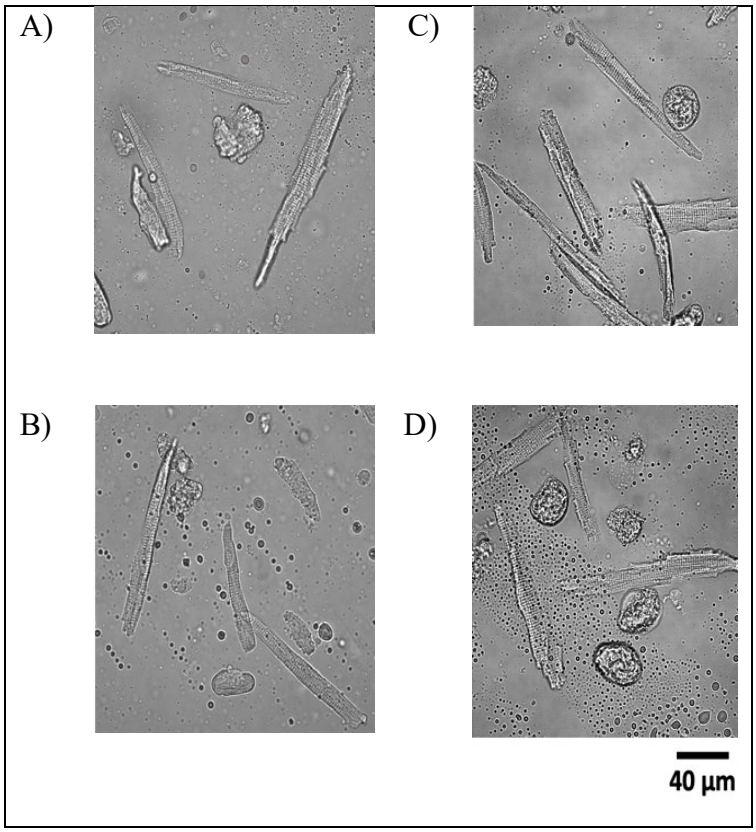

Figure 5.31. Single Cell Analysis of TS1 and WT Ventricular Cardiomyocytes at 40X Magnification.

Panel A: WT ventricular cardiomyocytes

Panel B: TS1 ventricular cardiomyocytes

Courtesy of Demetrio J. Santiago, PhD.

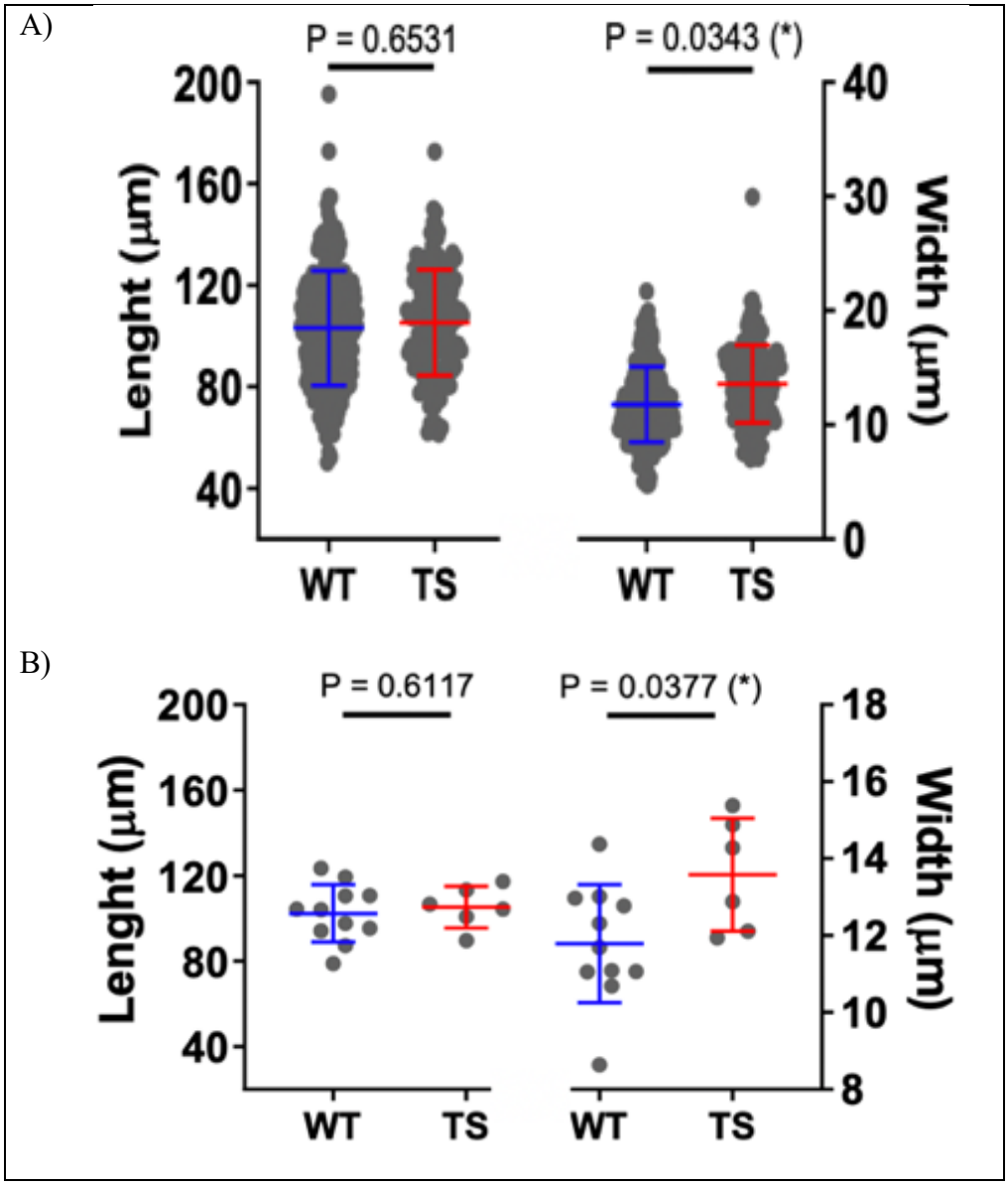

Figure 5.32. Cellular Size Analysis

Panel A: In a cell-oriented analysis, TS1 ventricular cardiomyocytes are significantly wider, but not longer.

Panel B: Animal-oriented analysis confirms the finding that TS1 ventricular cardiomyocytes are wider, but not longer, than WT ventricular cardiomyocytes.

Courtesy of Demetrio J. Santiago, PhD.

Following the demonstration that TS1 ventricular cardiomyocytes were significantly wider, we assessed the cellular capacitance. Elegant experiments from the laboratory of Prof. Bers have previously demonstrated that in different species cellular capacitance is an excellent surrogate of cellular volume[113].

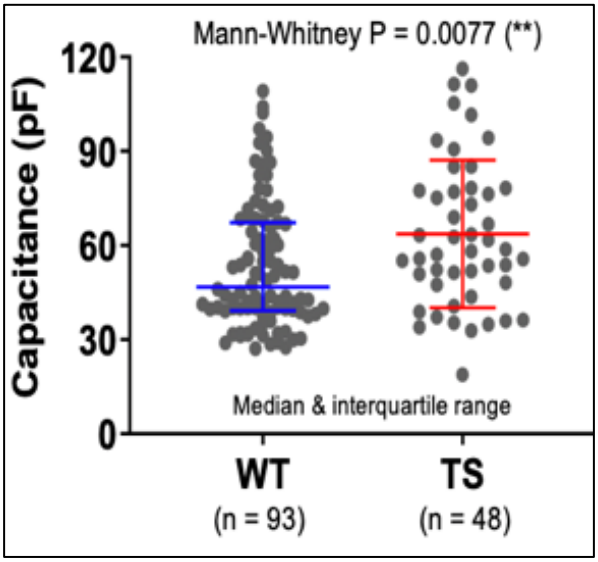

Figure 5.33. Cellular Capacitance in WT and TS1 Pigs.

Courtesy of Demetrio J. Santiago, PhD.

As shown in Figure 5.33, median cellular capacitance was significantly greater in TS1 animals (median capacitance 62.2 pF [IQR: 47.6-80.0 pF]) as compared to their WT littermates (median capacitance 50.9 pF [IQR: 39.9-67.6 pF]; p=0.008).

CMR demonstrated that TS1 animals present a structurally and functionally normal hearts. Importantly, CMR showed, and histological analysis confirmed, that TS1 pigs do not have intramyocardial fibrosis nor myocardial edema.

Interestingly, CMR identified increased intramyocardial mass in TS1 pigs, generating a hypothesis that TS1 pigs may present a modest degree of intracellular hypertrophy.

Single cell analysis and cellular capacitance studies confirmed that TS1 ventricular cardiomyocytes are indeed more voluminous than WT cardiomyocytes, corroborating the CMR hypothesis.

5.2.1.4 Advanced Electrophysiological Characterization

Following the demonstration that our novel knock-in porcine model of LQTS is characterized by a **significantly prolonged QTc interval** in the setting of a structurally normal heart, and that TS1 pigs develop **spontaneous life-threatening ventricular arrhythmias**, akin to ones observed in human patients, which leads to a notable excess mortality in TS1 pigs, we focused on an in-depth assessment of the underlying electrophysiology.

Hitherto, mapping of the ventricular repolarization using ultra-high density electroanatomical mapping system was not possible. Therefore, in collaboration with the Research and Development team of Boston Scientific Germany (Düsseldorf, Germany), our group has developed a technique for the annotation of repolarization (for more details please refer to the section Methods).

Considering that spontaneous life-threatening ventricular arrhythmias were often triggered by three premature ventricular beats and driven by the desire to gain novel insights into the arrhythmogenesis of our novel knock-in model, we mapped, for the first time ever, using state-of-the-art ultra-high density sequential mapping system, the repolarization patterns of the two ventricles on their endocardial and epicardial aspect during the delivery of the third extra-stimulus from the right ventricular apex in a group of age- and sex-matched WT and TS1 pigs. This protocol conducted in knock-in pigs, whose cardiac anatomy and physiology closely resemble the human ones, was chosen to mimic as closely as possible the electrophysiological state just before arrhythmia onset.

As expected, and in line with the marked prolongation of the QTc interval demonstrated previously, local recovery time (LRT) was significantly longer in TS1 pigs, both as a mean value (LRT_{WT} mean 303.6±21.7 ms *vs.* LRT_{TS} mean 378.1±54.0 ms; +25%; p=0.004) (Table 5.39 and Figure 5.34), as well as all examined percentiles.

Consistently with these data, total recovery time (TRT) was almost twice longer in TS1 pigs (TRT_{WT} 156.3±56.8 ms *vs.* TRT_{TS} 309.6±114.1 ms; +98%; p=0.006).

Whole Heart Mapping	WT	TS1	Δ (%)	p value
Number of animals, N	7	9		
EGMs per animal, N	5145±1946	5734±2168	+589 (+11%)	0.583
Mean LRT (ms), mean ± SD	303.6±21.7	378.1±54.0	+74.5 (+25%)	***0.004***
LRT SD (ms), mean ± SD	28.9±6.9	55.0±18.2	+26.1 (+90%)	***0.003***
LRT 10th Percentile (ms), mean ± SD	264.4±24.1	298.4±33.3	+34.0 (+13%)	***0.040***
LRT 25th Percentile (ms), mean ± SD	281.4±24.8	345.7±51.7	+64.3 (+23%)	***0.009***
Median LRT (ms), mean ± SD	303.9±23.4	382.9±58.5	+79.0 (+26%)	***0.005***
LRT 75th Percentile (ms), mean ± SD	327.5±22.1	421.2±64.9	+93.7 (+29%)	***0.003***
LRT 90th Percentile (ms), mean ± SD	341.8±20.3	446.2±70.4	+104.4 (+31%)	***0.002***
TRT (ms), mean ± SD	156.3±56.8	309.6±114.1	+153.3 (+98%)	***0.006***
LRT Δ90-10 (ms), mean ± SD	77.4±18.7	147.8±50.4	+70.4 (+91%)	***0.004***
LRT gradient (ms/mm), mean ± SD	2.3±0.6	4.1±1.5	+1.8 (+78%)	***0.010***
Maximal LRT gradient (ms/mm), mean ± SD	7.2±1.9	13.3±5.3	+6.1 (+85%)	***0.012***

Table 5.39. Comparison of LRT Parameters in WT and TS1 pigs

Pioneering works by the group of Prof. El-Sherif, conducted in canine drug-induced models of type 3 Long QT Syndrome in the 1990s demonstrated that the dispersion of local refractoriness is a fundamental prerequisite for arrhythmogenesis[12]. Therefore, following the unequivocal prolongation of ventricular repolarization, we focused on a robust assessment of dispersion of ventricular repolarization.

To this end, we have used two different approaches.

Firstly, we used the standard deviation of LRT and the difference between the 90th and 10th percentile as a distributive proxy for dispersion of repolarization.
Relevantly, LRT was also significantly more dispersed in TS1 pigs as compared to their WT littermates, as evidenced both by significantly greater standard deviation (LRT_{WT} SD 28.9±6.9 ms *vs.* LRT_{TS} SD 55.0±18.2 ms; +90%; p=0.003) and Δ90-10 (LRT_{WT} Δ90-10 77.4±18.7 ms *vs.* LRT_{TS} Δ90-10 147.8±50.4 ms; +91%; p=0.004) (see Table 5.28).

Secondly, exploiting the unprecedented coverage of the endocardial and epicardial surface of the two beating ventricles, made possible by ultra-high density mapping, we calculated the gradients of LRT and constructed gradient maps. Crucially, TS1 pigs showed a very steep gradient of repolarization, as evidenced both by significantly larger mean LRT gradient (LRT $gradient_{WT}$ mean 2.3±0.6 ms *vs.* LRT $gradient_{TS}$ mean 4.1±1.5 ms; +78%; p=0.010) and maximal LRT gradient (LRT $gradient_{WT}$ max 7.2±1.9 ms *vs.* LRT $gradient_{TS}$ max 13.3±5.3 ms; +85%; p=0.012) (Figure 5.35).

Findings from electroanatomical mapping suggest that ventricular repolarization is not only significantly prolonged, as demonstrated by marked QTc interval prolongation, but is also significantly dispersed. The dispersion of repolarization results in areas of high gradients of ventricular repolarization, which have been demonstrated to be highly arrhythmogenic.

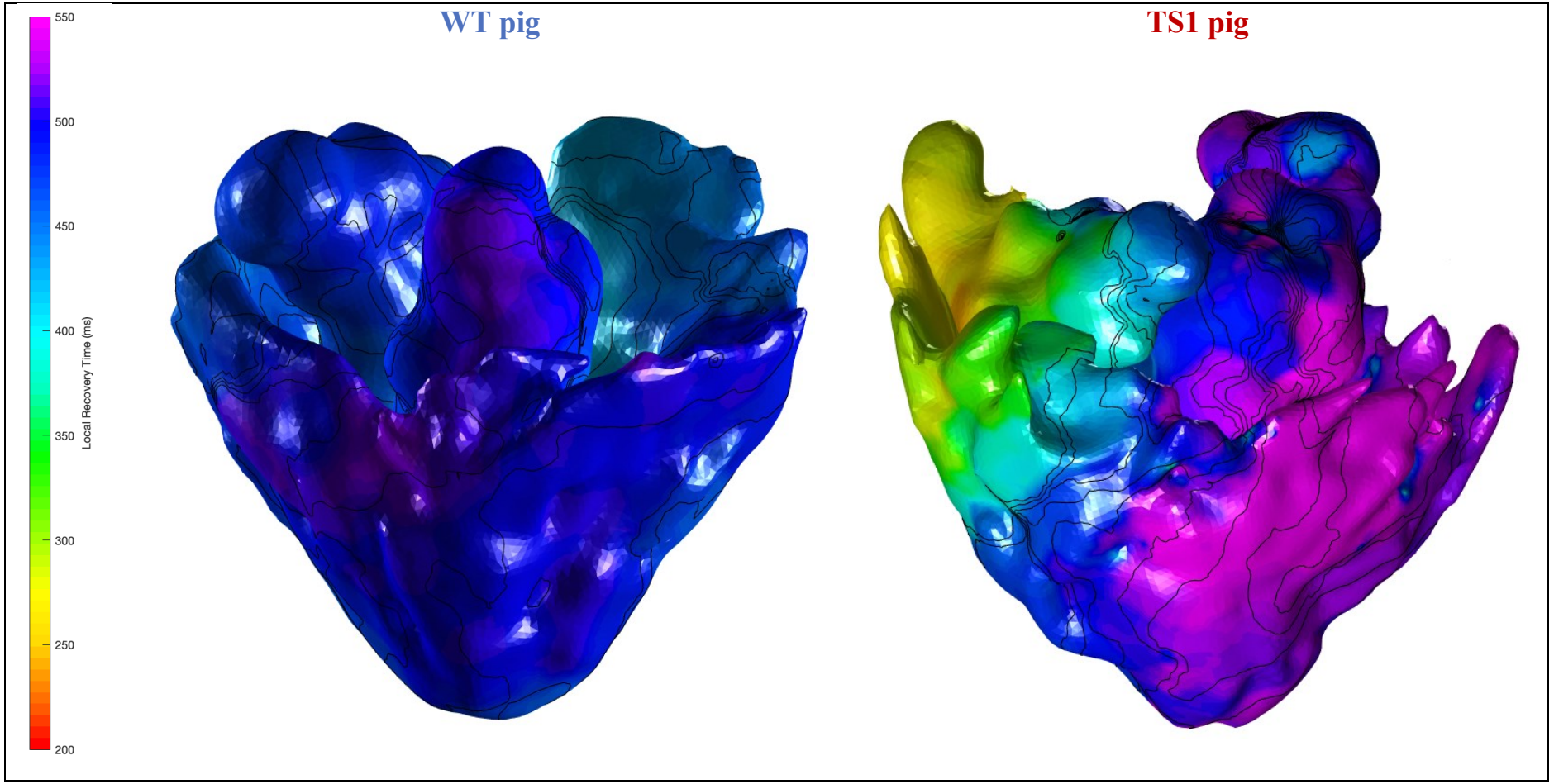

Figure 5.34. Electroanatomical Maps of Local Recovery Times in a WT and a TS1 Pig

Recovery times of whole heart are plotted using the canonical color spectrum used in electrophysiology, with red indicating the earliest recovery and purple the latest recovery and correspond to exact local recovery times. Isochrones, in steps of 10 ms, are overlaid.

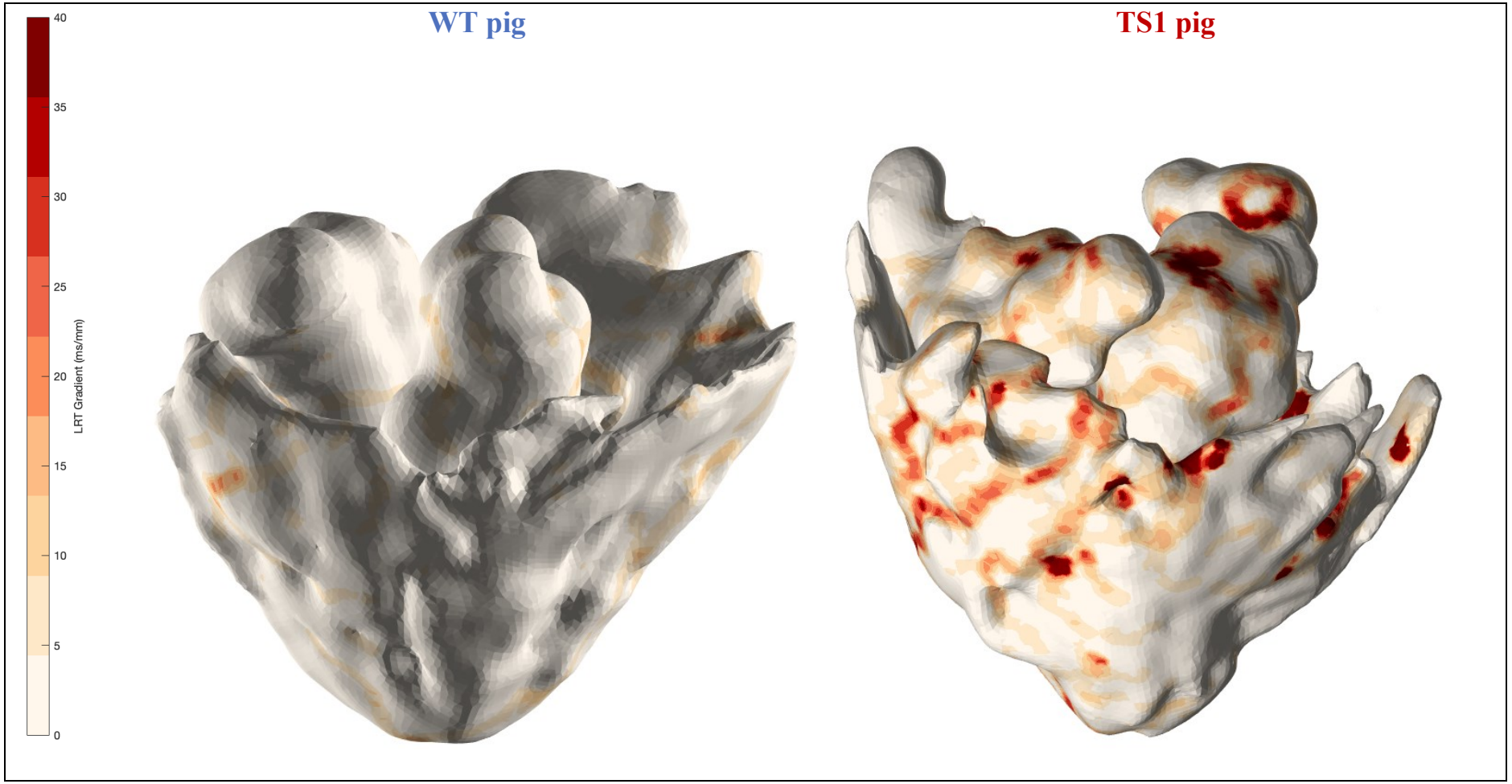

Figure 5.35. Electroanatomical Maps of Gradients of Local Recovery Times in a WT and a TS1 Pig

Gradients of local recovery times of whole heart are plotted using color spectrum, with red indicating the steepest gradient and white absence of any gradient of recovery.

5.2.2 In Vivo Testing of HERG1 Channel Agonists in Knock-in Model of Long QT Syndrome

Following our successful *in vivo* preliminary testing of HERG channel agonists in drug-induced models of LQTS, we investigated the efficacy and safety of HERG channel agonists in our knock-in model of LQTS.

5.2.2.1 Electrocardiographic Effects of ICA-105574

Our assessment of the electrocardiographic effects of ICA-105574 was divided into two sets of experiments: experiments with a single 3 mg/kg dose, followed by experiments with multiple doses.

5.2.2.1.1 Single Dose

As a first step, we assessed the effects of ICA-105574 at a dose of 3 mg/kg intravenously on the QTc interval. As shown in Table 5.40 and Figures 5.36 and 5.37, intravenous administration of 3 mg/kg ICA-105574 resulted in an immediate, pronounced and statistically significant shortening of the QTc interval in all TS1 pigs. Despite marked QTc shortening induced by ICA-105574, during the prolonged electrocardiographic registration no proarrhythmic events were observed.

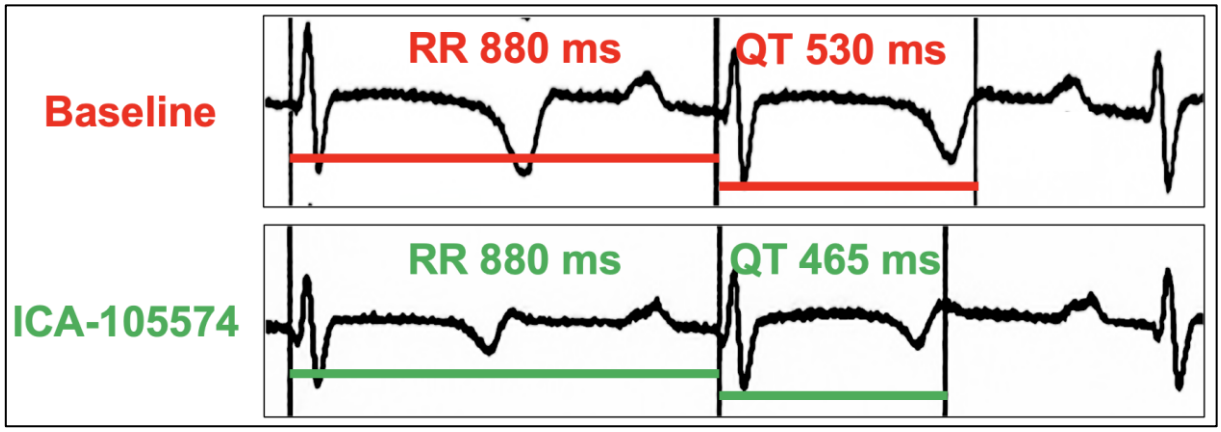

Figure 5.36. Exemplificative Electrocardiogram of a TS1 Pig at Baseline and After ICA-105574

N=5 animals	QTcB, ms (median, IQR)	ΔQTcB, ms (%)	p value
Baseline	620, 581-634	Ref.	Ref.
ICA-105574 1 mg/kg	602, 595-611	-18 (-3%)	0.526
ICA-105574 2 mg/kg	588, 550-597	-32 (-5%)	0.206
ICA-105574 3 mg/kg	540, 514-560	-80 (-13%)	***0.007***
1 minute after ICA-105574	502, 487-521	-118 (-19%)	***0.001***
2 minutes after ICA-105574	506, 473-518	-114 (-18%)	***<0.001***
3 minutes after ICA-105574	483, 460-507	-137 (-22%)	***<0.001***
4 minutes after ICA-105574	467, 460-470	-153 (-25%)	***<0.001***
5 minutes after ICA-105574	447, 443-457	-173 (-28%)	***<0.001***
6 minutes after ICA-105574	500, 489-509	-120 (-19%)	***0.001***
7 minutes after ICA-105574	502, 493-515	-118 (-19)	***0.001***
8 minutes after ICA-105574	512, 494-530	-108 (-17%)	***0.007***
9 minutes after ICA-105574	509, 508-510	-111 (-18%)	***0.006***
10 minutes after ICA-105574	509, 501-542	-111 (-18%)	***0.008***

Table 5.40. Effect of 3 mg/kg ICA-105574 on the QTc Interval in TS1 Pigs.

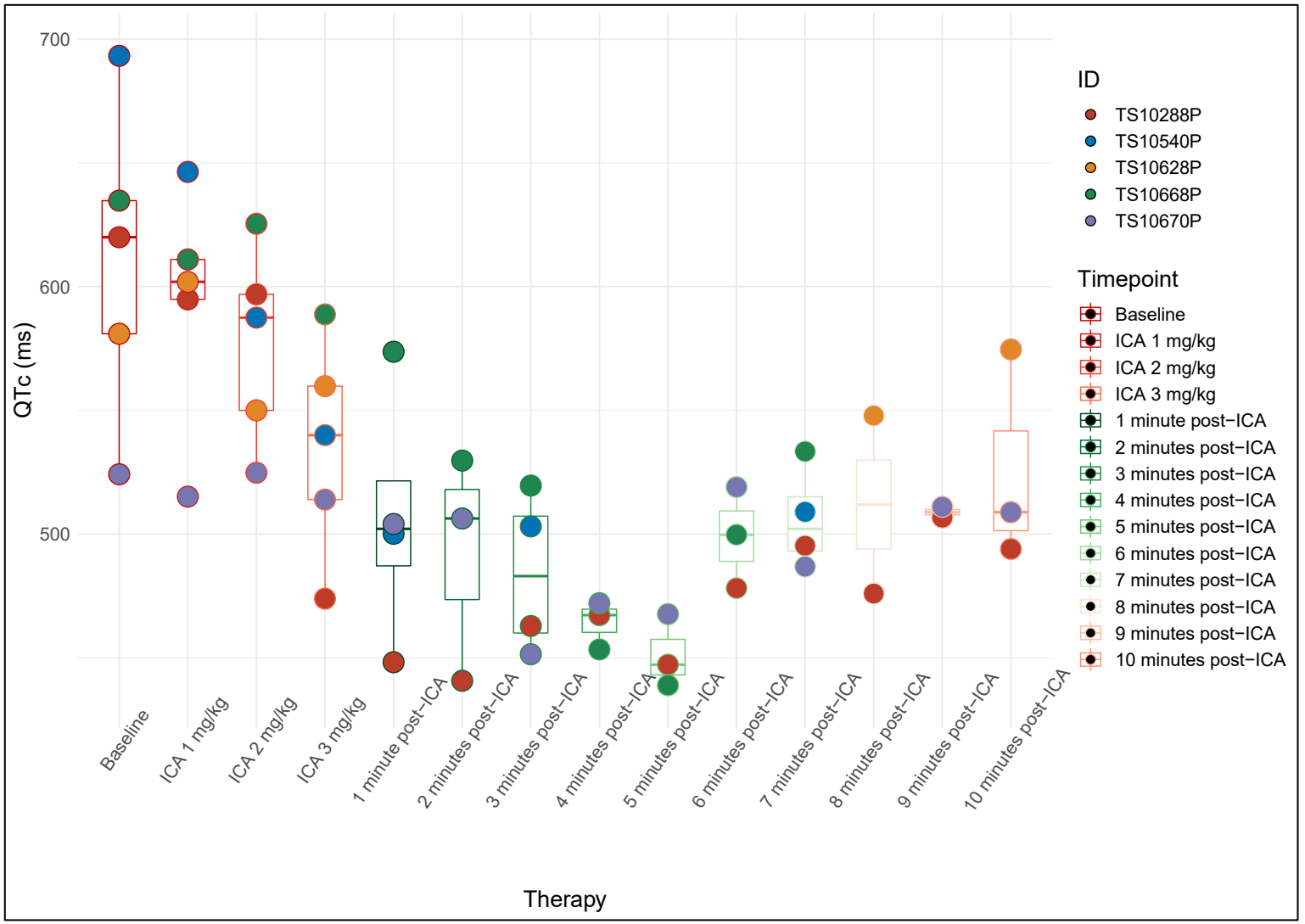

Figure 5.37. Effect of ICA-105574 on the QTc Interval Duration in TS1 Pigs

Each colored dot represents an animal.

5.2.2.1.2 Repeated Dosing

Following the demonstration of efficacy and safety of a single dose of 3 mg/kg i.v. of ICA-105574, we focused on investigating the efficacy and safety of multiple dosing. Specifically, we investigated repeated intravenous administrations of 3 mg/kg doses for a total of 4 doses (i.e., overall drug dose of 12 mg/kg).

As shown in Table 5.41 and Figure 5.38, intravenous administration of four doses of 3 mg/kg ICA-105574, for a total of 12 mg/kg ICA-105574, caused a modest dose-dependent QTc shortening. Specifically, 3 mg/kg increments shortened the QTc interval by one third 5 minutes after administration (QTcB $_{3\ mg/kg}$ 447 ms [IQR: 443-457 ms]; QTcB $_{6\ mg/kg}$ 457 ms [IQR: 432-463 ms]; QTcB $_{12\ mg/kg}$ 460 ms [IQR: 419-465 ms]; QTcB $_{12\ mg/kg}$ 433 ms [IQR: 407-459 ms]) as compared to baseline values (620 ms [IQR: 581-635 ms]; $p<0.001$ for all) (Table 5.41). Regarding safety, at any point in time, we did not observe excessive QTc shortening, nor did we observe any proarrhythmic events in any of the animals studied.

N=5 animals	QTcB, ms (median, IQR)	ΔQTcB, ms (%)	p value
Baseline	620, 581-635	Ref.	Ref.
Administering ICA-105574 3 mg/kg	540, 514-560	-80 (-13%)	***0.016***
5 minutes after 3 mg/kg of ICA-105574	447, 443-457	-173 (-28%)	***<0.001***
10 minutes after 3 mg/kg of ICA-105574	509, 501-542	-111 (-18%)	***0.019***
Administering ICA-105574 6 mg/kg	497, 490-509	-123 (-20%)	***0.002***
5 minutes after 6 mg/kg of ICA-105574	457, 432-463	-163 (-26%)	***<0.001***
10 minutes after 6 mg/kg of ICA-105574	521, 519-523	-99 (-16%)	***0.029***
Administering ICA-105574 9 mg/kg	482, 474-490	-138 (-22%)	***0.003***
5 minutes after 9 mg/kg of ICA-105574	460, 419-465	-160 (-26%)	***<0.001***
10 minutes after 9 mg/kg of ICA-105574	469, 467-510	-151 (-24%)	***0.002***
Administering ICA-105574 12 mg/kg	481, 454-508	-139 (-22%)	***0.003***
5 minutes after 12 mg/kg of ICA-105574	433, 407-459	-187 (-30%)	***<0.001***
10 minutes after 12 mg/kg of ICA-105574	395	-225 (-36%)	***<0.001***

Table 5.41. Effect of Repeated ICA-105574 Dosages on the QTc Interval in TS1 Pigs.

Overall, these findings demonstrate that ICA-105574 effectively and safely shortens the ventricular repolarization in a knock-in model of LQTS. Relevantly, repeated dosing appears to cause only a modest dose-dependent reduction in QTc.

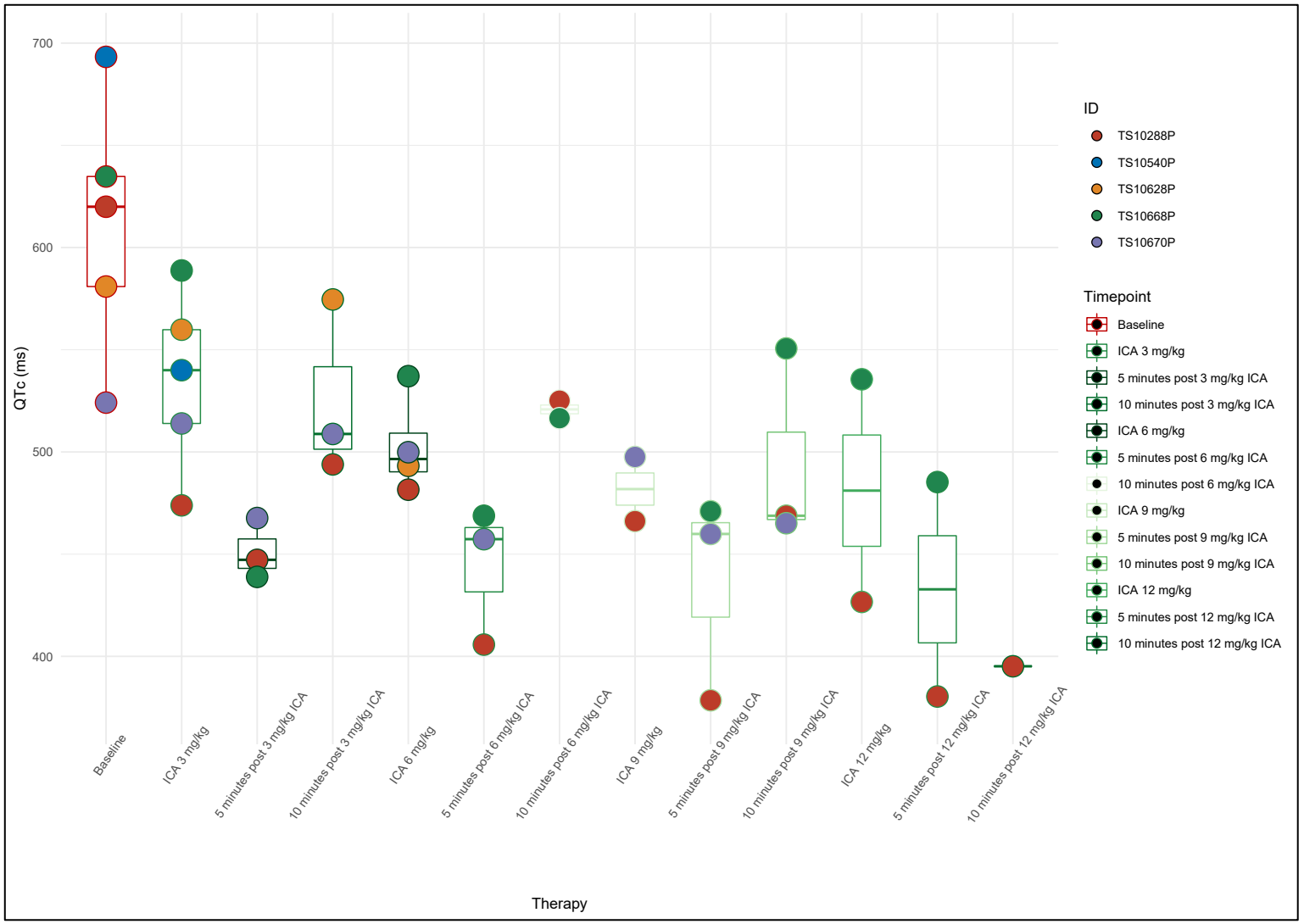

Figure 5.38. Effect of Repeated ICA-105574 Doses on the QTc Interval Duration in TS1 Pigs

Each colored dot represents an animal.

5.2.2.2 Advanced Electrophysiological Characterization of the Effects of HERG1 Channel Agonists

As shown previously, preliminary testing in three different drug-induced models of LQTS, including a model mimicking LQT8, has shown that the use of a novel HERG1 channel agonist, ICA-105574, is an efficacious and safe strategy to abbreviate the duration of ventricular repolarization.

Although the duration of ventricular repolarization (i.e., QTc interval) is itself is a potent predictor of arrhythmic effects[16,34], as mentioned earlier, pioneering works on drug-induced models of LQTS have demonstrated that dispersion of local refractoriness is a fundamental prerequisite for arrhythmogenesis[12]. This concept has been further corroborated by the classical work of Prof. Hondeghem and colleagues, who analyzed the proarrhythmic and antiarrhythmic effects of more than 700 compounds, demonstrating elegantly that in terms of both shortening and lengthening of the action potential duration, inhomogeneity is fundamental for arrhythmogenesis[114].

In our knock-in model of LQTS, in-depth assessment of the principal electrophysiological parameters performed in baseline suggests that the ventricular repolarization is not only extremely prolonged, as testified by significantly prolonged mean local repolarization time, but is markedly dispersed, creating steep gradients of repolarization, offering a mechanistic explanation for the marked excess of sudden cardiac deaths observed in TS1 pigs.

Therefore, for a compound to exert an antiarrhythmic effect in the setting of congenital LQTS, it is not merely sufficient that it shortens the duration of the ventricular repolarization. Fundamentally, the antiarrhythmic effect is likely to be dependent on the compound's ability to exert a net positive effect not only on the electrophysiological parameters related to the duration of ventricular repolarization, but also on those related to dispersion of ventricular repolarization.

We set out to investigate *in vivo*, using ultra-high density electroanatomical mapping, the effects of a novel HERG1 channel agonist, ICA-105574, on local repolarization times and on dispersion of repolarization.

Using ultra-high density sequential electroanatomical mapping (EAM) system, we mapped the repolarization patterns of the two ventricles on their endocardial and epicardial aspect during the delivery of three extra-stimuli from the right ventricular apex in TS1 pigs at baseline, and then we repeated the same protocol following the administration of 12 mg/kg of ICA-105574 intravenously.

Importantly, upon administration of ICA-105574 both the mean LRT shortened significantly ($LRT_{baseline}$ mean 406.8±46.8 ms *vs.* $LRT_{ICA\text{-}105574}$ mean 320.2±25.1 ms; -21%; p=0.032) (Table 5.42, Figures 5.39 and 5.40), as well as almost all LRT percentiles. The total recovery time shortened notably upon treatment ($TRT_{baseline}$ 358.0±97.4 ms *vs.* $TRT_{ICA\text{-}105574}$ 358.0±97.4 ms; -30%; p=0.006).

Regarding the assessment of the dispersion of ventricular repolarization, as in the baseline study, we have adopted two approaches.

Firstly, we assessed the distribution of the data, as the proxy for dispersion of repolarization. Relevantly for arrhythmogenesis, dispersion of repolarization reduced significantly after ICA-105574 as evidenced both by significantly smaller standard deviation ($LRT_{baseline}$ SD 65.3±12.3 ms *vs.* $LRT_{ICA\text{-}105574}$ SD 37.0±7.4 ms; -43%; p=0.009) and Δ90-10 ($LRT_{baseline}$ Δ90-10 175.9±38.2 ms *vs.* $LRT_{ICA\text{-}105574}$ Δ90-10 96.1±22.3 ms; -45%; p=0.012) (see Table 5.52).

Exploiting the unprecedented coverage of the endocardial and epicardial surface of the two beating ventricles, made possible by ultra-high density mapping, we calculated the gradients of LRT and constructed gradient maps. Crucially, ICA-105574 reduced significantly the gradient of repolarization, as evidenced both by a significant reduction of mean LRT gradient (LRT $gradient_{baseline}$ mean 5.1±1.6 ms/mm *vs.* LRT $gradient_{ICA\text{-}105574}$ mean 1.4±0.5 ms/mm; -73%; p=0.009) and maximal LRT gradient (LRT $gradient_{baseline}$ max 30.5±8.8 ms/mm *vs.* LRT $gradient_{ICA\text{-}105574}$ max 12.2±3.4 ms/mm; -60%; p=0.020) (Figure 5.41).

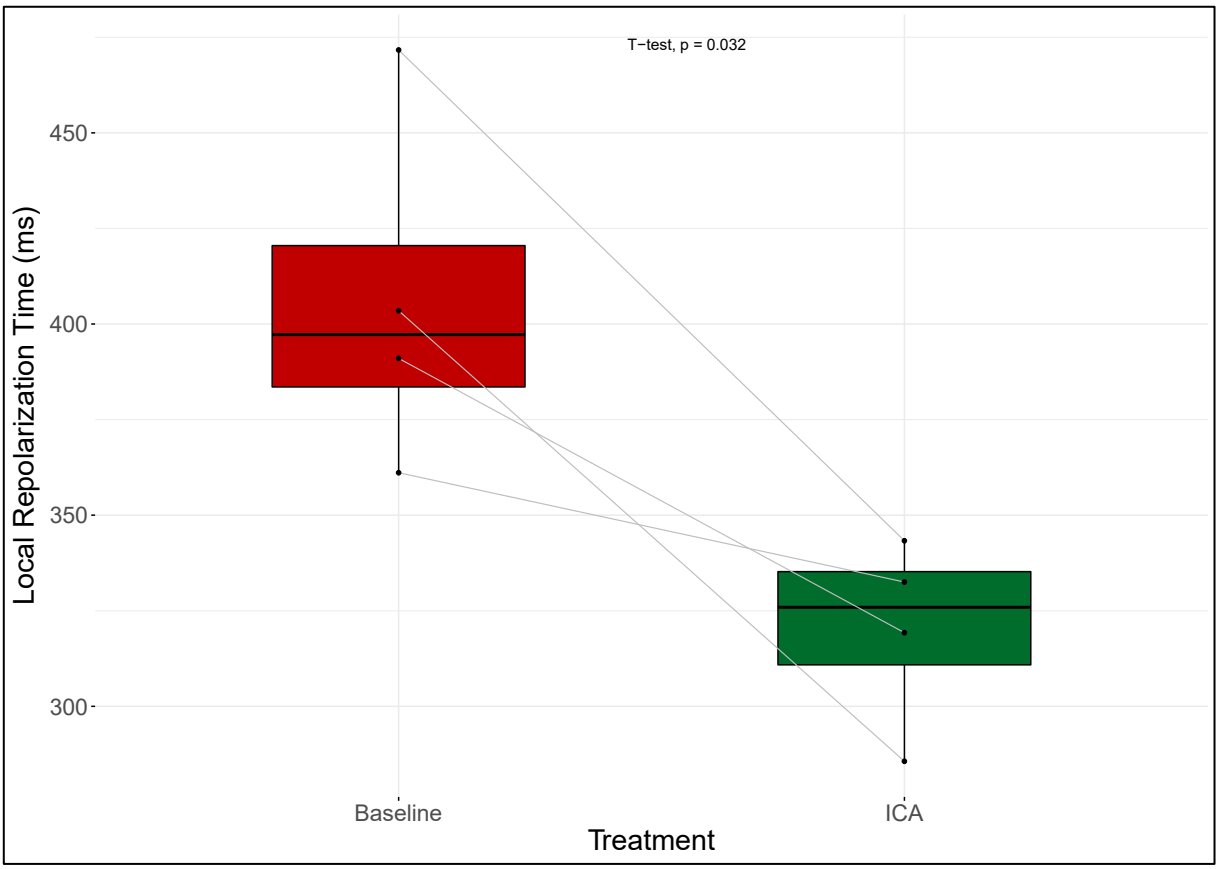

Figure 5.39. Boxplot Summarizing the Effects of ICA-105574 on LRT

ICA-105574 significantly shortens and homogenizes the ventricular repolarization, counterbalancing the arrhythmogenic gradient of ventricular repolarization identified in our knock-in model of LQTS.

Whole Heart Mapping	TS1 Cohort Overall (from Table 5.28)	Baseline (N=4)	ICA-105574 (N=4)	Δ (%)	p-value
EGMs per animal, N	5734±2168	5988±1737	3674±1261	-2313 (-39%)	0.066
Mean LRT (ms), mean ± SD	378.1±54.0	406.8±46.8	320.2±25.1	-86.6 (-21%)	***0.032***
LRT SD (ms), mean ± SD	55.0±18.2	65.3±12.3	37.0±7.4	-28.3 (-43%)	***0.009***
LRT 10th Percentile (ms), mean ± SD	298.4±33.3	309.6±26.3	273.3±23.4	-36.3 (-12%)	0.109
LRT 25th Percentile (ms), mean ± SD	345.7±51.7	370.6±49.0	292.7±22.0	-77.9 (-21%)	0.055
Median LRT (ms), mean ± SD	382.9±58.5	412.1±56.1	317.2±25.5	-94.9 (-23%)	***0.032***
LRT 75th Percentile (ms), mean ± SD	421.2±64.9	460.8±52.3	351.6±30.9	-109.2 (-24%)	***0.023***
LRT 90th Percentile (ms), mean ± SD	446.2±70.4	485.5±53.9	369.3±33.4	-116.2 (-24%)	***0.022***
TRT (ms), mean ± SD	309.6±114.1	358.0±97.4	249.7±83.8	-108.3 (-30%)	***0.006***
LRT Δ90-10 (ms), mean ± SD	147.8±50.4	175.9±38.2	96.1±22.3	-79.8 (-45%)	***0.012***
LRT gradient (ms/mm), mean ± SD	4.1±1.5	5.1±1.6	1.4±0.5	-3.7 (-73%)	***0.009***
Maximal LRT gradient (ms/mm), mean ± SD	13.3±5.3	30.5±8.8	12.2±3.4	-18.3 (-60%)	***0.020***

Table 5.42. Comparison of LRT Parameters in TS1 pigs at baseline and after ICA-105574

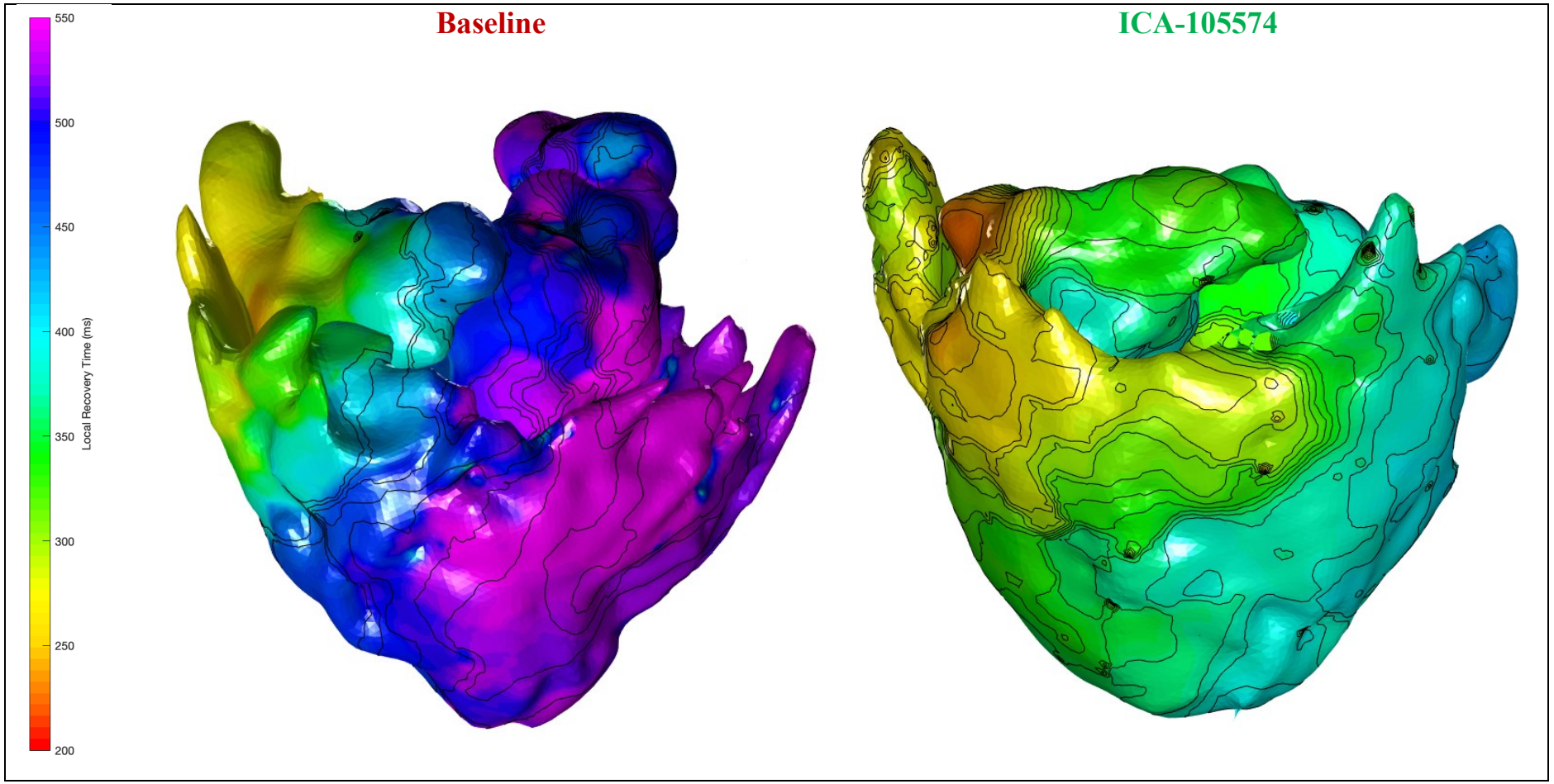

Figure 5.40. Sequential Electroanatomical Maps of Local Recovery Times in a TS1 Pig at Baseline and After ICA-105574

Recovery times of whole heart are plotted using the usual color spectrum, with red indicating the earliest activation and purple the latest activation.

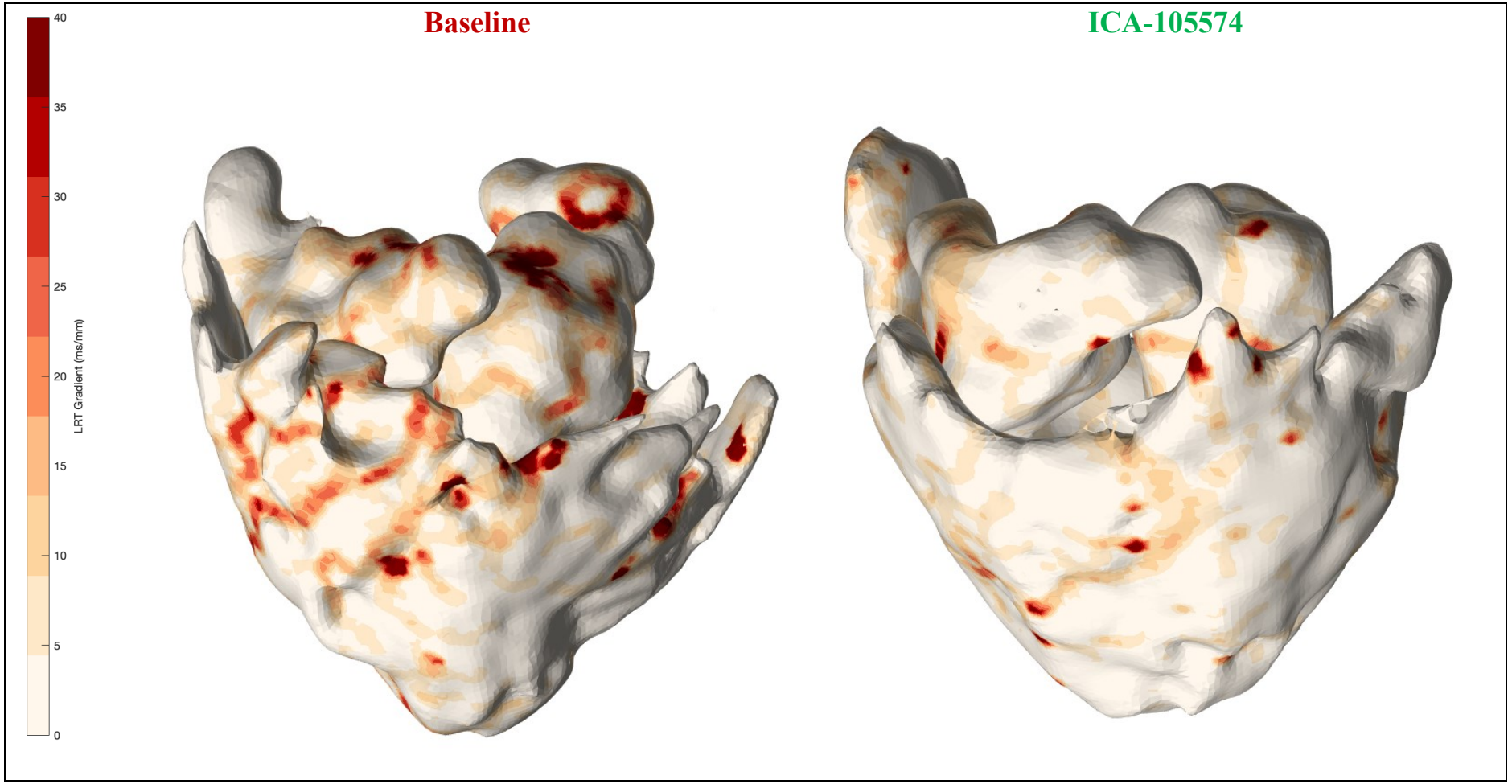

Figure 5.41. Electroanatomical Maps of Gradients of Local Recovery Times in a TS1 Pig in Baseline and After ICA-105574

Gradients of local recovery times of whole heart are plotted using color spectrum, with red indicating the steepest gradient and white absence of any gradient of recovery.

6 DISCUSSION

This doctoral dissertation demonstrates the transversal feasibility of phenotype correction of different forms of QT interval prolongation, efficaciously and safely using HERG1 potassium channel agonists. Our data, deriving from both drug-induced models of Long QT Syndrome (LQTS; type 2 [LQT2], type 3 [LQT3] and type 8 [LQT8]) and a knock-in model of LQT8, demonstrate that ventricular repolarization may be normalized, both in terms of electrocardiographic parameters (i.e., QT interval) and advanced electrophysiological parameters (i.e., gradients of local repolarization time), without excessive repolarization shortening nor induction of proarrhythmia.

Unmet Clinical Needs of Patients with LQTS

LQTS is a common inherited arrhythmogenic condition, characterized by prolongation of ventricular repolarization, which predisposes young and otherwise healthy individuals to sudden cardiac death[1].

The clinical management of LQTS was designed in the 1970s, in absence of pathophysiological insights explaining the prolongation of the QTc interval. Starting from the observation that patients affected by LQTS develop life-threatening arrhythmias during stress and/or strong emotions, treatment with beta-blockers (βB), pharmacological agents contrasting the effects of catecholamines was suggested. Despite the quantum leaps in our understanding of the pathophysiology of LQTS, the mainstay of treatment remains the use of βB[1], based on seminal studies which confirm marked changes in natural history of the disease as a result of treatment[40]. The use of βB, preferentially nadolol[34], has been shown to reduce, but not to completely abolish, the arrhythmic risk[34,40].

Considering the incomplete arrhythmic protection conferred by βB therapy in patients with most malignant forms of LQTS (such as LQT2, LQT3 and LQT8)[34,44], different novel therapeutic approaches have been investigated. Keeping in mind that the duration of the QTc interval is one of the most potent predictors of arrhythmic events[2,34], our group has pioneered a substrate-oriented approach, aimed at abbreviating the ventricular repolarization. Specifically, we demonstrated that the use of mexiletine[42], a sodium channel blocker which contrasts the effects of gain-of-function mutations causing LQT3[7], to abbreviate and normalize the pathologically prolonged QTc interval translated into a clinically meaningful benefit for patients treated, with reduction of the number of patients with arrhythmic events, the number

of events per patient, and the annual event rate[43]. The strongest testimonial to this approach is the recent endorsement by the 2022 European Society of Cardiology guidelines for the management of patients with ventricular arrhythmias and the prevention of sudden cardiac death[1], which state that mexiletine is indicated in all patients with LQT3.

This challenges the dogma that βB therapy, aimed at controlling the arrhythmic trigger, is the only treatment for all forms of LQTS, and instead suggests that the abbreviation of repolarization, in principle may be potentially a novel, exciting but also rather feasible therapeutic approach for *all* forms of LQTS.

Mexiletine as a Proof-of-Concept for Substrate-Specific Approach

Repolarization abbreviation, using mexiletine, has been attempted also in other malignant forms of LQTS, such as LQT2[50] and LQT8[51]. The results, unfortunately, have been only partially successful. Specifically, while most patients with LQT2 do respond to mexiletine therapy, the extent of QTc shortening is markedly inferior as compared to one observed in LQT3, with some patients responding incompletely or not responding[50]. These findings mimic a clinically relevant issue observed in LQT3 with, identified already in the early days of mexiletine therapy for LQT3: the existence of specific LQT3-causing mutations which are known to be mexiletine-resistant[72,115]. In LQT8, instead, the clinical investigations have failed to identify a drug able to significantly shorten QT interval in patients[51–53].

Therefore, considering the groundbreaking potential espoused by the success of mexiletine in LQT3[1,43], and keeping in mind the pressing clinical need for novel treatments for the most malignant forms of LQTS, novel compounds capable of safely and efficaciously abbreviating the ventricular repolarization, and not merely in a subtype-specific manner, represent the holy grail of treatment of LQTS in the twenty-first century.

HERG1 Channel Activation as a Novel Therapeutic Approach for LQTS

A promising therapeutic target to further explore this concept is represented by HERG1-conducted I_{Kr} current[65], one of the principal determinants of ventricular repolarization[6]. HERG1 has gained notoriety for the large number of chemically unrelated drugs which strongly inhibit HERG1, causing drug-induced LQTS[116]. In the context of HERG1 blocking screening, a serendipitous discovery of RPR260243[64], a first molecule of a novel antiarrhythmic class, HERG1 channel agonists, was made. Several other compounds were discovered shortly after, each modulating the HERG1 channel in a different way. Today, four principal mechanisms by which HERG1 channel agonists exert their effect are recognized: slowed rate of channel

deactivation, attenuation of C-type inactivation, shift of channel opening to more negative potentials, and increase in channel open probability[65].

For this proof-of-concept study, we selected 3-nitro-N-(4-phenoxyphenyl) benzamide (ICA-105574)[66], the most potent HERG1 channel agonist[65]. Relevantly, ICA-105574 has already been tested in different models of LQTS, *in silico*[71], *in vitro*[67,69,71] and *in vivo*[70], and it has been demonstrated to shorten the action potential duration (APD) in ventricular cardiomyocytes in a concentration-dependent manner[69], by causing an important positive shift in voltage-dependent of the C-type inactivation[65].

The study was divided into two distinct phases. In the first phase, we tested the efficacy and safety of ICA-105574 in three different drug-induced models of LQTS: LQT2, LQT3, and LQT8. Aware of the limitations of drug-induced models of LQTS, in the Phase Two, we exploited the opportunity to study *in vivo* the effects and safety of ICA-105574 using the first successful knock-in large mammal model of a cardiac channelopathy, our TS1 pig. Thanks to the similarities in anatomy and electrophysiological properties between pigs and humans[111,112], our porcine model of TS1 allows for studying the pharmacological effects of ICA-105574 in physiological conditions and using clinical-grade equipment, including state-of-the-art electroanatomical mapping.

Feasibility of HERG1 Channel Agonists as a Therapeutic Approach

In line with the recommendations for the European Medicines Agency guidelines[78] for the assessment of the delay of ventricular repolarization by pharmaceuticals, we have used guinea pigs (*Cavia porcellus*) as the animal species of choice for the development of our drug-induced models of LQTS. We have used three previously used compounds to mimic three different forms of LQTS. Considering that LQT2 is caused by loss-of-function mutations in the *HERG*-encoded $K_V11.1$ potassium channel[6], we used DL-sotalol, a well-known blocker of $K_V11.1$ potassium channel[80], to develop drug-induced models of LQT2[79]. Similarly, considering that LQT3 is caused by gain-of-function mutations in the *SCN5A*-encoded $Na_V1.5$ sodium channel, which augment the late I_{Na} current, we used Anthopleurin-A, an inhibitor of the inactivation of INa current, which had been previously used by our group to develop a drug-induced models of LQT3[42]. Lastly, considering that LQT8 is caused by gain-of-function mutations in the *CACNA1C*-encoded $Ca_V1.2$ calcium channel, Bay K8644, an enhancer of $Ca_V1.2$-conducted ICa current, has been used to develop drug-induced models of LQT8[82,88].

Following the successful development of three drug-induced models of LQTS in all animals studied, we tested the effects and safety of ICA-105574 in these three drug-induced

models, using cutting-edge statistical methodology that permits a robust assessment of the drug effect. Relevantly, in all three models, ICA-105574 successfully abbreviated and normalized the QT interval, without ever causing excessive QT interval shortening or causing proarrhythmia.

Notably, the duration of the drug effect was type-specific, and it was shortest in the LQT2 model. A possible mechanistic explanation for this phenomenon may be suggested from two considerations. Firstly, seminal work of Wang and MacKinnon identified that HERG1 blocking compounds, such as DL-Sotalol, strongly bind amino acids from Tyr-652 to Phe-656[62] which are located in a hydrophobic pocket in the pore[61]. Similarly, works of Garg and colleagues identified that ICA-105574 binds between the pore helices stabilizing the ion selectivity filter[67]. Therefore, it is possible that the effect of ICA-105574 is attenuated as a result of the aforementioned.

Novel Knock-In Model of LQTS as a Fundamental Tool for Drug Discovery and Testing

Following the successful demonstration that ICA-105574 can safely abbreviate the QT interval in three different models of LQTS, we decided to investigate in depth its effects on the ventricular repolarization. For this purpose, we exploited the availability of our novel knock-in model of LQT8, the first successful knock-in large mammal model of a cardiac channelopathy, developed within the framework of the European Research Council Grant "EU-Rhythmy" ERC-ADG-2014-ID:669387-2015-2021.

Over the past years, we have been characterizing extensively our TS1 pig. Firstly and most importantly, the TS1 pig presents a notably prolonged QT interval. Such extreme prolongation of the QT interval, one of the strongest determinants of arrhythmic risk in patients with LQTS[2,16,34], predisposes TS1 pigs to die suddenly. Implantation of clinical-grade subcutaneous loop recorders demonstrated that the cause of excessive sudden cardiac death mortality documented in TS1 pigs is due to the onset of spontaneous, life-threatening ventricular arrhythmias.

To ascertain that the cause of death is exclusively electrical in nature, we also performed in-depth CMR studies on our TS1 pig. Leveraging on the experience accrued during the first year of my PhD at the Department of Cardiac Imaging, where I trained under supervision of Dr. Gianluca Pontone, an internationally recognized expert in the field, we demonstrated that TS1 pigs present a structurally and functionally normal heart. Specifically, multiparametric tissue characterization, showed the absence of intramyocardial fibrosis and myocardial edema. However, an unexpected finding of increased intramyocardial mass in TS1 pigs generated a

hypothesis that TS1 pigs may present a modest degree of intracellular hypertrophy. To this end, we conducted single cell analysis and cellular capacitance studies, which confirmed that TS1 ventricular cardiomyocytes are indeed more voluminous than WT cardiomyocytes. Put together with the histological data confirming the absence of fibrosis and edema, these findings permitted us to confidently proceed, knowing that the arrhythmic substrate is devoid of substrate modifiers such as intramyocardial fibrosis.

To further characterize the arrhythmogenic substrate, we performed ultra-high density electroanatomical mapping using clinical-grade equipment. Considering that the primary focus of this dissertation is the ventricular repolarization and keeping in mind that until now mapping of ventricular repolarization was not possible, we worked in close collaboration with the Research and Development team of Boston Scientific Germany (Düsseldorf, Germany) to develop a technique for the annotation of signals relative to the ventricular repolarization. This prerequisite allowed us to map in unprecedented detail the patterns of ventricular repolarization. Since the spontaneous life-threatening ventricular arrhythmias were often triggered by three premature ventricular beats, we decided to map the repolarization patterns of the two ventricles on their endocardial and epicardial aspect during the delivery of three extra-stimuli from the right ventricular apex in a group of age- and sex-matched WT and TS1 pigs.

In silico studies predicted that mutations on *CACNA1C* would result in an inhomogeneous prolongation of cardiac action potential and dispersion of repolarization[117]. These findings are relevant, as the pioneering works by Prof. El-Sherif and colleagues, conducted in canine drug-induced models of LQT3 in the 1990s demonstrated that the dispersion of local refractoriness is a fundamental prerequisite for arrhythmogenesis in LQTS[12]. For the first time ever, we demonstrate using ultra-high density mapping *in vivo*, that ventricular repolarization in our TS1 pig is not only significantly prolonged, as demonstrated by marked QTc interval prolongation, but is also significantly dispersed with steep repolarization gradients, predisposing TS1 animals to arrhythmia onset.

Advanced Electrophysiological Investigations Confirm the Clinical Potential of HERG1 Channel Agonists

After these baseline investigations, we focused on a robust *in vivo* assessment of the efficacy and safety of ICA-105574 in our TS1 pig. Firstly, we tested the effect of ICA-105574 on the QT interval, showing that ICA-105574 effectively and safely shortens the ventricular repolarization. Additionally, considering the potential risk of proarrhythmia associated with excessive QT interval shortening, we assessed the effects of repeated doses of ICA-105574,

finding that even with repeated administrations, there was only a modest dose-dependent reduction in the QT interval.

However, we wanted to explore the electrophysiological effects of ICA-105574 more in depth, to offer a robust assessment of its efficacy and safety. Specifically, the classical work of Prof. Hondeghem and colleagues, who analyzed the proarrhythmic and antiarrhythmic effects of more than 700 compounds active on the duration of the cardiac action potential, showed that the resultant inhomogeneity of the APD was fundamental for arrhythmogenesis[114]. These considerations are even more relevant since ICA-105574 is an HERG1 channel agonist and considering the fact that arrhythmogenic APD inhomogeneity has been associated with compounds acting on Phase 3 of cardiac action potential[114].

Therefore, for a compound to exert an antiarrhythmic effect in the setting of LQTS, it is not merely sufficient that it shortens the duration of the ventricular repolarization. Fundamentally, the antiarrhythmic effect is likely to be dependent on the compound's ability to exert a net positive effect not only on the electrophysiological parameters related to the duration of ventricular repolarization, but also on those related to dispersion of ventricular repolarization.

The data from ultra-high density electroanatomical mapping demonstrate that ICA-105574 significantly shortens the ventricular repolarization. Crucially, data show that ICA-105574 does not worsen the gradient of repolarization, but rather that it counterbalances the arrhythmogenic gradient of ventricular repolarization identified in our knock-in model of LQTS, ameliorating it.

These results are of fundamental importance, as they offer evidence to support the view that development of HERG1 channel agonists, as a novel class of antiarrhythmics, could have clinical application. Specifically, this dissertation offers evidence that the use of these compounds in different, whole animal *in vivo* preclinical models of Long QT Syndrome is efficacious in abbreviating the duration of ventricular repolarization and, in the model of Long QT Syndrome type 8, counterbalancing the arrhythmogenic gradient of ventricular repolarization, reducing it. Additionally, this work demonstrates that ICA-105574, administered at a dosage previously reported in literature, is not associated with excessive shortening of the duration of ventricular repolarization and does not cause pro-arrhythmic events in different, whole animal *in vivo* preclinical models of Long QT Syndrome.

7 BIBLIOGRAPHY

1. Zeppenfeld, K. *et al.* 2022 ESC Guidelines for the management of patients with ventricular arrhythmias and the prevention of sudden cardiac death. *Eur. Heart J.* (2022). doi:10.1093/eurheartj/ehac262
2. Priori, S. G. *et al.* Risk Stratification in the Long-QT Syndrome. *N. Engl. J. Med.* **348**, 1866–1874 (2003).
3. Priori, S. G. *et al.* 2015 ESC Guidelines for the management of patients with ventricular arrhythmias and the prevention of sudden cardiac death: The Task Force for the Management of Patients with Ventricular Arrhythmias and the Prevention of Sudden Cardiac Death of the Europe. *Eur. Heart J.* **36**, 2793–2867 (2015).
4. Tisdale, J. E. *et al.* Prevalence of QT interval prolongation in patients admitted to cardiac care units and frequency of subsequent administration of QT interval-prolonging drugs: a prospective, observational study in a large urban academic medical center in the US. *Drug Saf.* **35**, 459–470 (2012).
5. Wang, Q. *et al.* Positional cloning of a novel potassium channel gene: KVLQT1 mutations cause cardiac arrhythmias. *Nat. Genet.* **12**, 17–23 (1996).
6. Curran, M. E. *et al.* A molecular basis for cardiac arrhythmia: HERG mutations cause long QT syndrome. *Cell* **80**, 795–803 (1995).
7. Wang, Q. *et al.* SCN5A mutations associated with an inherited cardiac arrhythmia, long QT syndrome. *Cell* **80**, 805–811 (1995).
8. Priori, S. G. *et al.* HRS/EHRA/APHRS expert consensus statement on the diagnosis and management of patients with inherited primary arrhythmia syndromes: document endorsed by HRS, EHRA, and APHRS in May 2013 and by ACCF, AHA, PACES, and AEPC in June 2013. *Hear. Rhythm* **10**, 1932–63 (2013).
9. Adler, A. *et al.* An International, Multicentered, Evidence-Based Reappraisal of Genes Reported to Cause Congenital Long QT Syndrome. *Circulation* **141**, 418–428 (2020).
10. Sanguinetti, M. C. & Tristani-Firouzi, M. hERG potassium channels and cardiac arrhythmia. *Nature* **440**, 463–469 (2006).
11. Priori, S. G. & Corr, P. B. Mechanisms underlying early and delayed afterdepolarizations induced by catecholamines. *Am. J. Physiol.* **258**, H1796-805 (1990).
12. el-Sherif, N., Caref, E. B., Yin, H. & Restivo, M. The electrophysiological mechanism of ventricular arrhythmias in the long QT syndrome. Tridimensional mapping of activation and recovery patterns. *Circ. Res.* **79**, 474–492 (1996).

13. Szabo, B., Sweidan, R., Rajagopalan, C. V & Lazzara, R. Role of Na+:Ca2+ exchange current in Cs(+)-induced early afterdepolarizations in Purkinje fibers. *J. Cardiovasc. Electrophysiol.* **5**, 933–944 (1994).
14. Yan, G. X. *et al.* Phase 2 early afterdepolarization as a trigger of polymorphic ventricular tachycardia in acquired long-QT syndrome: direct evidence from intracellular recordings in the intact left ventricular wall. *Circulation* **103**, 2851–2856 (2001).
15. Weiss, J. N., Garfinkel, A., Karagueuzian, H. S., Chen, P.-S. & Qu, Z. Early afterdepolarizations and cardiac arrhythmias. *Heart rhythm* **7**, 1891–1899 (2010).
16. Mazzanti, A. *et al.* Independent validation and clinical implications of the risk prediction model for long QT syndrome (1-2-3-LQTS-Risk). *Europace* (2021). doi:10.1093/europace/euab238
17. Sanguinetti, M. C., Jiang, C., Curran, M. E. & Keating, M. T. A mechanistic link between an inherited and an acquired cardiac arrhythmia: HERG encodes the IKr potassium channel. *Cell* **81**, 299–307 (1995).
18. Bohnen, M. S. *et al.* Molecular Pathophysiology of Congenital Long QT Syndrome. *Physiol. Rev.* **97**, 89–134 (2017).
19. Biliczki, P. *et al.* Trafficking-deficient long QT syndrome mutation KCNQ1-T587M confers severe clinical phenotype by impairment of KCNH2 membrane localization: evidence for clinically significant IKr-IKs alpha-subunit interaction. *Hear. Rhythm* **6**, 1792–801 (2009).
20. Ficker, E. *et al.* Novel characteristics of a misprocessed mutant HERG channel linked to hereditary long QT syndrome. *Am. J. Physiol. Heart Circ. Physiol.* **279**, H1748-56 (2000).
21. Mihic, A., Chauhan, V. S., Gao, X., Oudit, G. Y. & Tsushima, R. G. Trafficking Defect and Proteasomal Degradation Contribute to the Phenotype of a Novel KCNH2 Long QT Syndrome Mutation. *PLoS One* **6**, e18273 (2011).
22. Anderson, C. L. *et al.* Most LQT2 mutations reduce Kv11.1 (hERG) current by a class 2 (trafficking-deficient) mechanism. *Circulation* **113**, 365–73 (2006).
23. Anderson, C. L. *et al.* Large-scale mutational analysis of Kv11.1 reveals molecular insights into type 2 long QT syndrome. *Nat. Commun.* **5**, 5535 (2014).
24. JANUARY, C. T., GONG, Q. & ZHOU, Z. Long QT Syndrome: Cellular Basis and Arrhythmia Mechanism in LQT2. *J. Cardiovasc. Electrophysiol.* **11**, 1413–1418 (2000).
25. Moss, A. J. *et al.* Increased risk of arrhythmic events in long-QT syndrome with mutations in the pore region of the human ether-a-go-go-related gene potassium channel.

Circulation **105**, 794–799 (2002).

26. Bennett, P. B., Yazawa, K., Makita, N. & George, A. L. Molecular mechanism for an inherited cardiac arrhythmia. *Nature* **376**, 683–685 (1995).
27. Splawski, I. *et al.* Ca(V)1.2 calcium channel dysfunction causes a multisystem disorder including arrhythmia and autism. *Cell* **119**, 19–31 (2004).
28. Zhang, J. F., Ellinor, P. T., Aldrich, R. W. & Tsien, R. W. Molecular determinants of voltage-dependent inactivation in calcium channels. *Nature* **372**, 97–100 (1994).
29. Peterson, B. Z., DeMaria, C. D., Adelman, J. P. & Yue, D. T. Calmodulin is the Ca2+ sensor for Ca2+ -dependent inactivation of L-type calcium channels. *Neuron* **22**, 549–558 (1999).
30. Bazett, H. An analysis of the time-relations of electrocardiograms. *Heart* **1**, 353–370 (1920).
31. Moss, A. J. *et al.* ECG T-wave patterns in genetically distinct forms of the hereditary long QT syndrome. *Circulation* **92**, 2929–2934 (1995).
32. Zhang, L. *et al.* Spectrum of ST-T-wave patterns and repolarization parameters in congenital long-QT syndrome: ECG findings identify genotypes. *Circulation* **102**, 2849–2855 (2000).
33. Sugrue, A. *et al.* Architectural T-Wave Analysis and Identification of On-Therapy Breakthrough Arrhythmic Risk in Type 1 and Type 2 Long-QT Syndrome. *Circ. Arrhythm. Electrophysiol.* **10**, (2017).
34. Mazzanti, A. *et al.* Interplay Between Genetic Substrate, QTc Duration, and Arrhythmia Risk in Patients With Long QT Syndrome. *J. Am. Coll. Cardiol.* **71**, 1663–1671 (2018).
35. Zareba, W. *et al.* Modulating effects of age and gender on the clinical course of long QT syndrome by genotype. *J. Am. Coll. Cardiol.* **42**, 103–109 (2003).
36. Crotti, L. *et al.* Calmodulin mutations and life-threatening cardiac arrhythmias: insights from the International Calmodulinopathy Registry. *Eur. Heart J.* **40**, 2964–2975 (2019).
37. Schwartz, P. J. *et al.* The Jervell and Lange-Nielsen syndrome: natural history, molecular basis, and clinical outcome. *Circulation* **113**, 783–790 (2006).
38. Clemens, D. J. *et al.* International Triadin Knockout Syndrome Registry. *Circ. Genomic Precis. Med.* **12**, e002419–e002419 (2019).
39. Brink, P. A. *et al.* Phenotypic variability and unusual clinical severity of congenital long-QT syndrome in a founder population. *Circulation* **112**, 2602–2610 (2005).
40. Moss, A. J. *et al.* Effectiveness and limitations of beta-blocker therapy in congenital long-QT syndrome. *Circulation* **101**, 616–623 (2000).

41. Priori, S. G. *et al.* Association of long QT syndrome loci and cardiac events among patients treated with beta-blockers. *JAMA* **292**, 1341–1344 (2004).
42. Priori, S. G., Napolitano, C., Cantù, F., Brown, A. M. & Schwartz, P. J. Differential response to Na+ channel blockade, beta-adrenergic stimulation, and rapid pacing in a cellular model mimicking the SCN5A and HERG defects present in the long-QT syndrome. *Circ. Res.* **78**, 1009–1015 (1996).
43. Mazzanti, A. *et al.* Gene-Specific Therapy With Mexiletine Reduces Arrhythmic Events in Patients With Long QT Syndrome Type 3. *J. Am. Coll. Cardiol.* **67**, 1053–1058 (2016).
44. Dufendach, K. A. *et al.* Clinical Outcomes and Modes of Death in Timothy Syndrome: A Multicenter International Study of a Rare Disorder. *JACC Clin Electrophysiol* **4**, 459–466 (2018).
45. Benhorin, J. *et al.* Effects of flecainide in patients with new SCN5A mutation: mutation-specific therapy for long-QT syndrome? *Circulation* **101**, 1698–1706 (2000).
46. Windle, J. R., Geletka, R. C., Moss, A. J., Zareba, W. & Atkins, D. L. Normalization of ventricular repolarization with flecainide in long QT syndrome patients with SCN5A:DeltaKPQ mutation. *Ann. noninvasive Electrocardiol. Off. J. Int. Soc. Holter Noninvasive Electrocardiology, Inc* **6**, 153–158 (2001).
47. Moss, A. J. *et al.* Safety and efficacy of flecainide in subjects with Long QT-3 syndrome (DeltaKPQ mutation): a randomized, double-blind, placebo-controlled clinical trial. *Ann. noninvasive Electrocardiol. Off. J. Int. Soc. Holter Noninvasive Electrocardiology, Inc* **10**, 59–66 (2005).
48. Moss, A. J. *et al.* Ranolazine shortens repolarization in patients with sustained inward sodium current due to type-3 long-QT syndrome. *J. Cardiovasc. Electrophysiol.* **19**, 1289–1293 (2008).
49. Priori, S. G. *et al.* The elusive link between LQT3 and Brugada syndrome: the role of flecainide challenge. *Circulation* **102**, 945–947 (2000).
50. Bos, J. M. *et al.* Mexiletine Shortens the QT Interval in Patients With Potassium Channel-Mediated Type 2 Long QT Syndrome. *Circ. Arrhythm. Electrophysiol.* **12**, e007280 (2019).
51. Gao, Y. *et al.* Inhibition of late sodium current by mexiletine: a novel pharmotherapeutical approach in timothy syndrome. *Circ Arrhythm Electrophysiol* **6**, 614–622 (2013).
52. Shah, D. P., Baez-Escudero, J. L., Weisberg, I. L., Beshai, J. F. & Burke, M. C.

Ranolazine safely decreases ventricular and atrial fibrillation in Timothy syndrome (LQT8). *Pacing Clin Electrophysiol* **35**, e62--4 (2012).

53. Jacobs, A., Knight, B. P., McDonald, K. T. & Burke, M. C. Verapamil decreases ventricular tachyarrhythmias in a patient with Timothy syndrome (LQT8). *Hear. Rhythm* **3**, 967–970 (2006).
54. Mehta, A. *et al.* Identification of a targeted and testable antiarrhythmic therapy for long-QT syndrome type 2 using a patient-specific cellular model. *Eur. Heart J.* **39**, 1446–1455 (2018).
55. Schwartz, P. J. *et al.* From patient-specific induced pluripotent stem cells to clinical translation in long QT syndrome Type 2. *Eur. Heart J.* **40**, 1832–1836 (2019).
56. O'Hare, B. J. *et al.* Promise and Potential Peril With Lumacaftor for the Trafficking Defective Type 2 Long-QT Syndrome-Causative Variants, p.G604S, p.N633S, and p.R685P, Using Patient-Specific Re-Engineered Cardiomyocytes. *Circ. Genomic Precis. Med.* **13**, 466–475 (2020).
57. Yazawa, M. *et al.* Using induced pluripotent stem cells to investigate cardiac phenotypes in Timothy syndrome. *Nature* **471**, 230–234 (2011).
58. Song, L. *et al.* Sigma non-opioid receptor 1 is a potential therapeutic target for long QT syndrome. *Nat. Cardiovasc. Res.* **1**, 142–156 (2022).
59. Maguy, A. *et al.* KCNQ1 Antibodies for Immunotherapy of Long QT Syndrome Type 2. *J. Am. Coll. Cardiol.* **75**, 2140–2152 (2020).
60. Narayana Moorthy, N. S. H., Ramos, M. J. & Fernandes, P. A. Human ether-a-go-go-related gene channel blockers and its structural analysis for drug design. *Curr. Drug Targets* **14**, 102–113 (2013).
61. Wang, W. & MacKinnon, R. Cryo-EM Structure of the Open Human Ether-à-go-go-Related K(+) Channel hERG. *Cell* **169**, 422-430.e10 (2017).
62. Chen, J., Seebohm, G. & Sanguinetti, M. C. Position of aromatic residues in the S6 domain, not inactivation, dictates cisapride sensitivity of HERG and eag potassium channels. *Proc. Natl. Acad. Sci. U. S. A.* **99**, 12461–12466 (2002).
63. Perry, M. *et al.* Structural determinants of HERG channel block by clofilium and ibutilide. *Mol. Pharmacol.* **66**, 240–249 (2004).
64. Kang, J. *et al.* Discovery of a small molecule activator of the human ether-a-go-go-related gene (HERG) cardiac K+ channel. *Mol. Pharmacol.* **67**, 827–836 (2005).
65. Sanguinetti, M. C. HERG1 channel agonists and cardiac arrhythmia. *Curr Opin Pharmacol* **15**, 22–27 (2014).

66. Gerlach, A. C., Stoehr, S. J. & Castle, N. A. Pharmacological removal of human ether-à-go-go-related gene potassium channel inactivation by 3-nitro-N-(4-phenoxyphenyl) benzamide (ICA-105574). *Mol. Pharmacol.* **77**, 58–68 (2010).
67. Garg, V., Stary-Weinzinger, A., Sachse, F. & Sanguinetti, M. C. Molecular determinants for activation of human ether-à-go-go-related gene 1 potassium channels by 3-nitro-n-(4-phenoxyphenyl) benzamide. *Mol Pharmacol* **80**, 630–637 (2011).
68. Zangerl-Plessl, E.-M. *et al.* Toward a Structural View of hERG Activation by the Small-Molecule Activator ICA-105574. *J. Chem. Inf. Model.* **60**, 360–371 (2020).
69. Meng, J., Shi, C., Li, L., Du, Y. & Xu, Y. Compound ICA-105574 prevents arrhythmias induced by cardiac delayed repolarization. *Eur. J. Pharmacol.* **718**, 87–97 (2013).
70. Asayama, M. *et al.* Effects of an hERG activator, ICA-105574, on electrophysiological properties of canine hearts. *J. Pharmacol. Sci.* **121**, 1–8 (2013).
71. Perry, M. D. *et al.* Pharmacological activation of IKr in models of long QT Type 2 risks overcorrection of repolarization. *Cardiovasc. Res.* **116**, 1434–1445 (2020).
72. Zhu, W. *et al.* Predicting Patient Response to the Antiarrhythmic Mexiletine Based on Genetic Variation. *Circ. Res.* **124**, 539–552 (2019).
73. Mazzanti, A. *et al.* Arrhythmogenic Right Ventricular Cardiomyopathy: Clinical Course and Predictors of Arrhythmic Risk. *J. Am. Coll. Cardiol.* **68**, 2540–2550 (2016).
74. Mazzanti, A. *et al.* Natural History and Risk Stratification in Andersen-Tawil Syndrome Type 1. *J. Am. Coll. Cardiol.* **75**, 1772–1784 (2020).
75. Mazzanti, A. *et al.* Outcomes of Patients With Catecholaminergic Polymorphic Ventricular Tachycardia Treated With β-Blockers. *JAMA Cardiol.* **7**, 504–512 (2022).
76. Monserrat, L. *et al.* Non-sustained ventricular tachycardia in hypertrophic cardiomyopathy. *J. Am. Coll. Cardiol.* **42**, 873–879 (2003).
77. Oreto, G. *Elettrocardiogramma: un mosaico a 12 tessere (Vol. I + Vol. II)*. (Centro Scientifico Editore, 2009).
78. Agency, E. M. *Note for Guidance on The Nonclinical Evaluation of the Potential for Delayed Ventricular Repolarization (QT Interval Prolongation) by Human Pharmaceuticals*. (2005).
79. Ruppert, S., Vormberge, T., Igl, B.-W. & Hoffmann, M. ECG telemetry in conscious guinea pigs. *J. Pharmacol. Toxicol. Methods* **81**, 88–98 (2016).
80. Hohnloser, S. H. & Woosley, R. L. Sotalol. *N. Engl. J. Med.* **331**, 31–38 (1994).
81. El-Sherif, N., Caref, E. B., Chinushi, M. & Restivo, M. Mechanism of arrhythmogenicity of the short-long cardiac sequence that precedes ventricular tachyarrhythmias in the long

QT syndrome. *J. Am. Coll. Cardiol.* **33**, 1415–1423 (1999).

82. Sicouri, S. *et al.* Cellular basis for the electrocardiographic and arrhythmic manifestations of Timothy syndrome: effects of ranolazine. *Hear. Rhythm* **4**, 638–647 (2007).
83. Thomas, G., Chung, M. & Cohen, C. J. A dihydropyridine (Bay k 8644) that enhances calcium currents in guinea pig and calf myocardial cells. A new type of positive inotropic agent. *Circ. Res.* **56**, 87–96 (1985).
84. Schuster, A. *et al.* The IVS6 segment of the L-type calcium channel is critical for the action of dihydropyridines and phenylalkylamines. *EMBO J.* **15**, 2365–2370 (1996).
85. Sanguinetti, M. C., Krafte, D. S. & Kass, R. S. Voltage-dependent modulation of Ca channel current in heart cells by Bay K8644. *J. Gen. Physiol.* **88**, 369–392 (1986).
86. Artigas, P., Ferreira, G., Reyes, N., Brum, G. & Pizarro, G. Effects of the enantiomers of BayK 8644 on the charge movement of L-type Ca channels in guinea-pig ventricular myocytes. *J. Membr. Biol.* **193**, 215–227 (2003).
87. Hamilton, S. L., Yatani, A., Brush, K., Schwartz, A. & Brown, A. M. A comparison between the binding and electrophysiological effects of dihydropyridines on cardiac membranes. *Mol. Pharmacol.* **31**, 221–231 (1987).
88. Cheng, H. C., Incardona, J. & McCullough, B. Isolated perfused and paced guinea pig heart to test for drug-induced changes of the QT interval. *J. Pharmacol. Toxicol. Methods* **54**, 278–287 (2006).
89. Jinek, M. *et al.* A programmable dual-RNA-guided DNA endonuclease in adaptive bacterial immunity. *Science* **337**, 816–821 (2012).
90. Lagutina, I., Lazzari, G. & Galli, C. Birth of cloned pigs from zona-free nuclear transfer blastocysts developed in vitro before transfer. *Cloning Stem Cells* **8**, 283–293 (2006).
91. Brunetti, D. *et al.* Transgene expression of green fluorescent protein and germ line transmission in cloned pigs derived from in vitro transfected adult fibroblasts. *Cloning Stem Cells* **10**, 409–419 (2008).
92. Meijborg, V. M. F. *et al.* Electrocardiographic T wave and its relation with ventricular repolarization along major anatomical axes. *Circ. Arrhythm. Electrophysiol.* **7**, 524–531 (2014).
93. Rautaharju, P. M. *et al.* AHA/ACCF/HRS recommendations for the standardization and interpretation of the electrocardiogram: part IV: the ST segment, T and U waves, and the QT interval: a scientific statement from the American Heart Association Electrocardiography and Arrhythmias . *J. Am. Coll. Cardiol.* **53**, 982–991 (2009).

94. Galán-Arriola, C. *et al.* Serial Magnetic Resonance Imaging to Identify Early Stages of Anthracycline-Induced Cardiotoxicity. *J. Am. Coll. Cardiol.* **73**, 779–791 (2019).
95. Kelley, K. W., Curtis, S. E., Marzan, G. T., Karara, H. M. & Anderson, C. R. Body surface area of female swine. *J Anim Sci* **36**, 927–930 (1973).
96. Rogers, T. *et al.* Standardization of T1 measurements with MOLLI in differentiation between health and disease--the ConSept study. *J. Cardiovasc. Magn. Reson. Off. J. Soc. Cardiovasc. Magn. Reson.* **15**, 78 (2013).
97. Flett, A. S. *et al.* Equilibrium contrast cardiovascular magnetic resonance for the measurement of diffuse myocardial fibrosis: preliminary validation in humans. *Circulation* **122**, 138–144 (2010).
98. Seldinger, S. I. Catheter replacement of the needle in percutaneous arteriography; a new technique. *Acta radiol.* **39**, 368–376 (1953).
99. Anter, E., Tschabrunn, C. M., Buxton, A. E. & Josephson, M. E. High-Resolution Mapping of Postinfarction Reentrant Ventricular Tachycardia: Electrophysiological Characterization of the Circuit. *Circulation* **134**, 314–327 (2016).
100. Wyatt, R. F. *et al.* Estimation of ventricular transmembrane action potential durations and repolarization times from unipolar electrograms. *Am. J. Cardiol.* **47**, 488 (1981).
101. Gałecki, A. & Burzykowski, T. *Linear Mixed-Effects Models Using R*. (Springer New York, 2013). doi:10.1007/978-1-4614-3900-4
102. Laird, N. M. & Ware, J. H. Random-effects models for longitudinal data. *Biometrics* **38**, 963–974 (1982).
103. Cox, D. R. Regression Models and Life-Tables. *J. R. Stat. Soc. Ser. B* **34**, 187–220 (1972).
104. Therneau, T. M. & Grambsch, P. M. *Modeling Survival Data: Extending the Cox Model*. (Springer New York, 2000). doi:10.1007/978-1-4757-3294-8
105. Heinze, G. & Schemper, M. A Solution to the Problem of Monotone Likelihood in Cox Regression. *Biometrics* **57**, 114–119 (2001).
106. Firth, D. Bias Reduction of Maximum Likelihood Estimates. *Biometrika* **80**, 27–38 (1993).
107. Kenward, M. G. & Roger, J. H. Small sample inference for fixed effects from restricted maximum likelihood. *Biometrics* **53**, 983–997 (1997).
108. Rivaud, M. R. *et al.* Critical repolarization gradients determine the induction of reentry-based torsades de pointes arrhythmia in models of long QT syndrome. *Hear. Rhythm* **18**, 278–287 (2021).

109. Killeen, M. J., Sabir, I. N., Grace, A. A. & Huang, C. L.-H. Dispersions of repolarization and ventricular arrhythmogenesis: lessons from animal models. *Prog. Biophys. Mol. Biol.* **98**, 219–229 (2008).
110. Clauss, S. *et al.* Animal models of arrhythmia: classic electrophysiology to genetically modified large animals. *Nat. Rev. Cardiol.* **16**, 457–475 (2019).
111. Hughes, G. C., Post, M. J., Simons, M. & Annex, B. H. Translational physiology: porcine models of human coronary artery disease: implications for preclinical trials of therapeutic angiogenesis. *J. Appl. Physiol.* **94**, 1689–1701 (2003).
112. Bharati, S. *et al.* The conduction system of the swine heart. *Chest* **100**, 207–212 (1991).
113. Satoh, H., Delbridge, L. M., Blatter, L. A. & Bers, D. M. Surface:volume relationship in cardiac myocytes studied with confocal microscopy and membrane capacitance measurements: species-dependence and developmental effects. *Biophys. J.* **70**, 1494–1504 (1996).
114. Hondeghem, L. M., Carlsson, L. & Duker, G. Instability and triangulation of the action potential predict serious proarrhythmia, but action potential duration prolongation is antiarrhythmic. *Circulation* **103**, 2004–2013 (2001).
115. Ruan, Y., Liu, N., Bloise, R., Napolitano, C. & Priori, S. G. Gating properties of SCN5A mutations and the response to mexiletine in long-QT syndrome type 3 patients. *Circulation* **116**, 1137–1144 (2007).
116. Roden, D. M. Drug-induced prolongation of the QT interval. *N. Engl. J. Med.* **350**, 1013–1022 (2004).
117. Bai, J. *et al.* Computational Cardiac Modeling Reveals Mechanisms of Ventricular Arrhythmogenesis in Long QT Syndrome Type 8: CACNA1C R858H Mutation Linked to Ventricular Fibrillation. *Front. Physiol.* **8**, 771 (2017).